INFORMATION TO USERS

This manuscript has been reproduced from the microfilm master. UMI films the text directly from the original or copy submitted. Thus, some thesis and dissertation copies are in typewriter face, while others may be from any type of computer printer.

The quality of this reproduction is dependent upon the quality of the copy submitted. Broken or indistinct print, colored or poor quality illustrations and photographs, print bleedthrough, substandard margins, and improper alignment can adversely affect reproduction.

In the unlikely event that the author did not send UMI a complete manuscript and there are missing pages, these will be noted. Also, if unauthorized copyright material had to be removed, a note will indicate the deletion.

Oversize materials (e.g., maps, drawings, charts) are reproduced by sectioning the original, beginning at the upper left-hand corner and continuing from left to right in equal sections with small overlaps.

ProQuest Information and Learning
300 North Zeeb Road, Ann Arbor, MI 48106-1346 USA
800-521-0600

Université d'Ottawa • University of Ottawa

PERMISSION DE REPRODUIRE ET DE DISTRIBUER LA THÈSE

PERMISSION TO REPRODUCE AND DISTRIBUTE THE THESIS

NOM DE L'AUTEUR / NAME OF AUTHOR:	HINDS, Sean
ADRESSE POSTALE / MAILING ADDRESS:	810 Nicole Street Rockland, ON K4K 1L6
GRADE / DEGREE:	**ANNÉE D'OBTENTION / YEAR GRANTED**
M.A.Sc. (Electrical Engineering)	2003
TITRE DE LA THÈSE / TITLE OF THESIS:	
Negative Differentiated Optical Injection of Semiconductor Lasers	

L'auteur permet, par la présente, la consultation et le prêt de cette thèse en conformité avec les règlements établis par le bibliothécaire en chef de l'Université d'Ottawa. L'auteur autorise aussi l'Université d'Ottawa, ses successeurs et cessionnaires, à reproduire cet exemplaire par photograhie ou photocopie pour fins de prêt ou de vente au prix coûtant aux bibliothèques ou aux chercheurs qui en feront la demande.

Les droits de publication par tout autre moyen et pour vente au public demeureront la propriété de l'auteur de la thèse sous réserve des règlements de l'Université d'Ottawa en matière de publication de thèses.

The author hereby permits the consultation and the lending of this thesis pursuant to the regulations established by the Chief Librarian of the University of Ottawa. The author also authorizes the University of Ottawa, its successors and assignees, to make reproductions of this copy by photographic means or by photocopying and to lend or sell such reproductions at cost to libraries and to scholars requesting them.

The right to publish the thesis by other means and to sell it to the public is reserved to the author, subject to the regulations of the University of Ottawa governing the publication of theses.

N.B. LE MASCULIN COMPREND ÉGALEMENT LE FÉMININ

January 15, 2003
DATE

Sean Hinds
(AUTEUR) SIGNATURE (AUTHOR)

Université d'Ottawa · University of Ottawa

Université d'Ottawa • University of Ottawa

FACULTÉ DES ÉTUDES SUPÉRIEURES ET POSTDOCTORALES

FACULTY OF GRADUATE AND POSTDOCTORAL STUDIES

HINDS, Sean O'Reily

AUTEUR DE LA THÈSE - AUTHOR OF THESIS

M.A.Sc. (Electrical Engineering)

GRADE - DEGREE

School of Information Technology and Engineering

FACULTÉ, ÉCOLE, DÉPARTEMENT - FACULTY, SCHOOL, DEPARTMENT

TITRE DE LA THÈSE - TITLE OF THE THESIS

Negative Differentiated Optical Injection of Semiconductor Lasers

Peter Galko, Jean-Yves Chouinard and Jacek Chrostowski

DIRECTEUR DE LA THÈSE - THESIS SUPERVISOR

EXAMINATEURS DE LA THÈSE - THESIS EXAMINERS

J. Genest

B. Syrett

J.-M. De Koninck, Ph.D.

LE DOYEN DE LA FACULTÉ DES ÉTUDES SUPÉRIEURES ET POSTDOCTORALES

SIGNATURE

DEAN OF THE FACULTY OF GRADUATE AND POSTDOCTORAL STUDIES

Negative Differentiated Optical Injection of Semiconductor Lasers

By

Sean O'Reilly Hinds

A thesis submitted to the

School of Graduate Studies and Research

in partial fulfillment of the requirements for the degree of

Master of Applied Science

School of Information Technology and Engineering

Ottawa - Carleton Institute for Electrical Engineering

University of Ottawa

ABSTRACT

In this thesis, we present a new technique of semiconductor modulation that maintains simplicity of design and overcomes many deficiencies of current direct modulation technologies. This technique of negative differentiated optical injection locking, makes it possible to equal or improve the Q factor and reduce the chirp penalty of a directly modulated laser source. Using this new structure we stabilize the dielectric properties of the slave laser, beyond the performance of standard optical injection locking, by reducing the refractive index excursion in the active layer and minimizing optical frequency chirp. This enables more reliable bandwidth efficient communication without compromising linearity or demanding prohibitive control complexity. We contrast this technique with direct, standard injection locking, electro absorption and Mach-Zehnder modulators at various speeds and find that our particular technique demonstrates desirable trade-offs between performance, control flexibility and simplicity.

ACKNOWLEDGEMENTS

I wish to acknowledge the expert tutelage and encouragement of doctors Jean-Yves Chouinard, Jacek Chrostowski, and Peter Galko. I wish to express how much I appreciate the tools, resources, insights, and above all patience they provided me during my research. Their continued assistance allowed me to work independently and set my own focus and goals. At times, when the path of my research seemed most challenging, they allowed me to develop solutions and our discussions helped broaden my understanding of semiconductor optics in an interesting and rewarding manner. I should like to thank Dr. Chrostowski for providing me with excellent computing, simulation environments, and research grants to test the waters of my thesis work, buy books, attend seminars and ultimately to pursue knowledge.

The work and research I have done would not have been possible without the education I received in Canada at the University of Ottawa and in France at the École Nationale Supérieure des Télécommunications in their respective departments of electrical and optical engineering.

I would also like to thank my friends, teammates and coworkers for their incredible patience with me during the development of my thesis. Finally, I must thank my parents who have supported me vigilantly and unconditionally over the years with their love.

TABLE OF CONTENTS

LIST OF FIGURES

LIST OF TABLES

ACRONYMS

Abbreviation	Description
BER	Bit Error Rate
DM	Direct Modulation
DWDM	Dense Wavelength Division Multiplexing
Gbps	Gigabits Per Second
MZ	Mach-Zehnder
NDIL	Negative Differentiated Injection Locking
OCDMA	Optical Code Division Multiple Access
OTDM	Orthogonal Time Division Multiplexing
SHO	Simple Harmonic Oscillator
SIL	Standard Injection Locking

LIST OF SYMBOLS

Parameter	Definition
ω_{mo}	Angular frequency of free-running laser
ω_0	Angular frequency of master laser
N_0	Carrier number for transparency
N_w	Number of quantum wells
P	Cavity photons
P_i	Cavity injected photons
J	Current density
n_g	Group index of refraction
α	Linewidth enhancement factor
θ	Phase difference between injection and free-running laser fields
ϕ	Phase of the optical field rad
τ_{ph}	Photon lifetime
f_{RO}	Relaxation oscillation frequency
τ_e	Spontaneous carrier lifetime
J_{th}	Threshold current density
dg/dn	Differential gain
μ_e	Electron mobility
k	Boltzmann constant
η	Scaling parameter
v	Frequency
ω_p	Plasma frequency
ω_T	Natural frequency
$\varepsilon(\omega)$	Dielectric function
ε_0	Permittivity of free space
β	Wave propagation constant
n_{eff}	Effective refractive index
$\bar{E}$	Complex electric field
m	Mass
m^*	Effective mass
$\bar{P}$	Polarization field
$\bar{D}$	Displacement vector
ΔE	Energy change
h	Planck constant
d	Diffusion distance
$n(\omega)$	Refractive index

E_g	Bandgap energy
$\bar{k}$	Wave vector
V	Voltage
n_0	Local index of refraction in bulk material
n_{th}	Electron density at threshold
f_p	Relaxation oscillation gain peak
p	Hole density
t_{chirp}	Relaxation oscillation duration
τ_{RT}	Round trip time
Φ	Spontaneous emission coupling coefficient
ζ	Roll off factor
R'	Average spontaneous emission rate
$\overline{=}$ r	Linear electro-optic coefficient
A	Nonradiative recombination coefficient s^{-1}
B	Radiative recombination coefficient m^3/s
C	Auger recombination coefficient m^6/s
c	Speed of light
c'	Speed of light in medium m/s
g	Optical gain m^{-1}
I	Injection current
J	Injected current density A/m^2
L	Cavity length
L_z	Quantum-well thickness m
n	Electron density m^{-3}
N	Carrier number
q	Electronic charge C
R	Cavity facet reflectivity
S	Photon density m^{-3}
t	Time s
T	Temperature
Γ	Optical confinement factor

1. INTRODUCTION

1.1 THESIS MOTIVATION

The idea of confining electrons and holes in double heterojunction lasers was first published by Kroemer in 1963 [1]. This proposal eventually led to the development of attractive alloys, such as GaAs and InGaAsP, in semiconductors lasers for use over the 2nd and 3rd generation transmission windows of glass fiber. By 1974, Dingle, Weigmann and Henry [2], produced a double heterojunction active layer less than 30nm thick, resulting in a quantum confinement of injected carriers. These devices brought increased reliability and superior commercial telecommunications prospects through their higher gain, lower threshold biases, and superior efficiencies. In these devices, the thin active layers of quantum well designs break the energy-momentum profile (see Appendix B) of permissible energies from a parabolic continuum to a discrete set of permissible energy density states. Thus, larger portions of carriers contribute to lasing as well as improve the linewidth enhancement factor of the device. Another essential feature of semiconductor lasers is that modulating their input drive current can directly modulate their optical ouput. This has been shown [47], to be valid up to speeds near the relaxation oscillation frequency of the device, given by

$$f_{RO} = \frac{1}{2\pi}\sqrt{\frac{c'\,dg/dn\,S}{\tau_{ph}}}, \tag{1.1}$$

where c' is the velocity of light in a particular environment, $^{dg}/_{dn}$ is the differential gain, S is the photon density, and τ_{ph} is the photon lifetime. This rate is usually not achieved in practice as modulation speed is generally limited by driving electronics parasitic capacitance, which also limits the utility of electrical pre-distortion, and not by the relaxation oscillation frequency of the laser. The optical bandwidth of the modulated signal however is a very different problem altogether.

There are three important technologies, for optical fiber, which attempt to address user bandwidth demand [40]. The first is, Optical Time Division Multiplexing (OTDM), which uses interleavers to provide extremely high data rates. This technology has led to dispersion compensated signalling such as soliton transmission, pico and femto second pulse shaping. The second is, Optical Code Division Multiple Access (OCDMA), which admittedly is still in its infancy, but draws from a rich electrical heritage. It offers the possibility of reusing the same bandwidth over and over with simple efficient means for maximizing the practical spectral bit utilization of the channel. It remains in its infancy due to limitations in high-speed optical signal processing techniques. The third and more disruptive technology is that of Wavelength Division Multiplexing (WDM). Since the late 80's WDM has provided a measure of scalability attractive to the demands of data-driven traffic, requiring far less stringent timing complexity than is necessary using OTDM or OCDMA. In WDM, the channel capacity of the fiber is divided into equally spaced frequency bands over which multi-rate, multi-signalling and multi-users can be supported. In conjunction with optical switches, optical amplifiers and optical equalizers it makes for a very dynamic and effective telecommunication network solution. Since the

80's WDM has evolved, by reducing the channel frequency spacing and supporting more simultaneous users, by Dense Wavelength Division Multiplexing (DWDM) providing a more effective utilization the available optical bandwidth.

The most critical aspects of laser emission in Dense Wavelength Division Multiplexing (DWDM) systems are channel width, modulation rate and frequency stability. These issues are physically entangled with the laser structure and its operating parameters. In the forefront of semiconductor direct modulation optical frequency stability is the problem of "chirp". Chirp refers simply to a time-varying change in the oscillation frequency of the laser, measured by the rate of such a change. Chirp is the result of changes in the refractive index of the active layer of the lasing material and subsequent shifts in the laser's emission frequency resultant of instantaneous free carrier injection and relaxation. Its effects affect, on a system level, the modulation response, chromatic and to a lesser extent polarization dispersion [39] and represent a reduction of total fiber usable bandwidth because the actual bandwidth utilization per channel is increased. Thus channel capacity and bit error rate (BER) performance of an optical communications link are degraded.

There are three primary technologies that attempt to address the shortcomings of direct semiconductor modulation with respect to its chirp penalties. The first is the Mach-Zehnder (MZ) modulator, an external modulator that splits an optical signal into two paths of different optical length, recombining them and using the superposition principle of constructive and destructive interference to key the modulation. A second solution is

the electro-absorption modulator, which couples a gain cavity with a reverse biased semiconductor that modulates by absorption. In this instance, the frequency chirp shift is opposite to the chirp normally produced in direct modulation and thus presents the designer with a useful equalization mechanism over standard dispersion fiber. Finally, a third technology is optical injection locking modulation. It reduces frequency chirp in a directly modulated laser's output by injecting an unmodulated laser's output into the modulated laser, a technique known as optical injection. This technique reduces spontaneous emission interaction with the lasing field and mitigates the relaxation oscillation time through electro-optical carrier population control. These three modulation schemes represent the bulk of current commercial technology for high-access optical modulation. It is important for us to understand how each addresses the issue of chirp and the technological compromises they engineer to achieve this goal.

Semiconductor optical injection can significantly increases the intrinsic modulation rate and decreases the frequency chirp of a laser. Frequency chirp is reduced and peak modulation rate is enhanced because of the presence of optical carriers; overriding spontaneous influences and alleviating the electrical carrier pressures in the active region, thus reducing the relaxation oscillation intensity. This technique however has the disadvantage that it cannot produce modulation at rates as high as those possible with a MZ modulator. Still, it is a simple robust and highly effective means of low chirp high-speed modulation and remains linear in its electro-optical modulation. To us, this is a significant advantage if understated in the evolution of an optical system towards simpler

high data rate communication, higher access metro markets, and towards OCDMA modulation.

Until recently, the primary focus of the optical telecommunication community has been in long haul applications where the cost and complexity of Mach-Zehnder modulators were acceptable compromises in favor of their superior speed and frequency stability. This market has apparently proven to be dramatically overbuilt and thus has prompted a renewed interest in designing optical systems to meet the demands of more metro market type applications. With this in mind, companies are beginning to invest more heavily in developing systems that address the optical communications needs between cities rather than across oceans, where carrier modulation speed now plays a secondary role to cost efficiency and simplicity of design. It is in this context that we propose a new method of optical injection locking. Like direct modulation, the electro-absorption modulator and standard injection locking, our modulation does not solely attempt to compete in terms of speed, frequency stability, and optical bandwidth but also as a function of its simplicity and efficiency of design.

1.2 THESIS OBJECTIVES AND HYPOTHESIS

Our aim in this thesis is to improve the optical frequency chirp performance of direct semiconductor modulation through a simple signal dependent optical carrier injection locking mechanism. We attempt to reduce the relaxation oscillation duration, reduce chirp, and consequently improve the performance of systems employing direct modulation through this technique.

The principal causes of spectral broadening degradation in single mode directly modulated semiconductor lasers are phase noise and frequency chirp. Phase noise is an issue we shall consider largely addressed by the principle of standard injection locking as described in Chapter 3. (We present a short examination of this subject in Appendix C.). Optical frequency chirp however, is the primary focus of this thesis. It has two main sources: electrical carrier concentration changes and electro-optically coupled relaxation oscillations. The electrical carrier concentration changes are a fundamental property of direct modulation and remain a physical penalty to the process of direct modulation in the form of adiabatic chirp. Electrical carrier concentration changes influence the dielectric function of the laser active layer and consequently shift the refractive index of the material and its emission wavelength spectrum as depicted in Figure 1.1, which shows the typical evolution of these material parameters under a current step function and is intended to simplify the understanding of the relationships between them.

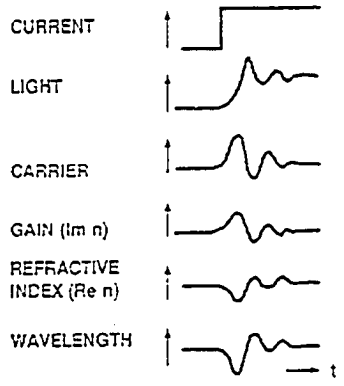

Figure 1.1 Semiconductor relationships of material properties due to a current step function.

The relaxation oscillation that occurs from instantaneous electrical carrier concentration changes results in an equilibrium searching condition between the changes in electrical carrier concentration and optical carrier concentration. This is an uncontrolled process in

direct modulation (DM) and standard injection locking (SIL), and one that we attempt to address in this thesis by modifying the practice of standard injection locking taking into account this effect.

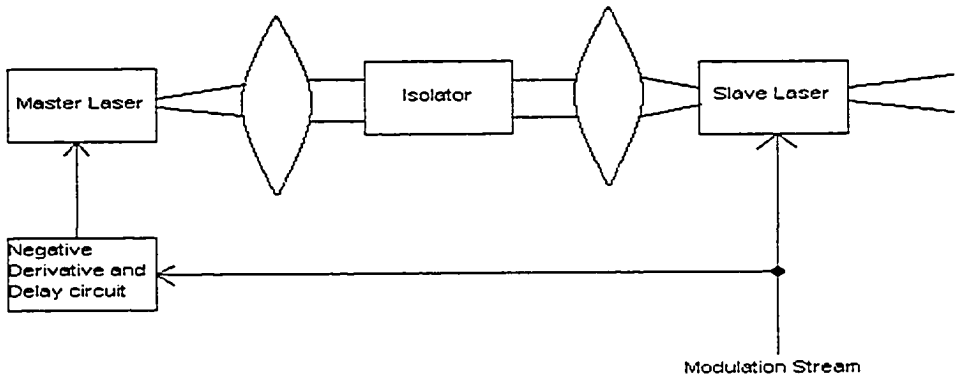

Figure 1.2 Schematic diagram of negative differentiated optical injection locking.

Figure 1.2, depicts the system topology of our proposed modulation. Essentially, a differentiated version of the electrical input signal is used to drive the optical characteristics of the master laser as it is injected into the modulated slave laser. Typically, the relaxation oscillation duration and the gain mechanism of the slave laser result in a birth-death process between electrical and optical carrier populations in the active layer of the laser. By optically controlling the relaxation oscillation mechanism we propose to mitigate a degree of the adiabatic and transient chirp, which brings us to the statement of our hypothesis:

Hypothesis:

Addressing the electro-optical carrier population dynamics with a proportionally negative differentiated optical injection field can mitigate the adiabatic and transient chirp of a directly modulated semiconductor laser.

Mitigating chirp focuses the spectral utilization of the signal and reduces the influence optical amplitude phase coupling. The technological audience of negative differentiated optical injection locking is not to address high power long haul telecommunications lasers. It is rather to present a simple solution in the emerging or future DWDM metro networks. Also, it is to present a solution to semiconductor laser applications that require a high degree of frequency stability upon modulation.

1.3 ORGANIZATION OF THESIS

In Chapter 2, we present a literature review of semiconductor electrical carrier confinement. Chapter 3 discusses direct modulation laser dynamics and investigates the theoretical justification of our proposed model. In Chapter 4, we review the significant results between the transmission line and rate equation simulation models and contrast them to contemporary external modulation devices. In Chapter 5, we conclude the thesis presentation and précis the work to date. There we also discuss possible future enhancements and research which might help better understand the physical limits of our new optical injection model. Finally, in the appendices we examine the relevant subjects of dispersion, quantum confinement, noise, and present the MATLAB engine developed to simulate the direct, standard injection locking, and negative differentiated injection locking models.

2. SEMICONDUCTOR ELECTRICAL CONFINEMENT REVIEW

2.1 MOTIVATION

In this chapter we review the static physical framework of the most important feature of semiconductor technology, that of electrical carrier confinement. The main feature of a semiconductor laser that makes it so attractive as a technology is that it can be directly modulated. Ironically, the mechanism of this feature is also the source of its greatest technical challenges as the effects of modulation rate, relaxation oscillation, and emission frequency stability are directly related to its structure as shall be demonstrated in Chapter 3. In this chapter, we will investigate the basic evolution of the semiconductor laser from the simple pn junction to heterojunction carrier confinement and relate refractive index to bandgap energy and emission wavelength for $Al_yGa_{1-y}As$. In Appendix B, we go further by investigating the quantum confinement of electrical carriers. Finally, we shall briefly review the implication of direct vs. indirect bandgaps in semiconductor lasers, which will set the stage for the next chapter, Chapter 3, investing the dynamics of the semiconductor laser under modulation.

2.2 THE HOMOJUNCTION DIODE

We begin with an exploration of the pn junction, which forms the core of semiconductor lasers and receivers. Doping part of a semiconductor crystal p-type and an adjacent part n-type creates a pn junction. By investigating the depletion region of the junction where the concentration of mobile carriers is reduced with respect to the bulk regions, we can investigate some of the semiconductors fundamental properties. Under equilibrium conditions we first make the assumption of charge neutrality for the device. We would initially expect diffusion to take place and equalize the carrier concentration throughout the semiconductor crystal, but we must also take into account the effect of charge balance. As majority carriers diffuse across the depletion region, they leave behind ionized atoms of opposite charge that are fixed in place within the crystal lattice. From Gauss's law [44], the net charge density produces an electric field in the semiconductor. The generated electric field opposes the diffusion of the majority carriers. The carrier concentration imbalance between regions will cause an inevitable charge imbalance. The ionic charge imbalance counteracts further carrier diffusion until an equilibrium point is reached where the net flow of carriers is nil. By integrating over the electric field we see that a built-in potential difference exists over the device under thermal equilibrium. If a forward bias is then applied, using Kirchhoff's voltage law, the depletion region must accordingly shrink. Similarly, the opposite effect occurs if the device is reverse biased.

Building on these notions in the depletion region, we might ask if minority carriers will slide down the built-in potential of the depletion region. If so, what happens to the null carrier flow in the bulk regions of the device? Clearly, to maintain flow neutrality

minority carrier drift must be compensated for by majority carrier diffusion in the opposite direction.

Applying a forward bias to this model decreases the potential hill in the depletion region. Thus the slope of the band edges in the energy band diagram of the device is reduced with respect to thermal equilibrium. Therefore, the electric field and potential difference at the ends of the diode must also be reduced. Subsequently, the barrier for electron diffusion is reduced and electrons are more likely to make their way through the depletion region. The same argument can be applied for the holes in the p-doped region. Drift current, however, usually remains near its thermal equilibrium level since its carrier supply is limited by thermal generation. This is the fundamental path that will lead electrons from the conduction band to recombine with holes from the valence band and produce light.

Applying a reverse bias to this model increases the potential height in the depletion region. Now the slope of the band edges in the energy band diagram is exaggerated with respect to thermal equilibrium and the potential barrier is increased. Thus the majority carriers are further blocked by the potential hill and minority carriers dominate current flow by drift. This flow may be significantly increased when excess carriers are created as is the principal of a photodiode.

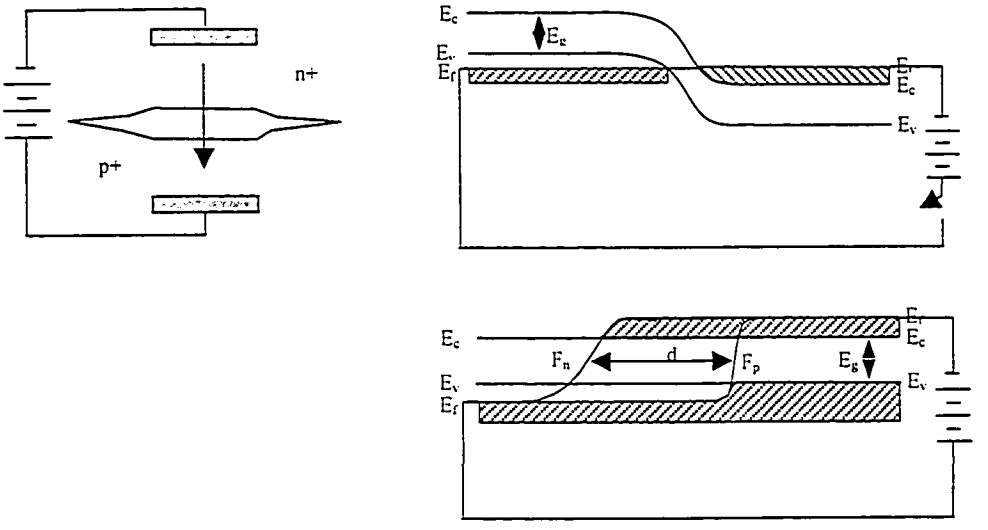

Figure 2.1 Semiconductor Fermi level and depletion width with bias conditions.

When the junction is forward biased according to [3], the Fermi levels between the bulk regions split because of the injection of minority carriers. This injection creates a region over the depletion region where there is a high concentration of both electrons and holes. Considering the higher mobility of the electrons, the majority of recombination events will occur in the p region after diffusing a distance d given by the diffusion length

$$d = \sqrt{\frac{\mu_e q \tau_e}{kT}}, \tag{2.1}$$

where τ_e is the carrier lifetime, q is the charge on an electron, k is Boltzmann's constant, T is the temperature and μ_e is the electron mobility. The rate equation governing the recombination/loss mechanisms of the minority carrier injection n_p into the p region is given as follows:

$$\frac{dn_p}{dt} = -(\eta p_p) n_p = -\frac{n_p}{\tau_e}, \tag{2.2}$$

where η is an arbitrary fitting parameter and p_p are majority hole carriers. If we were to assume the electron distribution at T=0K a few electron volts above the conduction band edge we could estimate the number of electrons per cm cubed as,

$$n = \frac{1}{3\pi^2}\sqrt[3]{\frac{2m_e^{*}\Delta E}{h^2}}, \tag{2.3}$$

where m_e^{*} is the effective mass of an average electron, ΔE is the electron energy and h is Planck's constant, this equation can be related to a current density by the relationship,

$$J = \frac{nqd}{\tau_e}. \tag{2.4}$$

Clearly one important feature is that the diffusion length and carrier lifetime play a pivotal role in the current density. For typical values in GaAs homojunction laser structures, J=23.5 kA/cm^2. Among the other disadvantages of homojunction lasers are lack of design freedom with respect to the depletion length; the dimensions of the cavity do not allow for a cylindrically symmetric beam pattern and the minority carriers are free to diffuse where they will. Another important feature according to (2.3) is that carrier concentration and effective mass are related to an energy change, which can be related to a change in emission wavelength. In Section 3.5, we will explicitly relate carrier concentration and refractive index changes.

In order for electron transitions to efficiently result in stimulated emission between the conduction and valence bands, energy and momentum must be preserved. Although photons can carry significant energy $hc/n(\omega)\lambda$, their momentum is quite small $h/n(\omega)\lambda$,

where c is the speed of light, and $n(\omega)$ is the refractive index of the medium. Semiconductors are classified into either direct bandgap or indirect bandgap for this reason. A direct bandgap material is one where electron and hole momentums are identical; during recombination, a photon is emitted with little other effect. However, in indirect bandgap materials the conduction band energy minimum and valence band energy maximum occur at different momentums. To conserve the momentum crystal lattice vibrations, called phonons make up in heat the difference in momentum. Apart from generating unwanted heat, the simultaneous combinational probabilities of recombination, with an appropriate phonon, make indirect bandgap materials generally less inviting for our purpose.

2.3 CARRIER CONFINEMENT

The main draw back of the pn junction is that the carrier confinement is so poor as to only allow a region of about 0.01 micrometer of sufficient gain to allow lasing to dominate over absorption. Such homojunctions generally have not been able to function at room temperature.

However, by using a heterojunction we can more efficiently confine electrical carriers in the active region in the plane perpendicular to the junction. In this configuration the active layer bandgap is sandwiched between two cladding layers of larger bandgap energies. When they are forward biased, the injected carriers can become trapped between the potential well of the cladding junctions. This confinement of carriers makes

lasing more easily achievable since the necessary current is greatly reduced even at room temperature.

Another important form of carrier confinement is lateral confinement. Lateral confinement improves laser efficiency and beam shape. One method commonly used to achieve this lateral confinement is by varying the refractive index discontinuity between the active and cladding layers by total internal reflection, as is similar to the fundamental practice of an optical fiber for photons but for the confinement of electrons in this instance.

2.4 DOUBLE HETEROJUNCTION DIODE

In [4], we learned that creating semiconductors between two dissimilar materials form heterojunctions, which enhance the electrical carrier confinement between them. To allow the growth of one layer, say of $Al_xGa_{1-x}As$, under another material layer, of say GaAs, it is important to have nearly matched lattice constants as shown in Figure 2.2. This matching is important to minimize lattice strain and to minimize the density of traps at the surface.

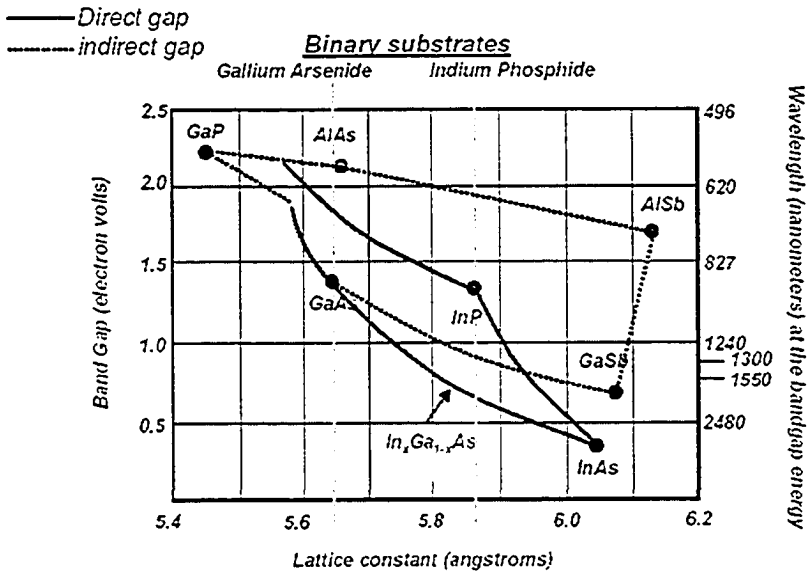

Figure 2.2 Lattice constant, bandgap and emission wavelengths for selected binary substrates.

The most important role, however, of this heterojunction is that as the percentage of Al directly increases the bandgap and it directly influences the index of refraction accordingly. This allows us to confine electrons and photons into a region using Snell's law and the band gap by growing a third layer, of say $Al_yGa_{1-y}As$, over the second layer. These effects allow for a generally wavelength designable device with dramatic reductions in threshold currents due to the enhanced electrical confinement of carriers in the active region.

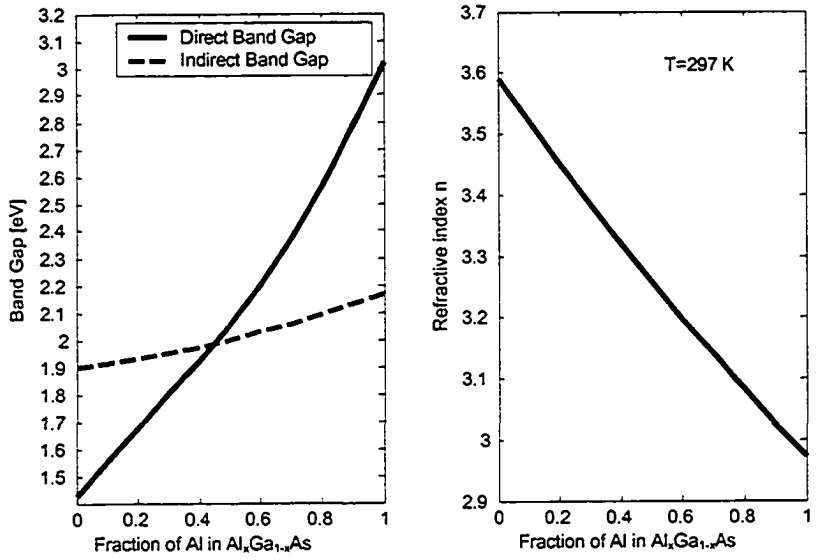

Figure 2.3 Bandgap and refractive index dependence of aluminium gallium arsenide.

Figure 2.3 depicts the dependence [5,6] of the bandgap and index of the refraction x, on the fraction of aluminium in the alloy. It is important to note that bandgap energy and refractive index are generally related. If we further increase the electrical confinement of a double heterojunction laser down to the DeBroglie wavelength of the active material we can break down the energy momentum profile into a discrete number of permissible energy levels as described in Appendix B. What is of general interest to this thesis is that in all the semiconductor structures we have classified, they all conform to the relationship that changes in carrier density, effective mass in the active region, precipitate proportional changes in refractive index, and emission wavelength as detailed in Section 3.5. The particulars of this relationship we shall postpone until then however; what is of interest to our current literature review is that dependence on material active layer refractive index remains a fundamental property of any directly modulated semiconductor laser.

2.5 POPULATIONS IN A SEMICONDUCTOR LASER

We are interested in the lasing action that is possible within a semiconductor, which can be described by the following chemical equation

$$\text{electron} + \text{hole} \rightarrow (h\nu) > E_g . \tag{2.5}$$

For this reaction to occur with high probability, it is necessary to conserve the momentum of the involved electron and hole population interactions. This conservation of momentum usually translates itself into favouring direct bandgap materials for light emission. The conservation of momentum requirement in this context corresponds [7], to the following equation

$$\hbar\bar{k}_f + \hbar\bar{k}_p = \hbar\bar{k}_i , \tag{2.6}$$

where $\hbar$ is Planck's constant over 2π, $\bar{k}$ is the wave vector, where the subscript f indicates the wave vector of the final electron state, p the photon state, and i the initial state. Considering the following conservation of energy assumption, letting the electron temperature equal the lattice temperature, we can approximate the momentum of the electron $\left|\hbar\bar{k}\right|$ by using the relationship

$$\frac{m_c^* v^2}{2} = \frac{3kT_c}{2}, \tag{2.7}$$

where v is the speed of the electron. When comparing the momentum of an electron $\left|m_c^* v\right|$ to that of a photon h/λ ,we generally observe a large discrepancy. Thus without involving lower probability interactions with events such as phonons, the hole

momentum must account for the difference between electron and photon momenta and thus necessitate an almost direct bandgap transition in order to conserve momentum and energy.

During direct amplitude modulation, of direct bandgap materials, the amplitude change couples itself to changes in the phase of the output in part through the material refractive index change of the laser altering the effective optical length of the resonator and its output wavelength. Typically in standard injection locking the frequency of the master laser is negatively detuned from the free-running slave laser optical frequency. According to Schunk [43], negative detuning is favoured because the electro-optic conversion of the injected field tends to reduce the carrier concentration in the slave laser. This increases the active layer's refractive index thus lowering its emission frequency and all but eliminates the phase deviation response based on spontaneous emission. Since coupling is enhanced when the frequencies of the master and slave lasers more closely coincide, this activity favours the master laser being negatively detuned from the slave free running laser emission frequency.

Under injection locking the coherent light already in the optical cavity reduces the degree of amplitude phase coupling by reducing the phase deviation in the transition from spontaneous to a stimulated emission lasing process by suggesting an emission frequency to the cavity. However, to additionally mitigate the residual frequency chirping that exists during the transition relaxations of modulation is the principal target of this thesis.

2.6 SUMMARY

In this chapter we reviewed the essential feature of semiconductor lasers that of electrical carrier confinement. We discussed the failings of homojunction lasers and described the general characteristics of heterojunction lasers. Finally, we introduced the concepts of bandgap energy and momentum transitions and ultimately introduced the relationship between emission frequency and electrical carrier injection. We will now focus on developing these notions further and investigate how controlling carrier densities can be related to the index of refraction and how such a relationship will present an opportunity to mitigate transient frequency chirp for directly modulated semiconductor lasers.

3. LASER MODULATION DYNAMICS

3.1 MOTIVATION

Essential to this thesis is the modulation dynamics of a semiconductor laser. In the previous chapter we examined, in part, some of the physical structure of the types of semiconductor lasers we are interested in; a more detailed perspective on quantum confinement is also addressed, in part, in Appendix B. Now that the necessary physical and historical appreciation of the semiconductor structure have been briefly reviewed we turn our attention to models of laser dynamics under modulation. The models we will consider are the standard rate equation model and the phonon-polariton and lattice absorption/emission simple harmonic oscillator (SHO) model. We will also review salient laser dynamics relevant to carrier induced frequency chirp and concentrate our focus on an analysis of direct modulation, injection locking and our proposed negative differentiated optical injection locking method.

Using the standard laser rate equation model, we will study how the relaxation oscillation induces a chirp penalty to the device, how injection locking can be used to mitigate the performance degradation of these effects, how negative differentiated optical injection locking would compare to standard injection locking in terms of chirp, distortion, modulation response, stability over injected optical frequency range, Q factor statistics of

the laser source in relation to amplitude phase coupling, and finally, to contrast these result to external modulation techniques.

The reason for including the SHO model is to have a physical model to support the hypothesis of negative differentiated injection locking. We seek to explain why the change in index of refraction is caused by a change of electrical carriers that can be directly countered by an opposite change in optical carrier density, and why this will lead to a optical frequency chirp reduction that will improve the laser source figures of merit.

3.2 MODULATION OF LASER DIODES

In Keiser [8], it was reported that the fundamental limitation on direct carrier injection modulation speed depends on cavity photon lifetime and spontaneous electrical carrier lifetime respectively. Spontaneous carrier lifetime is dependent on semiconductor band structure and carrier concentration and has a radiative lifetime of about 1ns for average dopant concentrations in GaAs type materials. The cavity photon lifetime is the average time it takes a photon to either be emitted or reabsorbed from the cavity and is usually on the order of 2 ps. Therefore, to operate the device the direct modulation duration of the laser must be longer than the relaxation oscillation duration of the lasing field. If we assume a linear dependence of optical gain on carrier density, we can approximate the relaxation oscillation duration as

$$t_r \approx \frac{2\pi\sqrt{\tau_c \tau_{ph}}}{\sqrt{\frac{I}{I_{th}} - 1}}, \tag{3.1}$$

where τ_e is the electron lifetime, τ_{ph} is the photon lifetime, I is current and I_{th} is the threshold current for lasing.

3.3 CAVITY PHOTON LIFETIME

The photon lifetime is a time constant describing the decay of energy in the optical cavity. This process is depicted in Figure 3.1 below:

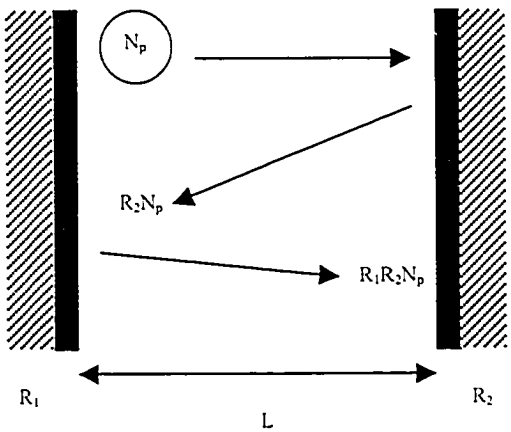

Figure 3.1 Schematic description of photon lifetime mechanism.

Using the analysis presented in [10], assuming we begin with N_p photons, the energy in the cavity will be $N_p h\upsilon$. The number of photons surviving one round trip in the cavity is $N_p R_1 R_2$, where R_1, R_2 represent the reflectivity factor of the cavity walls. Thus, the number of photons lost in one round trip is $[1 - R_1 R_2]N_p$. Taking the limit as the number of photons lost in one round trip divided by the time taken to complete one round trip, we obtain the rate of change of photons in the cavity.

$$\frac{dN_p}{dt} = -\frac{[1 - R_1 R_2]N_p}{\tau_{RT}} \equiv -\frac{N_p}{\tau_{ph}}, \tag{3.2}$$

where, by definition, we have labeled the photon lifetime as τ_{ph}. One solution of the differential equation is obviously,

$$N_p(t) = N_p(0)e^{-\frac{t}{\tau_{ph}}}. \tag{3.3}$$

For the assumed cavity $\tau_{RT} = \frac{2n(\omega)L}{c}$, defined to be the round trip time, where L is the cavity length. One extra point to consider is that we might model a round trip "lossy" transmission through the cavity as $R_1R_2e^{-\eta 2L}$, where η represents and arbitrary loss coefficient. We make this point to illustrate that any process that changes the photon concentration can be incorporated into our model in this fashion.

Later in the thesis, we will contrast our various modulation techniques as a function of their relaxation oscillation durations as described by (3.1), (3.2) and (3.3) thus relating the envelope of the relaxation oscillation to the photon lifetime.

3.4 LINEWIDTH BROADENING

Linewidth describes the spectral spread of a laser about a particular frequency, which is derived largely from its phase fluctuations, which can be divided into phase noise and frequency chirp. Phase noise, has its origins rooted in spontaneous emissions, which change the phase of the lasing field through the gain mechanism of the laser. It was shown, in [18], that spontaneous emissions add new components to the lasing field in the form of a random phase deviation $\theta_i(t)$. Thus field intensity gives rise to, two phase

changes, an instantaneous one $\Delta\phi_i^{'}(t)$ and a delayed phase change. The instantaneous phase change is related through spontaneous emissions is given by

$$\Delta\phi_i^{'}(t)=\frac{\sin(\theta_i(t))}{\sqrt{I}}. \tag{3.4}$$

The phase change after the relaxation oscillation was given to be

$$\Delta\phi_i^{''}(\infty)=-\frac{\alpha\cos(\theta_i(t))}{\sqrt{I}}. \tag{3.5}$$

A more detailed presentation on phase noise is presented in Appendix C. Frequency chirp then is largely the result of an instantaneous adiabatic change in electrical carrier concentration. This change causes the laser to go through relaxation oscillations, which typically last, using direct modulation, on the order of 1ns. According to Henry [19] during the relaxation oscillation there will be a net gain change of

$$\Delta g(t)=\frac{-2\omega\Delta n''(t)}{c}, \tag{3.6}$$

where $n''(t)$, is the imaginary refractive index change during this time. This change is caused by a change in carrier density and will affect the real part of the refractive index $n'(t)$ as well. The ratio of changes in the real and imaginary refractive indices called the linewidth enhancement factor is defined by:

$$\alpha=\frac{\Delta n^{'}}{\Delta n^{''}} \tag{3.7}$$

Henry's formulation of linewidth enhancement factor [19], encapsulates both the effects of changing gain and changing index of refraction. It has been described in [21] that

measuring the coupling between AM and FM noise essentially describes the linewidth enhancement factor of the laser and is given by,

$$\alpha = -2\left(\frac{2\pi}{\lambda_0}\right)\frac{\left(\frac{d\bar{n}}{dn}\right)}{\left(\frac{dg}{dn}\right)}. \tag{3.8}$$

Electron density changes cause changes in phase. Thus ultimately, we find that electron density changes change the photon density, refractive index, and optical output intensity (gain). Since deviations in phase result in variations in frequency dispersion, we can relate the changes in phase to changes in frequency chirp and its evolution by

$$\Delta f(t) = \frac{1}{2\pi}\frac{d(\Delta\phi(t))}{dt} \tag{3.9}$$

where, $\Delta\phi(t)$, represents changes in the laser field phase deviation and , $\Delta f(t)$, is its coupled frequency deviation. Thus linewidth broadening can be computed from the spectral density of the phase given as described in [20], by

$$\Delta f = \frac{1}{4\pi}\frac{\Phi B n_{th}^2}{S_0}\left(1+\alpha^2\right). \tag{3.10}$$

Where S is the photon density, Φ is the spontaneous emission coupling coefficient, B is the radiative recombination coefficient, n is the carrier density and α is the linewidth enhancement factor.

3.5 PHONON-POLARITONS AND LATTICE ABSORPTION, SIMPLE HARMONIC OSCILLATOR MODEL

According to [30], a laser will oscillate at the wavelength at which gain exceeds loss by the largest amount with the consideration of the mode spacing of the cavity. To study this we can employ the plasma equation, the Drude model [14], which relates negative changes to the refractive index of the material caused by the injection of free carriers

$$\Delta n(\omega) = n(\omega) - n_0 = -\frac{\omega_p^2}{n_0 \omega^2} = -\frac{n_c q^2 \lambda^2}{4\pi c^2 n_0 m_c^* \varepsilon_0}, \tag{3.11}$$

where ε_0 is the permittivity of free space, ω_p is the plasma frequency, n_0 is static refractive index and is so labelled to distinguish this quantity from the carrier concentration n. In Figure 3.2, we show the carrier density $n(t)$, for a typical semiconductor laser under standard optical injection locking.

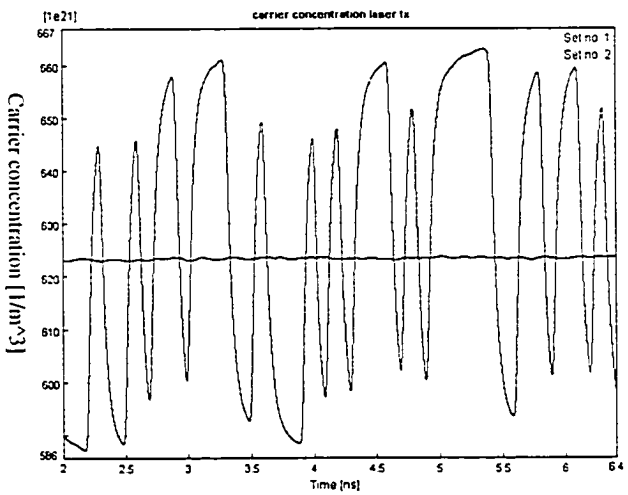

Figure 3.2 VPI simulation of typical electrical carrier concentration in active region of semiconductor laser under standard injection locking.

For quantum well distributed feedback structures two guides have their phase velocities differing by the wave number periodicity of the grating, thereby maximizing the energy between the guides

$$|\beta_2 - \beta_1| = \frac{2\pi}{\Lambda}, \tag{3.12}$$

where $\Lambda = \lambda_B / 2n_{w=0}$ is the mechanical periodicity that maximized the energy interchange between the two guides. Using the definition of the phase constant (see Appendix A)

$$\beta = 2\pi n_{eff} / \lambda_0 . \tag{3.13}$$

We can express the wave number as

$$\lambda_0 = \Lambda \left| n_{2eff} - n_{1eff} \right| . \tag{3.14}$$

We observe that the output wavelength is especially susceptible to the refractive index difference. In this section, we shall present a more detailed development of the Drude plasma model and relate it to our proposed model of negative differentiated injection locking.

From [13] and [14], if we consider phonons that interact with the lattice by way of electromagnetic radiation, we might quantify the dielectric properties of an isotropic medium by quantized simple harmonic oscillators. Consider the applied electrical field

$$\vec{E}(t) = \vec{E}_0 e^{j\omega t}, \tag{3.15}$$

inside the medium. Consider also that the harmonic oscillators are of mass m and charge q and are displaced by a distance x from their equilibrium positions by the application

of the electric field. Thus, the equation of motion can be approximated by the universal equation describing an oscillating system driven by a complex exponential field

$$m\frac{d^2x}{dt^2} - m\eta\frac{dx}{dt} + m\omega_T^2 x = q\bar{E}_0 e^{jwt}, \tag{3.16}$$

where η is the damping constant, and ω_T is the natural vibration frequency. One possible steady state solution is

$$x = x_0 e^{jwt}, \tag{3.17}$$

where substitution back into the differential equation (3.16) yields

$$x_0 = \frac{q\bar{E}_0}{m\left(\omega_T^2 - \omega^2 - j\eta\omega\right)}. \tag{3.18}$$

The displacement of the charges produces a polarization field

$$\bar{P} = Nq\bar{x}, \tag{3.19}$$

where N is the density of simple harmonic oscillators. Finally, relating polarization, displacement vector, electric field and dielectric function, we have

$$\bar{D} = \bar{E} + 4\pi\bar{P} = \varepsilon(\omega)\bar{E}, \tag{3.20}$$

where $\varepsilon(\omega)$ is the dielectric function of the material, and so the complex dielectric function is then expressed by

$$\begin{aligned}\varepsilon(\omega) &= \varepsilon_\infty + \frac{4\pi Nq^2}{m\left(\omega_T^2 - \omega^2 - j\eta\omega\right)} \\ &= \varepsilon_\infty + \frac{\varepsilon_0 - \varepsilon_\infty}{\left[1 - \left(\omega^2/\omega_T^2\right)\right] - j\left(\eta\omega/\omega_T^2\right)} \\ \varepsilon_\infty &: \varepsilon(\omega = \infty) \rightarrow \varepsilon_r \equiv 1 \\ \varepsilon_0 &: \varepsilon(\omega = 0)\end{aligned} \tag{3.21}$$

To express the free carrier contribution to the dielectric function we may proceed along the standard line of following the Drude model. Setting the term for the natural frequency

of the material to zero and appropriately changing the values for the density of oscillators, effective mass of carriers, and the damping coefficient accomplish this. Then it becomes a simple matter to decompose the real and imaginary parts of the dielectric function:

$$\varepsilon(\omega) = \varepsilon_\infty - \frac{4\pi N_c e^2}{m^*\left(\omega^2 + j\omega\gamma_c\right)}, \tag{3.22}$$

$$\varepsilon_r(\omega) = \varepsilon_\infty\left(1 - \frac{\omega_p^2}{\omega^2 + \gamma_c^2}\right), \tag{3.23}$$

$$\varepsilon_i(\omega) = \frac{\varepsilon_\infty \omega_p^2 \gamma_c}{\omega\left(\omega^2 + \gamma_c^2\right)}, \tag{3.24}$$

$$\omega_p^2 = \frac{4\pi N_c e^2}{m^* \varepsilon_\infty}. \tag{3.25}$$

where ω_p is the plasma frequency of the free carriers. Recalling the Lyddane-Sachs-Teller relation [13],

$$\frac{\varepsilon_0}{\varepsilon_\infty} = \frac{\omega_L^2}{\omega_T^2}. \tag{3.26}$$

The values of the constants ω_T, ω_L and γ_c from [15], in these equations are provided in Table 3.1.

Table 3.1 Semiconductor natural, longitudinal frequencies and damping constants for select materials.

Semiconductor	Temperature	ω_T [cm^{-1}]	ω_L [cm^{-1}]	γ_c / ω_T
InP	300	307.2	347.5	0.01
GaAs	296	268.2	291.5	0.007
GaP	300	366.3	401.9	0.003

Finally recalling, the relation between the refractive index and dielectric function

$$n(\omega) = \sqrt{\varepsilon(\omega)}. \tag{3.27}$$

If we neglect the damping constant for the moment using (3.22), (3.25) and (3.27) we obtain the following relationship using the binomial expansion

$$\begin{aligned} n_r(\omega) &= n_0 \frac{\omega_T}{\omega_L}\left(1 - \frac{\omega_p^2}{2\omega^2} + \cdots\right), \\ n_r(\omega) &\approx n_0 \frac{\omega_T}{\omega_L}\left(1 - \frac{\omega_p^2}{2\omega^2}\right), \\ \Delta n_r(\omega) &\approx -n_0 \frac{\omega_T}{\omega_L}\frac{2\pi n q^2}{m^* \varepsilon_\infty \omega^2}. \end{aligned} \tag{3.28}$$

Careful attention must be paid to the distinction between electrical carrier density n and the index of refraction $n(\omega)$, n_0. Equation (3.28) relates the change in refractive index to carrier concentration and electron effective mass. Since refractive index and emission energy are related $hc/n(\omega)\lambda$ we now have a picture of the influence of the carrier concentration on emission wavelength.

Therefore, for an opto-electrical transition, one can use the Drude model to approximate the dielectric function of a material with respect to the electromagnetic field frequency and carrier concentration. For instance, we show in Figure 3.3, the calculated dielectric impact for radiative transitions in gallium arsenide depicting the relationships between emission frequency and refractive index for various carrier concentrations.

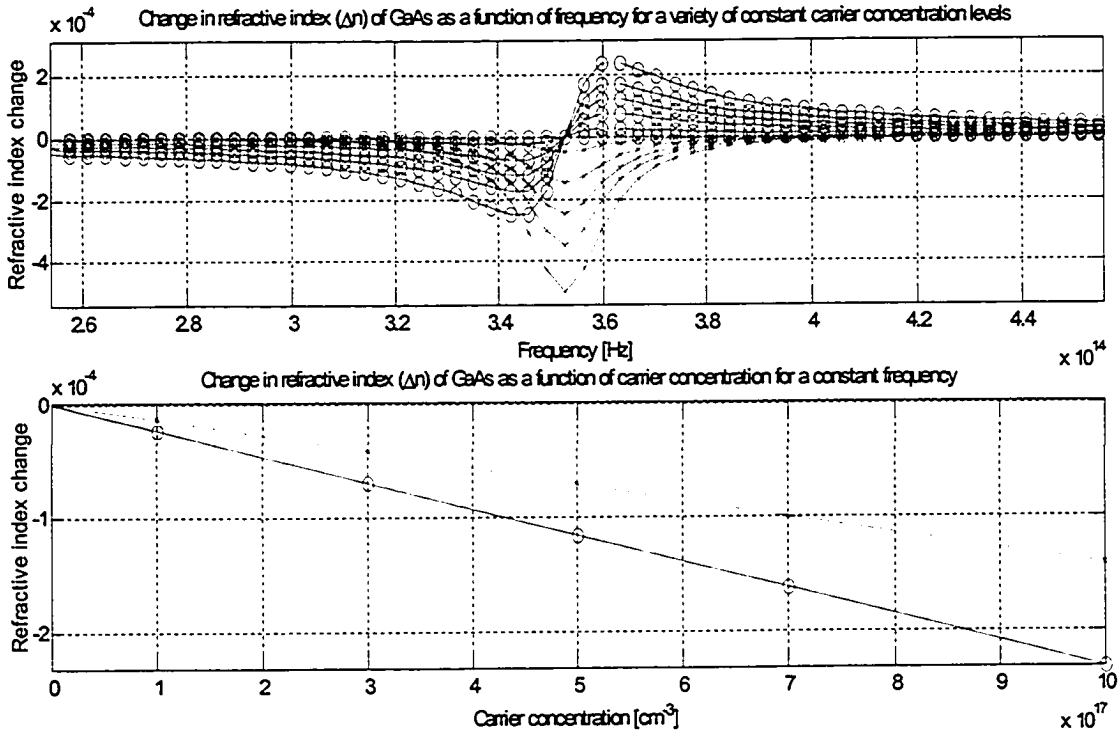

Figure 3.3 Refractive index dependence on emission frequency and carrier density for GaAs.

In the context of the current discussion of optical injection locking this presents an interesting symmetry between absorptive transition and stimulated emission. In the case of injection resulting in an absorptive transition from the valence band to the conduction band, one would expect the dielectric change to be opposite to the above figure, which would lead us to the conclusion that positive differentiated optical injection might counteract the swings in dielectric function due to modulation and thus reduce frequency chirp. However, in the case of stimulated or spontaneous emission electrical transitions occur in the other direction from conduction to valence. Thus the idea of using negative differentiated optical injection is to decrease the frequency chirp of the modulating laser by reducing the relaxation oscillation; this in turn results in minimizing the carrier induced refractive index change during modulation supported by this model.

3.6 CLASSICAL MAXWELL STANDARD RATE EQUATIONS

Semiconductor laser structures by virtue of their greater wavelength selectivity have greatly enhanced the optical telecommunications community. The dynamic properties of the active region in a semiconductor laser can be modeled by well-known rate equations. These equations describe the photon, electron and optical phase evolution of the laser are given in [11] as,

$$\frac{dn}{dt} = \frac{J}{qN_w L_z} - (An + Bn^2 + Cn^3) - \Gamma g c' S, \tag{3.29}$$

$$\frac{dS}{dt} = \Phi B n^2 + \Gamma g c' S - \frac{S}{\tau_{ph}}, \tag{3.30}$$

$$\frac{d\phi}{dt} = \frac{\alpha}{2}\left(\Gamma g c' - \frac{1}{\tau_{ph}}\right), \tag{3.31}$$

where the symbols in these equations are defined in Table 3.2.

Table 3.2 Direct modulation parameter definitions.

Parameter	Definition
J	Injected current density
N_w	Number of quantum-wells
L_z	Quantum-well thickness
A	Nonradiative recombination coefficient
B	Radiative recombination coefficient
C	Auger recombination coefficient
Γ	Optical confinement factor
g	Optical gain
S	Photon density
n	Electron density
Φ	Spontaneous emission coupling coefficient
c'	Speed of light in medium
α	Linewidth enhancement factor
ϕ	Phase

Once a population inversion is achieved within a forward biased semi-conductor stimulated minority carrier recombination can be made to dominate over spontaneous emission and give way to a coherent optical output. Equation (3.29), describes how the injected current relates to spontaneous losses and stimulated emission as a result of changing electron carrier density. Equation (3.30), describes the evolution of the photon density in the active region by spontaneous, stimulated, and absorptive processes. The last term in (3.30) describes light that is lost internally by absorption in the lasing cavity from [11], we have an expected photon lifetime given by

$$\tau_{ph} = \left[\Gamma c' \alpha_{\text{int}} - \frac{c'}{L} \ln(R) \right]^{-1}, \tag{3.32}$$

where Γ is the confinement factor, c' is the speed of light in a medium, L is the cavity length and R is the facet reflectivity. Equation (3.31) describes the evolution of optical phase in relation primarily to the linewidth enhancement factor. By ignoring the number of photons in play we may observe that the change in phase is proportional to the cavity gain minus the internal losses. This amplitude phase coupling forms the basis of our exploration into negative differentiated optical injection locking as a means to minimizing the duration of the relaxation oscillation's impact on gain and to stabilize the optical frequency chirp.

$$g = {}^{dg}\!/_{dn}(n - n_{th}). \tag{3.33}$$

Equation (3.33) refers to the gain function in a semiconductor laser as being a function of electron density, which in turn is a function of injected current. This is an important parameter in relation to how much light will actually escape the cavity. Since electron

density is directly related to phase through equation (3.31) optimizing the amplitude excursion of the relaxation oscillation also helps minimize the correlated phase excursion. This will be a key result in our effort to minimize chirp as it directly relates the mechanism of amplitude phase coupling. These equations model the active layer of the semiconductor under direct modulation of a single mode laser cavity. They will be explored in one form or another throughout the thesis to gain further insight into the laser dynamics of direct modulation.

3.7 Optical injection locking

Adler [48], presented a fundamental theoretical investigation on the injection locking of classical oscillators over half a century ago. Similar to the equations used to explore the dynamics of single cavity semiconductor lasers are the rate equations for an optical injection locking system as presented in [12] by Petitbon.

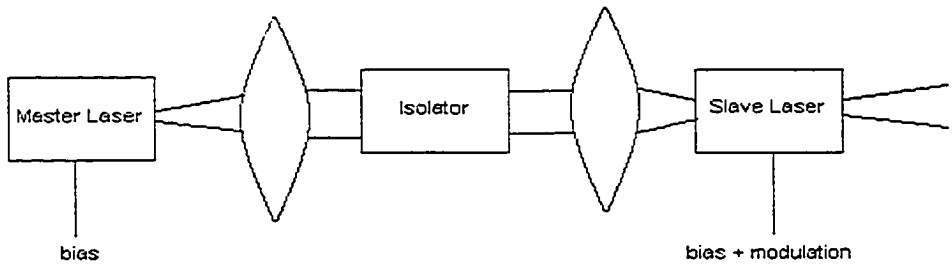

Figure 3.4 Schematic diagram of optical injection modulator.

In this regime, the master laser's optical field is decoupled from the slave laser by an isolator. The purpose of this field is to maintain a coherent lead emission wavelength for

the slave laser over its amplitude modulation range. This greatly improves the frequency stability of the slave laser thanks to the coherent lead of the master laser field. However, the slave laser still remains susceptible to frequency deviation due to dielectric function changes in the active layer caused by electro-optical carrier injection concentration changes due to ever present relaxation oscillations.

$$\dot{N} = \frac{J}{qN_w L_z} - GP - \frac{N}{\tau_e} - BN^2 - CN^3; \tag{3.34}$$

$$\dot{P} = \left[G - \frac{1}{\tau_p} + \Phi BN^2 + \frac{c}{n_g L}\left(\frac{P_i}{P}\right)^{1/2} \cos\theta \right] P; \tag{3.35}$$

$$\dot{\phi} = \left[\omega_{mo} - \omega_0 + \frac{c}{2n_g L}\left(\frac{P_i}{P}\right)^{1/2} \sin\theta + \frac{\alpha}{2}\left(G - \frac{1}{\tau_{ph}} \right) \right], \tag{3.36}$$

where the new symbols in these equations are as defined in Table 3.3.

Table 3.3 Standard injection locking parameter definitions.

Parameter	Definition
dg/dn	Differential gain
N_{th}	Carrier number for transparency
τ_{ph}	Photon lifetime
n_g	Group index of refraction
P	Cavity photons
P_i	Cavity injected photons
θ	Phase difference between injection and free-running laser fields
ω_0	Angular frequency of master laser
ω_{mo}	Angular frequency of free-running laser
τ_c	Spontaneous carrier lifetime
c	Speed of light
G	Optical gain
L	Cavity Length
N	Carrier number
q	Charge of electron

The optical gain G can be modeled by

$$G = \Gamma {}^{dg}\!/_{dn}(N - N_{th}). \tag{3.37}$$

These equations (3.34),(3.35) and (3.36) are identical to those presented for the single diode rate equations. However they are more complete in that they include the effect of injection locking on the dynamics of the active region. In fact, in order to solve the rate equations for standard injection locking it is necessary to solve equations (3.34),(3.35) and (3.36) twice simultaneously, once to establish the operating conditions of the master laser while simultaneously coupling the operation of the master laser to the dynamics of the slave laser operation. For the remainder of this subsection we will investigate two of the fundamental effects of injection locking on the standard rate equations. The first deals with the locking range of the laser pair and establishes under unmodulated conditions the frequency detuning the master laser can support relative to the free running optical frequency of the slave laser and still "lock" to the same frequency when coupled. The second investigates the locking stability under small signal conditions where the locking range is explored over a modulation rate.

3.7.1 INJECTION LOCKING RANGE

The locking range describes the range of frequencies where the unmodulated slave laser will lock to the frequency of the master laser. Proceeding with the analysis of [12], solving and equating the steady state solution for photon number and phase we can express the laser detuning as

$$\Delta\omega = \frac{c}{2n_g}\left(\frac{P_i}{P}\right)^{1/2}(\sin\theta - \alpha\cos\theta). \tag{3.38}$$

Defining $\theta_0 = \tan^{-1}(\alpha)$, we then have using the trigonometric relationship

$$\sin(A-B) = \sin A\cos B - \cos A\sin B, \tag{3.39}$$

$$\begin{aligned}\sin(\theta_0) &= \frac{\alpha}{\sqrt{1+\alpha^2}},\\ \cos(\theta_0) &= \frac{1}{\sqrt{1+\alpha^2}},\end{aligned} \tag{3.40}$$

from which we obtain,

$$\Delta\omega = \frac{c}{2n_g L}\left(\frac{P_i}{P}\right)^{1/2}\sqrt{1+\alpha^2}\,\sin(\theta-\theta_0). \tag{3.41}$$

Consequently, the locking range must be limited to

$$|\Delta\omega| \le \frac{c}{2n_g L}\left(\frac{P_i}{P}\right)^{1/2}\sqrt{1+\alpha^2}\,. \tag{3.42}$$

Another limit must be that the gain of stimulated emission must be greater than the amplification of spontaneous emission or stated another way that the photon lifetime must be longer than the gain process time of the cavity

$$\frac{1}{G} < \tau_{ph}\,. \tag{3.43}$$

This means that in our steady state solution,

$$G - \frac{1}{\tau_{ph}} = -\frac{c}{n_g L}\left(\frac{P_i}{P}\right)^{1/2}\cos\theta_0. \tag{3.44}$$

Both LHS and RHS must remain negative. Consequently, the limitation is $|\theta| < \frac{\pi}{2}$ which puts us in the situation of re-expressing the detuning range as

$$\Delta\omega = \frac{c}{2n_g L}\left(\frac{P_i}{P}\right)^{1/2}\left(\sqrt{1-\cos^2(\theta)} - \cos(\theta)\tan(\theta_0)\right). \tag{3.45}$$

Maximizing this quantity yields $|\theta| = \frac{\pi}{2}$ which bounds the locking range by

$$-\frac{c}{2n_g L}\left(\frac{P_i}{P}\right)^{1/2}\sqrt{1+\alpha^2} < \Delta\omega < \frac{c}{2n_g L}\left(\frac{P_i}{P}\right)^{1/2}. \tag{3.46}$$

The locking range is asymmetric due to the phase amplitude coupling and favours theoretically negative master laser optical frequency detuning with respect to the optical frequency of the free running slave laser.

3.7.2 INJECTION LOCKING STABILITY

A laser is stable if after some time it returns to its original operating point after a slight perturbation. One method of examining the stability of our system is to linearize the rate equations by:

$$\begin{bmatrix} \frac{d\Delta P}{dt} \\ \frac{d\Delta\theta}{dt} \\ \frac{d\Delta N}{dt} \end{bmatrix} = \begin{bmatrix} \frac{\partial}{\partial P}\dot{P} & \frac{\partial}{\partial\theta}\dot{P} & \frac{\partial}{\partial N}\dot{P} \\ \frac{\partial}{\partial P}\dot{\theta} & \frac{\partial}{\partial\theta}\dot{\theta} & \frac{\partial}{\partial N}\dot{\theta} \\ \frac{\partial}{\partial P}\dot{N} & \frac{\partial}{\partial\theta}\dot{N} & \frac{\partial}{\partial N}\dot{N} \end{bmatrix} \begin{bmatrix} \Delta P \\ \Delta\theta \\ \Delta N \end{bmatrix}, \tag{3.47}$$

yielding,

$$\begin{bmatrix} \frac{d\Delta P}{dt} \\ \frac{d\Delta\theta}{dt} \\ \frac{d\Delta N}{dt} \end{bmatrix} = \begin{bmatrix} \rho\cos\theta & -2\rho P\sin\theta & A\Gamma P \\ \frac{-\rho\sin\theta}{2P} & \rho\cos\theta & \frac{\alpha A\Gamma}{2} \\ \left(2\cos\theta - 1/\tau_{ph}h\right) & 0 & -\left(1/\tau_e - A\Gamma P\right) \end{bmatrix} \begin{bmatrix} \Delta P \\ \Delta\theta \\ \Delta N \end{bmatrix}, \tag{3.48}$$

where $\rho = (c/2n_g L)\sqrt{P_i/P}$ .Under usual experimental conditions and weak injection ($P_i/P < 10^{-3}$), the system reduces to the results given in [12] as:

$$(1/\tau_c + \Gamma AP) > \rho(\alpha \sin\theta - \cos\theta), \tag{3.49}$$

which implies that for low injection rates where $\rho < (1/\tau_c + \Gamma AP)\sqrt{1+\alpha^2}$,for the laser to remain unconditionally stable.

3.8 NEGATIVE DIFFERENTIATED INJECTION LOCKING

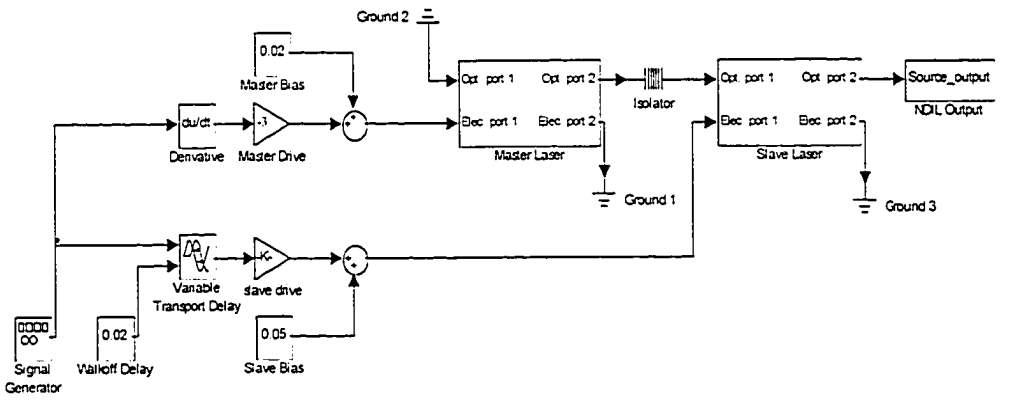

Figure 3.5 Block diagram of negative differentiated injection locking modulator (NDIL).

Figure 3.5, depicts a more detailed description of our negative differentiated injection locking model. Unlike standard injection locking however both the master and slave laser fields are modulated. This is accomplished via both the traditional mechanisms of bias and scaling as well as a new mechanism of delay and differentiation to compensate for optical frequency chirping effects upon modulation of the slave laser.

Though the mechanism of negative differentiated injection locking is generic our particular characterization in this thesis is based on a binary modulation. The modulation rise and fall characteristics are controlled via modelling the signal by a time domain raised cosine pulse train. This modulation format greatly resembles the conventional signalling in DWDM binary networks. The model of this signal in MATLAB is presented in Appendix D. Solving the large signal model rate equations (3.34),(3.35) and (3.36) is generally studied using numerical simulations. Our simulations in MATLAB and VPI allow us to investigate the electro-optical properties and performances of the model while optimizing control parameters such as gain, bias and delay of electrical input signals to the master and slave lasers. In the MATLAB model the input signal is modeled by a time domain raised cosine whose pulse shape is given by

$$X_{RC}(t)=\eta\begin{cases}T_b & 0\le|t|\le\dfrac{1-\zeta}{2T_b}\\ \dfrac{T_b}{2}\left(1+\cos\left[\dfrac{\pi T_b}{\zeta}\left(|t|-\dfrac{1-\zeta}{2T_b}\right)\right]\right) & \dfrac{1-\zeta}{2T_b}\le|t|\le\dfrac{1+\zeta}{2T_b}\\ 0 & |t|\ge\dfrac{1+\zeta}{2T_b}\end{cases}, \qquad (3.50)$$

where ζ is the roll off factor, η is an arbitrary scaling constant and T_b is the bit period. We must also note that in our simulation models we have assumed a perfect ideal isolator.

The rate equations defining negative differentiated injection locking are identical to those that describe standard injection locking. The master laser however is distinct from the standard case in that it is both biased and modulated. The modulated signal is a delayed scaled derivative of the slave laser modulation stream. The purpose of this is to mitigate

the refractive index shifts in the slave laser that coincide with electrical carrier concentration injection as detailed in the section using the simple harmonic oscillator model. Essentially looking at equations (3.34), (3.35) and (3.36), we recognize that the relaxation oscillation of the slave laser links to a birth-death process between the photon and electron densities in the active region of the slave laser. Modulated optical injection provides a means of controlling the evolution of this relaxation oscillation and thus provides a means of further controlling the frequency deviation of the slave laser due to refractive index changes; possibly beyond what is currently achievable using standard injection locking. Also, this method circumvents the effects of parasitic capacitance that prevent us from using direct electric pre-distortion near the resonant frequency of the cavity.

3.9 SEMICONDUCTOR LASER SIMULATION MODELS

To verify, at least from a theoretical perspective, the premise of this thesis we shall explore two numerical simulation models to verify the hypothesis we formulated based upon the SHO model. As explained in the previous section we have chosen a binary modulation format that is consistent with current DWDM transmission systems. The reason we have chosen to study a binary modulation format is because it is exceptionally susceptible to chirp induced relaxation oscillations.

The first numerical simulation we designed to study negative differentiated injection locking is a modification to the standard injection locking model, (3.34), (3.35) and

(3.36), where the master laser field is modified from a strictly biasing condition to a modulating one using our time domain raised cosine modulation as a base electrical input signal. The MATLAB code we have written (see Appendix D.2) to model this system was solved using standard Runge-Kutta numerical methods and optimized over the parameters of bias, drive and delay. We also wrote code to analyze some of the salient performance characteristics we are interested in investigating and optimizing. These codes include the following: source Q factor estimation, optical frequency chirp, modulation response, relaxation oscillation duration, optical power spectral density, optical frequency chirp-power index, electro-optical distortion analysis, slave laser optical stability analysis, dielectric function analysis, carrier evolution and various optimization codes.

The second set of numerical simulations, used to verify our theoretical negative differentiated injection locking model, was constructed using the active photonics, photonics and signal processing modules of the Virtual Photonics simulation software package. The core functionality of this piece of software is very similar to the MATLAB Simulink environment. What was of particular interest was the transmission line modeling of the MQW DFB laser. Both simulations were used to model the laser dynamics under negative differentiated optical injection locking.

Our first simulation uses a time driven variation of the raised cosine modulation waveform (see Appendix D.2) to simulate the variable rise and fall time of a given modulator. This waveform, once differentiated, is also used as an input to the master laser

modulator where the signal is scaled in terms of injection depth, delayed and optimized for a source Q factor estimate constraint. The Q factor estimates are based upon the knowledge of amplitude phase coupling influence on adiabatic and transient chirp. We have written such a statistic estimator and optimization code in MATLAB as well as routines to measure a variety of other figures of merit.

We must also note that we attempted to use the internal VPI language estimators of these quantities but unfortunately discovered a critical error in the software, which produced results that were inconsistent in the frequency responses of the simulations. The VPI model performs a transmission line spectral analysis on the interaction inside or between connected components as displayed in Figure 3.6. This model has a more complete control over the parameters and responses of individual components but lacks some of the functionality, user language interface, and complexity of analysis provided by the MATLAB language environment. Also as mentioned we discovered a design error in the VPI simulation language that favored the development and analysis of the MATLAB simulations. For these reasons the performance characteristics estimators of the optical output signal were implemented in MATLAB. Both models however present cogent results with respect to the analysis of direct modulation and optical injection locking mechanisms. However the VPI model, could not be optimized in the same manner as the MATLAB model could; consequently, we have made a much greater effort in the development of the MATLAB codes.

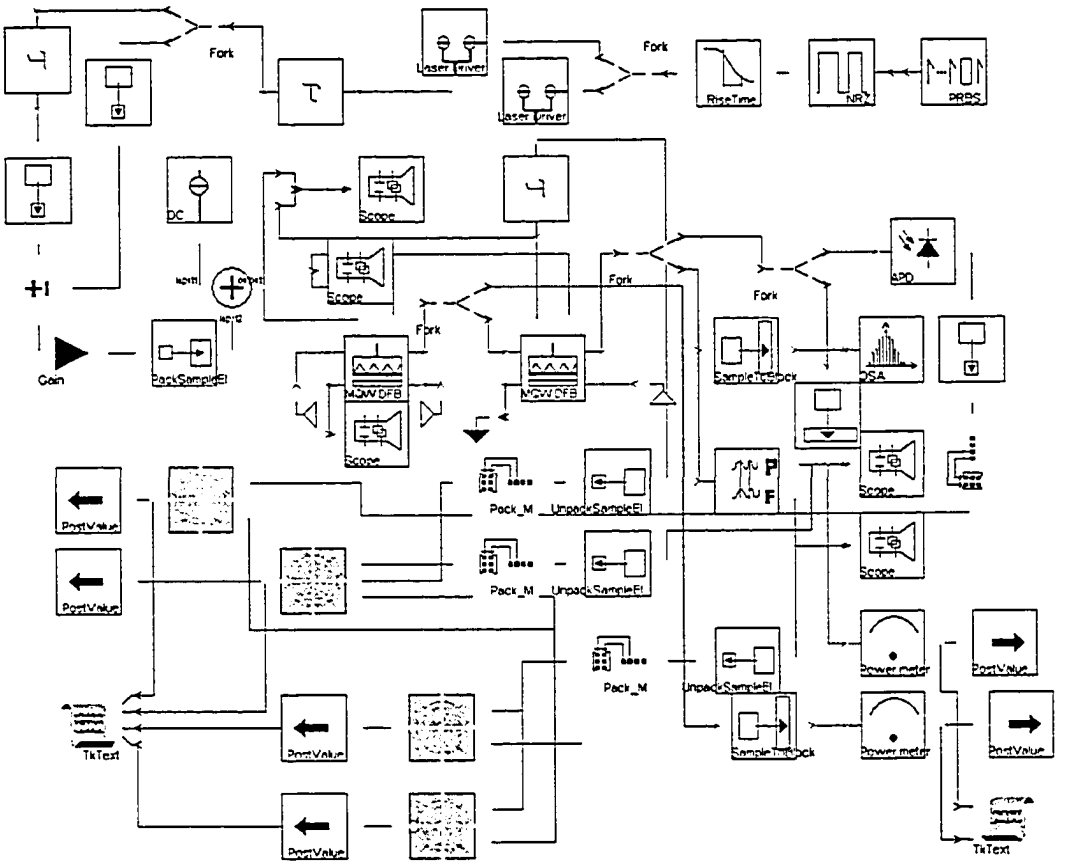

Figure 3.6 Schematic of VPI simulation model of negative differentiated injection locking.

In Figure 3.6, we depict the VPI model used to investigate our proposed modulator. This schematic model displays the modulation, differentiation circuit, laser structure and analysis functions used to probe the device's performance. In the top right quadrant of Figure 3.6 we observe the pseudo random bit source feeding into a non return to zero modulation formatting block which is fed into a rise/fall time pulse shaping block. The signal at this point is branched off into two paths. The first path is conditioned in terms of bias, gain, delayed and then fed into the slave laser MQW DFB block as an electrical input. The second path is numerically differentiated conditioned in terms of bias, gain, delayed and then fed into the master laser MQW DFB block as an electrical input. Both

master and slave laser blocks are then optically coupled using a perfect ideal isolator. The optical output signal of the slave laser is then presented to a number of analysis blocks which monitor power, frequency and convert the signal into text output for further signal processing. Simulation results and interpretations are presented in Chapter 4.

3.10 SUMMARY

In this chapter we reviewed the theory behind semiconductor laser modulation dynamics. We began by developing a model for cavity photon lifetime and related it to the duration of the envelope of the relaxation oscillation. We then defined the linewidth enhancement factor and related it to the changes in real and imaginary refractive index changes. Tying these concepts together using the simple harmonic oscillator model, we related changes in carrier density, refractive index and emission wavelength excursion in the form of transient frequency chirp. We then explored the fundamental rate equations for a generic semiconductor laser followed by one under standard optical injection locking and related the effect of amplitude phase coupling on frequency chirp, optical locking bandwidth and the stability of the slave laser optical output for our proposed negative differentiated injection locking mechanism. We then presented under the conditions of large scale binary signal modulation the salient parameters of the MATLAB simulation. Having examined the MATLAB simulation model we discussed the equivalent VPI simulation and reported on the structure and discoveries we made using this software. In Chapter 4, we will review and analyse the results of these simulations.

4. SIMULATION PARAMETERS AND RESULTS

4.1 MOTIVATION

In this chapter we review the results of simulation comparisons among direct modulation, standard injection locking, negative differentiated injection locking in terms of relaxation oscillation duration, optical frequency chirp, source Q factor estimates, power spectral density, master laser optical frequency detuning, chip-power index, constrained modulation response, and constrained slave laser electro-optic distortion. Also, we present the typical performance of Mach-Zehnder and electro-absorption modulators as a framework to our discussion on modulation compromises engineered to meet user demand. Finally we must note that because of the variable step differential equation solver used in MATLAB to solve the rate equations our MATLAB simulations lack Langevin noise source influences; however this might be resolved in future work by using a fixed step solver.

4.2 RELAXATION OSCILLATION DURATION

The relaxation oscillation is a transient response caused, typically, by current swings in direct modulation. As the electron density increases, physical loss mechanisms come into play such as nonradiative recombination and spontaneous emission. However, stimulated radiative recombination, in the instances just after current onset drive the electron concentration back down, possibly below the lasing threshold concentration. Such a

system will then try to equilibrate itself reaching towards either a steady state or unstable evolution of photon and electron decay rates.

It was believed, prior to 1983, that the spectrum of single mode semiconductor lasers would be consistent with the Lorentzian shape developed in gas laser theory. Flemming and Mooradian [17], found single mode AlGaAs lasers to have a Lorentzian spectrum width inversely proportional to their drive intensity but 30 times larger than can be explained by the corrected Schawlow-Townes formulae. More detailed studies [16], of the spectrum have turned up a substructure line shape equally spaced in resonance with the relaxation oscillation frequency of the laser; it was shown this enhanced linewidth is due to refractive index changes occurring as a result of relaxation oscillations.

The derivative of phase variation due to the relaxation oscillation is equal to the shift of the cavity resonance angular frequency caused by carrier density changes. Since the carrier density undergoes damped forced oscillations, it is reasonable to model it proportionately along classical differential equation lines as $e^{-\eta t}\sin(\Omega t)$ where Ω is the angular frequency and η is the damping rate. Also, according to Henry [16], the integration of our carrier density is proportional to the time fluctuation function of the delayed phase changes and is related by:

$$f(t) = 1 - e^{-\eta t}\frac{\sqrt{\Omega^2 + \eta^2}\cos(\Omega t - \delta)}{\Omega}, \tag{4.1}$$

where,

$$\cos(\delta) = \frac{\Omega}{\sqrt{\Omega^2 + \eta^2}}. \tag{4.2}$$

Thus the total phase change over a time $[0,t]$ is given by

$$\Delta\phi = \sum_i \frac{\sin(\theta_i)}{\sqrt{I}} - \sum_i \frac{\alpha\cos(\theta_i)}{\sqrt{I}}[f(t-t_i) - f(0-t_i)], \tag{4.3}$$

and the mean square value of this phase change is given by

$$\left\langle \Delta\phi^2(t) \right\rangle = \frac{R'}{2I}\left\{(1+\alpha^2)t - \alpha^2\left[\frac{e^{-\eta t}\cos(\Omega t - 3\delta) - \cos(3\delta)}{2\eta\cos(\delta)}\right]\right\}, \tag{4.4}$$

where R' is the average spontaneous emission rate. Expanding in powers of t the delayed phase change due to the relaxation oscillations can be expressed as

$$\left\langle \Delta\phi^2(t) \right\rangle = \frac{R'}{2I}\left[t + \alpha^2\frac{(\Omega^2-\eta^2)}{2\eta}t^2\right] + \text{higher order terms.} \tag{4.5}$$

The first term is an adiabatic chirp and is due to instantaneous amplitude change. The second term is due to transient chirp resulting from relaxation oscillations following from amplitude phase coupling as a result of the instantaneous amplitude change. The salient features pertinent to our discussion can be summarized as follows. Electron density increases with current injection. Electron density decreases with radiative and non-radiative recombination. Photon density increases with radiative and non-radiative recombination. Photon density decreases with photon lifetime. The key result of these features in terms of the relaxation oscillation is that they are dependent essentially on two parameters f_0 and f_d. The parameter f_0 results from the birth-death concentration equalization process between electro-optic carriers and is directly related to the electron and photon lifetimes in the cavity. The parameter f_d is the damping frequency and is related to the photon lifetime and dielectric function. In [21], under the condition of small signal analysis, the following equations describe in more detail these relationships:

$$f_0 = \frac{1}{2\pi\sqrt{\tau_n \tau_{ph}}},$$
$$f_d = \frac{\varepsilon S}{2\pi\tau_{ph}}. \tag{4.6}$$
$$f_p^2 = f_0^2 - \frac{f_d^2}{4},$$

where f_p is the relaxation oscillation gain peak frequency. In (3.1), we observed that the relaxation oscillation gain peak frequency is also dependent on the square root of the bias current. However, according to [31], increasing the bias current degrades the maximum possible extinction as expressed by (4.14). Thus, in theory, it would be advantageous to devise a modulation technology that addresses the relaxation oscillation of a laser without changing the biasing levels, as we have attempted to do by negative differentiated injection locking.

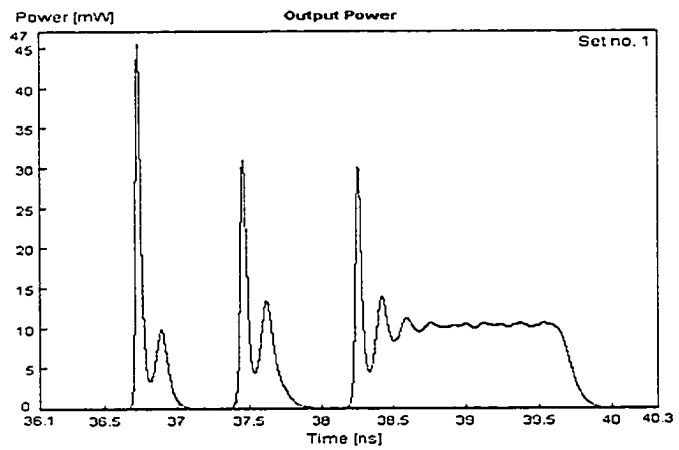

Figure 4.1 Output power of direct modulation.

Figure 4.1 and Figure 4.2 illustrate the relaxation oscillation of a directly modulated semiconductor laser. These oscillations are electro-optically coupled with a Markovian birth-death process [45]. These oscillations are the result of the interplay between the electro-optic re-balancing of carriers. Figure 4.1, depicts the laser optical output power

and details its relaxation oscillation, whereas Figure 4.2 details the coupled relaxation oscillation experienced by the electrical carrier population over time.

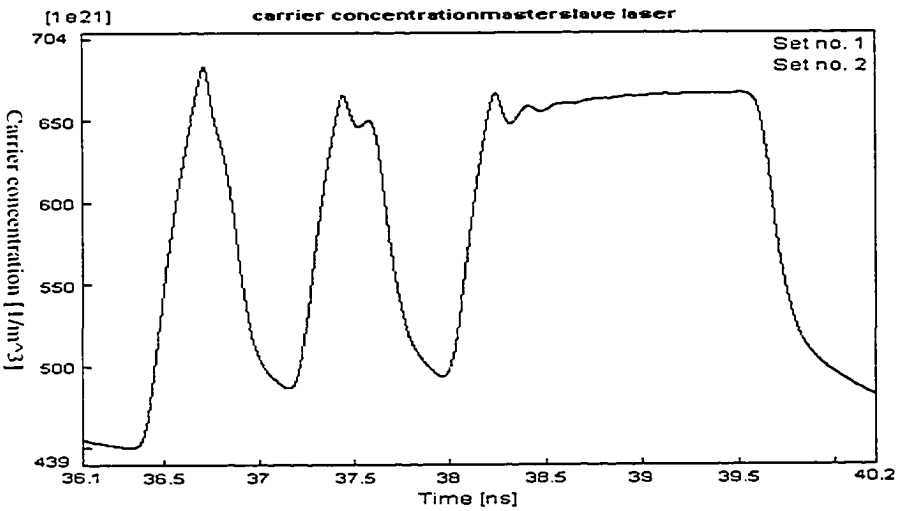

Figure 4.2 Carrier concentration of direct modulation.

Figure 4.3, contrasts the computed relaxation oscillation duration with respect to standard injection locking and negative differentiated injection locking using identical common biasing parameters similar to those presented in Appendix D. In general, for modulation rates where the relaxation oscillation is appreciable, not critically damped, we note that negative differentiated injection locking outperformed standard injection locking over similar physical biasing contexts. Specifically, at a constant master laser injection level of 0.6, we note that both the relaxation oscillation duration offsets of, 0.01 vs. 0.03, and exponential slopes of, 0.26 vs. 0.25, of the data fitting, for a standard best fit analysis, parameters show superior performance for negative differentiated injection locking than for standard injection locking for the four simulated transmission rates. This clear advantage is carried over to the higher injection level of 0.8 where the model of our best-fit approach changes from an exponential to a linear model. The fit parameters for NDIL

relaxation oscillation duration of, offset 0.21 and slope –0.08, again out perform those of SIL, offset 0.22 and slope –0.07. Going beyond these injection levels, and modulation rates revealed that the relaxation oscillations are either critically damped or insignificant in terms of oscillation strength. A situation which might be addressable by extending the injection duration and thus changing the modulation design. This has not been investigated yet within the scope of our current research.

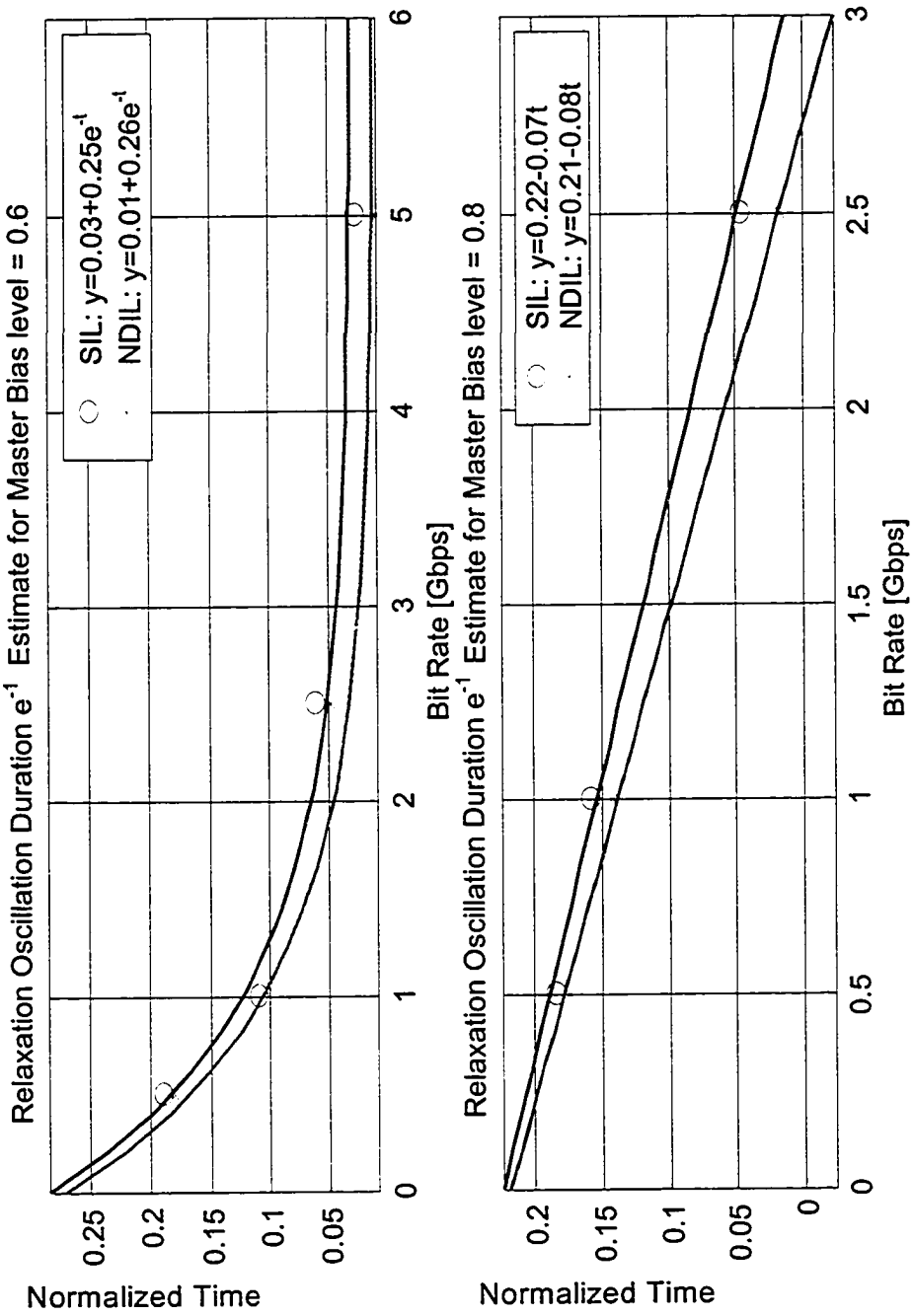

Figure 4.3 Comparison of relaxation oscillation durations between NDIL and SIL.

4.3 OPTICAL FREQUENCY CHIRP

The injection current of direct modulation leads to a linewidth broadening of a laser's optical output spectrum. This broadening is a frequency chirp associated with carrier density changes influencing the refractive index of the active layer of a semiconductor directly modulated laser. This effect can be decomposed into two essential features, adiabatic and transient chirp. Adiabatic chirp is a direct result of the sudden change in electrical carrier concentration in the active layer as a result of direct modulation applying a sudden "pressure" to the material "volume" and precipitating a rapid change in emission frequency. Transient chirp is a result of the relaxation oscillation and results in a variation in the refractive index that oscillates proportionally to the electro-optical carrier population interplay. In a DWDM network, laser chirp may push a signal outside the receiver's passband representing a significant loss to channel passband utilization appearing as cross talk in adjacent channels or carrying signal power away from dispersion compensation devices. To a reasonable approximation the extent of time dependant frequency chirp can be expressed according to Keiser [9] by,

$$\Delta f = \frac{-\alpha}{4\pi}\left[\frac{d}{dt}\ln(S(t)) + \eta S(t)\right] \tag{4.7}$$

where η is an arbitrary scaling factor. One can increase the bias level of the electrical drive of a laser to reduce frequency chirp. However, this occurs typically at the cost of a lower extinction ratio which usually imposes a significant system penalty by reducing the signal to background noise ratio. This is one situation where negative differentiated injection locking clearly attempts to reduce chirp while preserving the extinction ratio without increasing the bias level.

The second derivative of the phase response is usually called the frequency dispersion and it describes the change in instantaneous frequency of a signal. This is given by

$$\Delta f(t)=\frac{1}{2\pi}\frac{d(\Delta\phi)}{dt}. \tag{4.8}$$

Phase and chirp are related through their derivatives. As such, if the linewidth enhancement factor was zero the only contribution to phase deviation would come from the Langevin phase noise. From texts [22],[23],[25], chirp is essentially defined under laser modulation such that the previous small signal analysis, discussed in Sections 3.7.1 and 3.7.2 , may not always be applicable. However, taking the approach of [25], as current density deviations must now be non zero, one can model the Fourier representation of the injection current by

$$\Delta\tilde{I}(\omega)=\int_{-\infty}^{+\infty}\Delta I(t)\cdot e^{-j\omega t}dt\,, \tag{4.9}$$

and the noise-driven frequency domain rate equations can be used to determine the phase variation, resulting in the expressions

$$\begin{aligned}\Gamma_S &= \frac{\Phi B n_{th}^2}{S_0}-\frac{dg}{dS}S_0\\ \Gamma_N &= 2\Phi B n_{th}+\frac{dg}{dS}\Gamma c' S_0\,,\\ \Gamma_R &= (\Gamma_N+\Gamma_S)/2\end{aligned} \tag{4.10}$$

$$\Omega_R=\sqrt{\Gamma c'\left(g+\frac{dg}{dS}S_0\right)\left(\Gamma c'\frac{dg}{dn}S_0+2\Phi B n_{th}\right)-\Gamma_R^2}\,, \tag{4.11}$$

$$\Delta\tilde{\phi}(\omega)=-\frac{\alpha\frac{dg}{dn}\delta\tilde{I}(\omega)(\omega-j\Gamma_S)}{2q\omega[\omega-(\Omega_R+j\Gamma_R)][\omega-(-\Omega_R+j\Gamma_R)]}. \tag{4.12}$$

Knowing that a multiplication by $j\omega$ in the Fourier domain corresponds to differentiation in time we can express chirp using (4.8), (4.12) as

$$\Delta f(t)=\int_{-\infty}^{\infty}\left\{\frac{\frac{1}{(2\pi)^2}\alpha\frac{dg}{dn}\delta\tilde{I}(\omega)(\omega-j\Gamma_S)}{2jq[\omega-(\Omega_R+j\Gamma_R)][\omega-(-\Omega_R+j\Gamma_R)]}\right\}e^{j\omega t}d\omega. \tag{4.13}$$

In [24], when chirp is small, the eye diagram closure can be approximated by,

$$\Theta=\left(\frac{4}{3}\pi^2-8\right)t_{chirp}DLB^2\delta\lambda\left[1+\frac{2}{3}\left(DL\delta\lambda-t_{chirp}\right)\right], \tag{4.14}$$

where D is the fiber dispersion, L is the fiber length and $\delta\lambda$ the chirp induced wavelength excursion, and the power penalty for an APD system can be estimated as

$$p_{chirp}=10\frac{x+2}{x+1}\log(1-\Theta). \tag{4.15}$$

Even single mode lasers [27], exhibit chirping by as much as 1nm when they are directly modulated. These observations of chirp are consistent with the relaxation oscillations of carrier density. The reduction in index of refraction is paramount to a reduction in the optical path length of the cavity. The turn off characteristics result in the opposite effect, an increase in the output frequency of the laser. Restating the simple model for the duration of the excursion of carrier density during the relaxation oscillation given by [28],

$$t_{chirp}\approx 2\pi\left[\frac{1}{\tau_s\tau_{ph}}\left(\frac{J}{J_{th}}-1\right)\right]^{-1/2}. \tag{4.16}$$

The fraction of energy contained in the chirp is related to the bit rate and is given as $2t_{chirp}B$. When coupled with a dispersive fiber D (ns/km*nm), we will get temporal diffusion with blue shifted wavelength arriving at earlier times and red shifted

wavelength arriving later. All the chirped power will escape the bit interval when $LD = t_{chirp} / \Delta\lambda$. The resulting power penalty assuming the remaining power is the difference between the powers in and out of the bit period is given by

$$P(dB) = -10\log(1 - 4LDB\Delta\lambda) \text{ for } LD < {}^{t_c}/_{\Delta\lambda} \tag{4.17}$$

Therefore, the less energy confined in the fraction $2t_{chirp}B$ the less sensitive the laser will be to the effects of cross talk, receiver passband range and channel passband utilization.

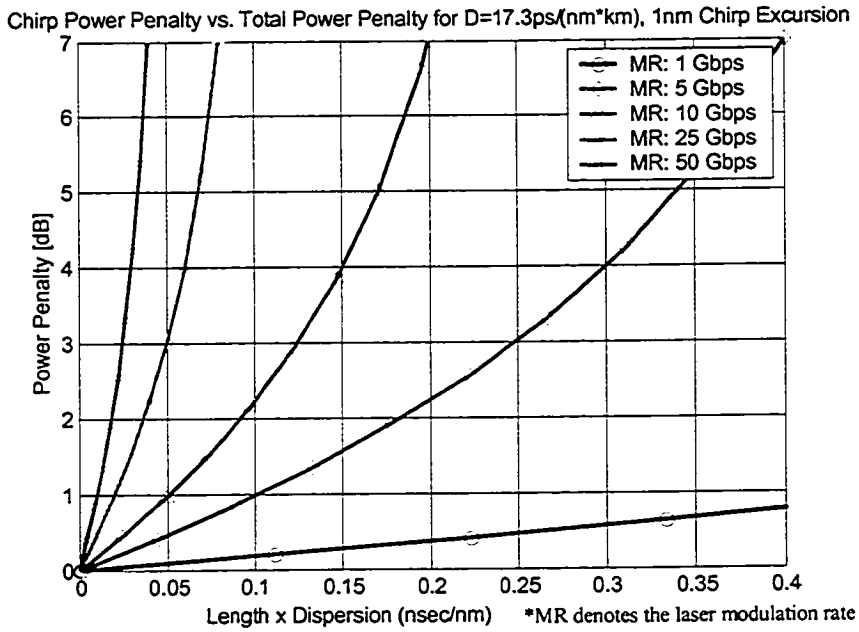

Figure 4.4 Chirp bandwidth power penalty vs. dispersion.

Figure 4.4 depicts a typical chirp bandwidth power penalty for a frequency excursion of 1 nm over a single mode fiber with dispersion 17.3 $ps/(nm \cdot km)$. Clearly increasing the modulation rate exponentially increases the chirp penalty.

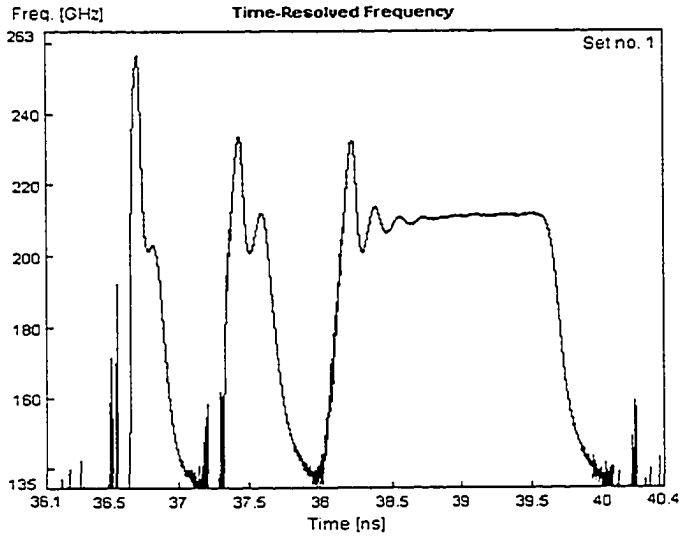

Figure 4.5 Chirp simulation of direct modulation from VPI.

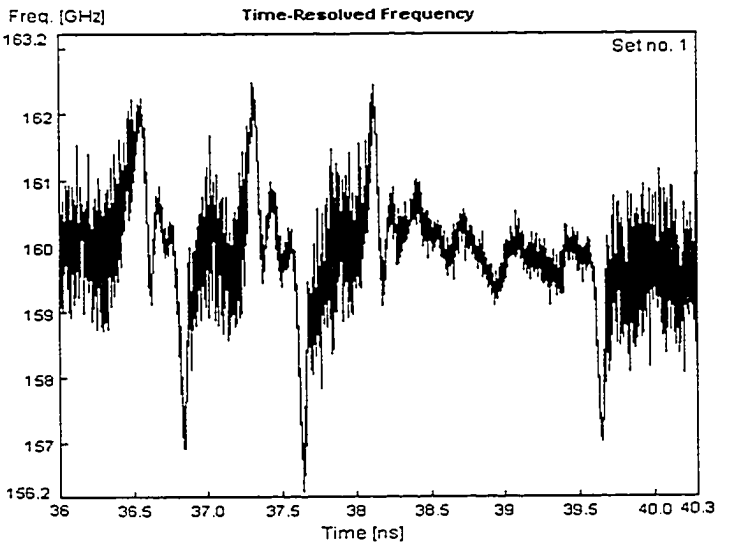

Figure 4.6 Chirp simulation of standard injection locking from VPI.

In Figure 4.5 and Figure 4.6 we observe the degree of chirp for direct modulation and standard injection locking respectively in the context of the VPI software simulation model. We observe a significant improvement on the frequency stability of the slave laser due to the master field in standard injection locking. However, with standard injection locking we also clearly observe the effects of adiabatic and transient chirp.

The next three diagrams, Figure 4.7, Figure 4.8, and Figure 4.9 depict the optimized chirp responses of direct modulation, standard injection locking, and negative differentiated injection locking respectively under the conditions described in the MATLAB chirp parameters of Appendix D and identical common biasing conditions. We clearly observe a distinct improvement under these conditions from direct modulation, standard injection locking toward negative differentiated injection locking in both adiabatic and transient chirp response.

Figure 4.7 shows the normalized chirp of a directly modulated laser and exhibits the greatest normalized frequency excursion $\Delta f > 40$; however, magnitude aside, another point to note is that the relaxation oscillation excursion is relatively unconfined, meaning that the energy of the signal is spread out over a large frequency range. Figure 4.8 shows the normalized chirp for standard injection locking. The normalized frequency excursion of the relaxation oscillation in this instance is greatly reduced $\Delta f < 10$ and though the excursion is more controlled it is still largely unconfined over this frequency span. Figure 4.9 depicts the normalized chirp for negative differentiated injection locking. This modulation shows the smallest relaxation oscillation frequency excursion $\Delta f < 6$ and reflects the most confined excursion range of ± 1. This indicates that the power is largely confined to a narrow frequency span and thus would be less sensitive to the previously mentioned system penalty effects of chromatic dispersion, cross talk interference and poor channel energy confinement.

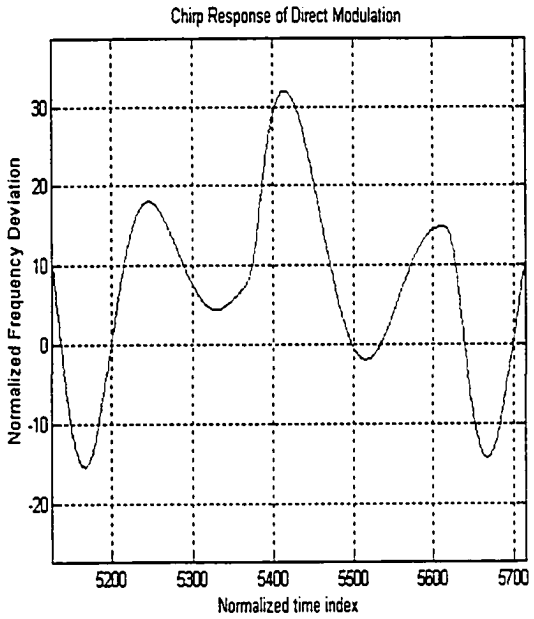

Figure 4.7 Chirp response of semiconductor laser under direct modulation.

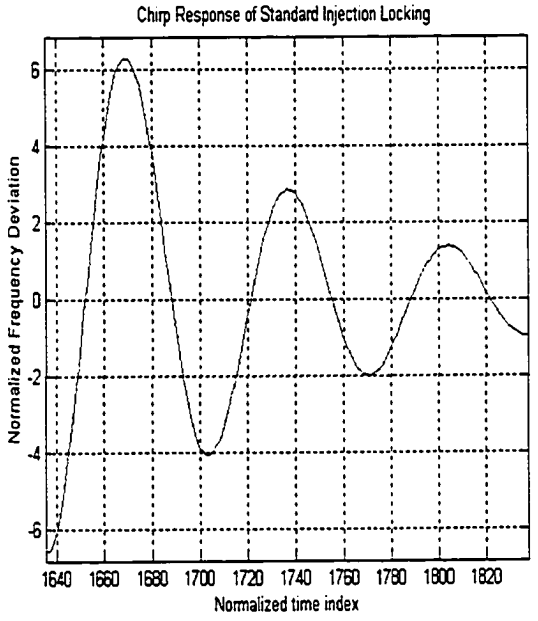

Figure 4.8 Chirp response of a semiconductor under standard injection locking conditions.

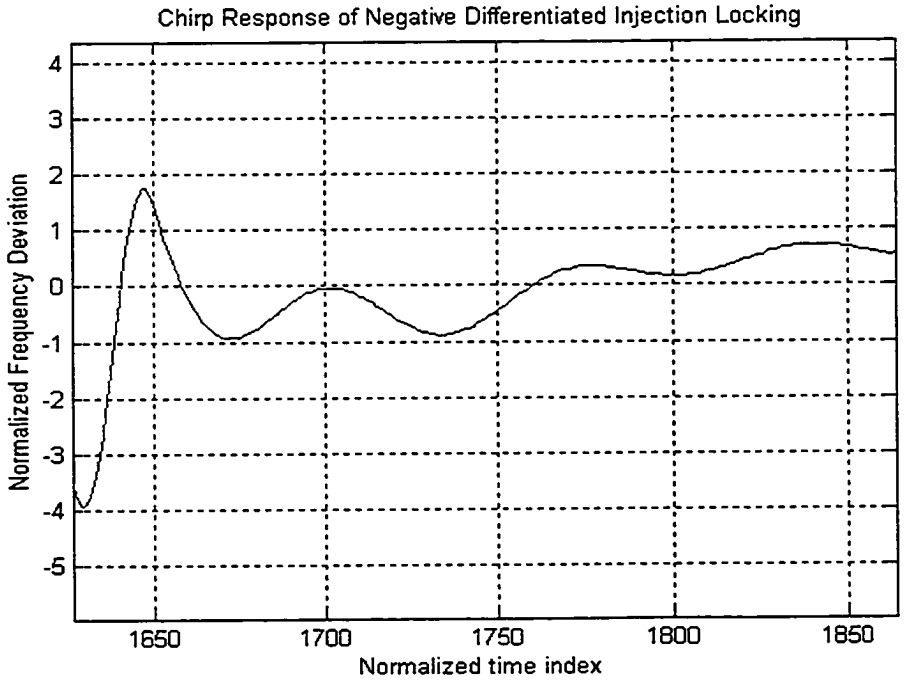

Figure 4.9 Chirp response of semiconductor laser under negative differentiated injection locking conditions.

From these computations we conclude frequency stability can be greatly enhanced using negatively differentiated optical injection locking for conditions where relaxation oscillation effects are significant.

4.4 SOURCE Q FACTOR ESTIMATES

There exist many ways of estimating the bit error rate (BER) of an arbitrary binary signal based on threshold detection. The most obvious [29], is to divide the number of errors Ne by the number of transmitted bits Nt over a sufficiently long sequence:

$$BER = \frac{Ne}{Nt}. \tag{4.18}$$

Since the error rate is dependent on the signal to noise ratio, knowing the probability distribution of the signalling levels about a decision threshold would allow us to calculate the BER based upon signal statistics without resorting to bit counting. However in general, the probability distribution function of the signal is unknown due to the interaction of different distorting noise forces. The most common approach is then to assume the noise perturbing the signal level has a Gaussian probability distribution function. Under this assumption, the probability that the signal falls into the range s to $s + ds$ is given by

$$f(s)ds = \frac{1}{\sqrt{2\pi\sigma^2}} e^{-(s-m)^2/2\sigma^2} ds. \tag{4.19}$$

where $f(s)$ is the assumed Gaussian probability distribution function and σ is the noise standard deviation. Using such a probability distribution function we can estimate the

error rate of the signal. For instance, the probability the noise will exceed the threshold decision voltage v_{th} and be mistaken for the opposite signalling level is given by

$$\begin{aligned} P_0(v_{th}) &= \int_{v_{th}}^{\infty} p(y|0)dy = \int_{v_{th}}^{\infty} f_0(y)dy \\ &= \frac{1}{\sqrt{2\pi\sigma_{off}}} \int_{v_{th}}^{\infty} e^{-\frac{(v-b_{off})^2}{2\sigma_{off}^2}} dv \\ P_1(v_{th}) &= \int_{-\infty}^{v_{th}} p(y|1)dy = \int_{-\infty}^{v_{th}} f_1(y)dy \\ &= \frac{1}{\sqrt{2\pi\sigma_{off}}} \int_{-\infty}^{v_{th}} e^{-\frac{(b_{on}-v)^2}{2\sigma_{on}^2}} dv \end{aligned} \tag{4.20}$$

If we assume the on and off statistics are equiprobable, then the bit error rate can be written as

$$\begin{aligned} BER = P_e(Q) &= \frac{1}{\sqrt{\pi}} \int_{Q/\sqrt{2}}^{\infty} e^{-x^2} dx \\ &= \frac{1}{2}\left(1 - erf\left(\frac{Q}{\sqrt{2}}\right)\right) \approx \frac{e^{-Q^2/2}}{\sqrt{2\pi}Q} \\ Q &= \frac{v_{th} - b_{off}}{\sigma_{off}} = \frac{b_{on} - v_{th}}{\sigma_{on}} \\ erf(x) &= \frac{2}{\sqrt{\pi}} \int_0^x e^{-y^2} dy \end{aligned} \tag{4.21}$$

The following figures compare the computed Q factors and associated Gaussian statistic source, and not system level, BER estimates for direct modulation, standard injection locking, and negative differentiated injection locking under similar common biasing conditions as described in Appendix D. We observe a net improvement from direct modulation towards negative differentiated injection locking.

Figure 4.10 depicts the estimated Q factor of 2.7244 (source BER estimate of 0.0032) for direct modulation under the conditions labelled in the graph. The normalized rise time from this simulation is 0.05 and the poor mean and standard deviation spread of this signal's statistics are responsible for its poor Q factor estimate. Figure 4.11 shows the estimated Q factor of 4.5819 (source BER estimate of $2.6651x10^{-6}$) and a normalized rise time of 0.1 for this standard injection locking simulation under the conditions labelled in the graph. Figure 4.12 depicts the estimated Q factor statistic of 17.3539 (source BER estimate of $9.3846x10^{-47}$) and a normalized rise time of 0.05 for the simulation of negative differentiated injection locking under the conditions labelled in the graph. It demonstrates superior performance among these simulations with a quicker rise time and better stability than was demonstrated by standard injection locking or direct modulation under similar common biasing conditions.

The Q factor is a signal statistic that is independent of the probability distribution function and is related to a perception of signal strength and clarity. It is a measure of the signal to noise ratio and through the previously described mechanism of amplitude phase coupling, is directly related to the inherent chirp of the signal for directly modulated semiconductor lasers. The Q factor will directly influence the eye diagram of the laser output and is therefore considered along with its relation to amplitude phase coupling to be a key figure of merit.

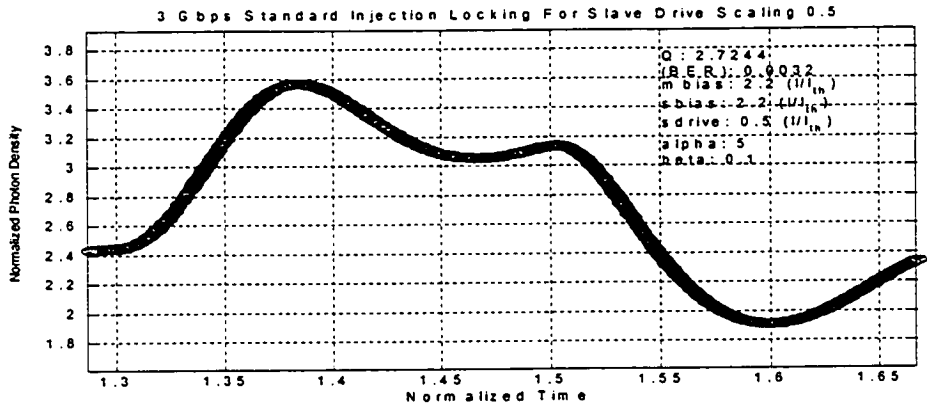

Figure 4.10 Q factor (BER) estimate of direct modulation.

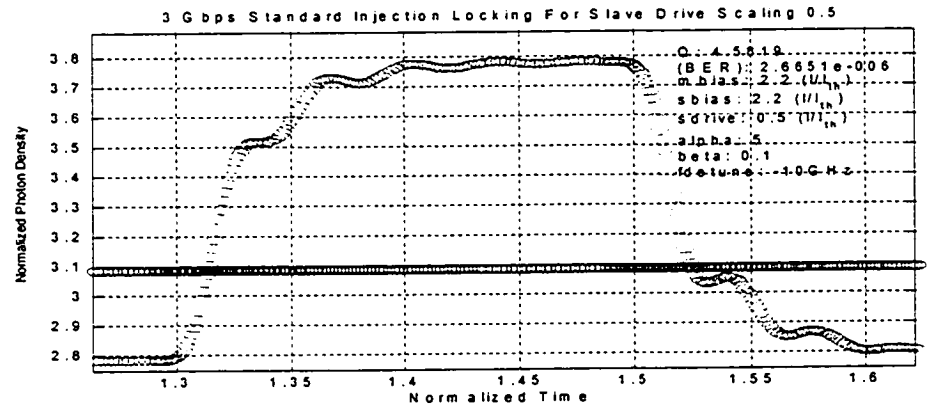

Figure 4.11 Q factor (BER) estimate of standard injection locking.

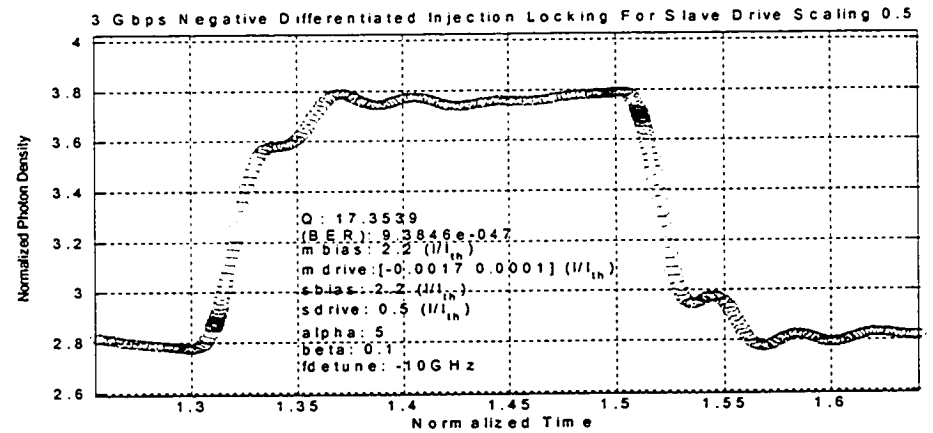

Figure 4.12 Q factor (BER) rate estimate of negative differentiated injection locking.

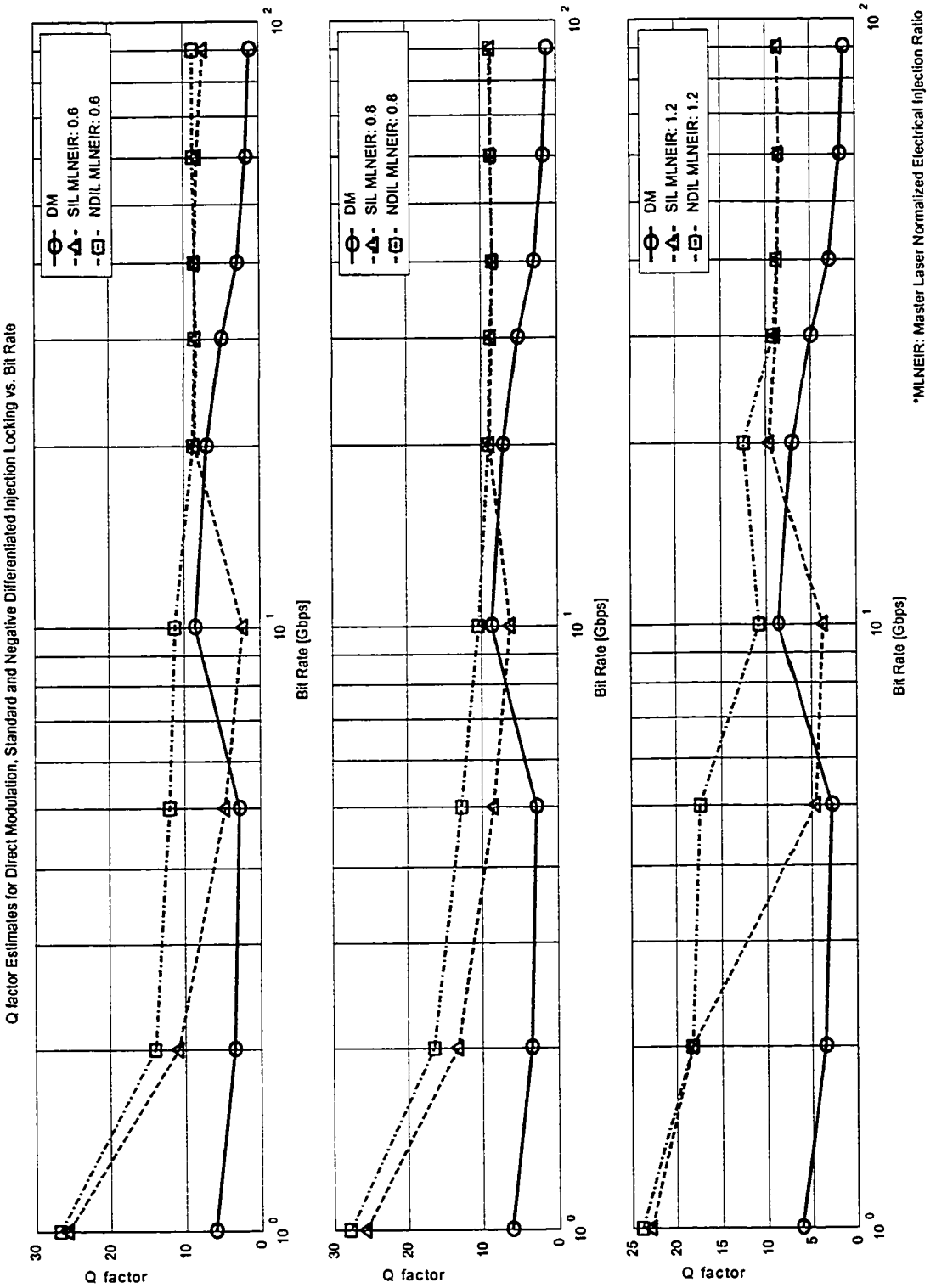

Figure 4.13 Q factor estimation vs. bit rate comparison between NDIL, SIL and DM for 0.5 slave drive scaling.

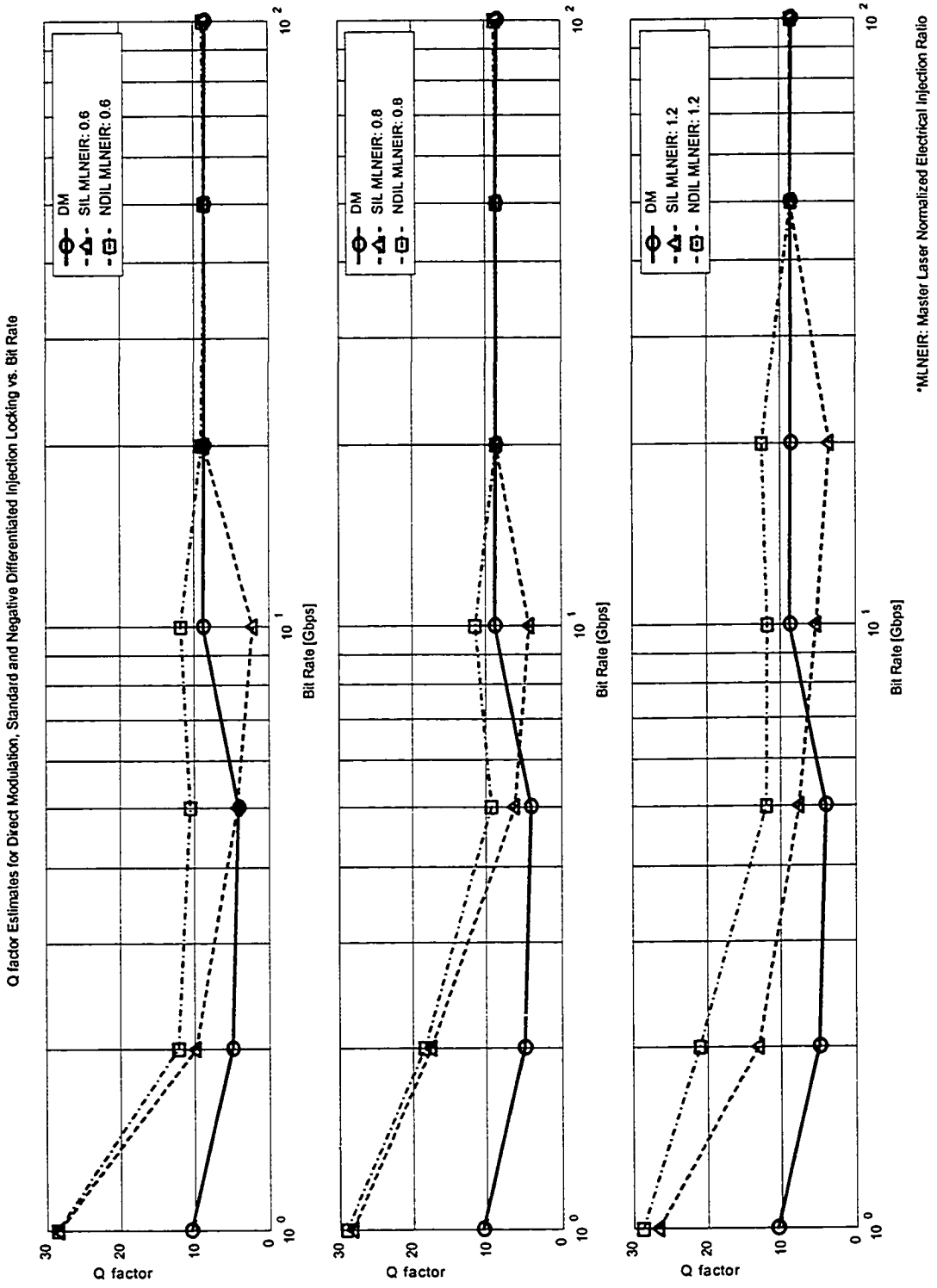

Figure 4.14 Q factor estimates vs. bit rate comparison between NDIL, SIL and DM for 2.5 slave drive scaling.

Figure 4.13 and Figure 4.14 contrast the Q factor estimates over a large class of modulation rates between weak and moderate slave drive extinction ratio scaling conditions of 0.5 and 2.5 respectively. Our analysis shows that Q factor optimization is bias level dependent as well as modulation rate dependent. In all the cases we have studied the Q factors of optimized negative differentiated injection locking outperform standard injection locking and direct modulation. In our simulation NDIL clearly achieved superior performances at normalized injection levels of 0.6, 0.8 and 1.2 between 1 and 20-50 Gbps with up to a 5 times improvement in the NDIL modulation Q factor source signal statistic. An interesting reversal in Q factor performance was also observed between SIL and DM where it is believed that the interplay between relaxation oscillation and signal distortion due to the optical injection forcing field in SIL degrade its performance with respect to direct modulation at rates below 10 Gbps. Beyond these rates the relaxation oscillation effect is diminished and thus SIL performance reclaims its Q factor superiority, or at least equality, with respect to direct modulation. Finally, above 10 Gbps NDIL performance was only marginally better than standard injection locking which itself remains significantly superior to direct modulation for a slave laser scaling of 0.5. These statistics were computed under conditions reported in Appendix D and optimized in MATLAB. As such we have imposed a negative detuning of 10 GHz of the master laser optical frequency relative to the free running slave laser optical frequency in all these computations. It may be of interest to future researchers to compute the Q factor performance improvement simultaneously over a range of master laser optical frequency detuning.

4.5 POWER SPECTRAL DENSITY OF PHOTON DENSITY

The optical power spectrum output derived from equations (3.29), (3.30), (3.31) and (3.34) are computed using not only photon concentration but also phase information as well. According to Agrawal [37], using the following relationship

$$E(t)=\frac{\sqrt{I+S(t)}}{2}e^{-i(\omega_0 t+\theta+\phi(t))}, \tag{4.22}$$

where $E(t)$ is the complex energy of the signal, the power spectrum is then given through the Fourier transform of the autocorrelation function,

$$G(\omega)=\frac{1}{2\pi}\int_{-\infty}^{\infty}\langle E(\tau)\,E(\tau)\rangle e^{i\omega\tau}d\tau\,. \tag{4.23}$$

Applying these relations to our simulation models for direct modulation, standard injection locking and negative differentiated injection locking, we observe in Figures 4.15, 4.16 and 4.17, that negative differentiated injection locking, under the conditions presented, can achieve a crisper more compact spectral profile than either direct modulation or standard injection locking. In these illustrations we have used common parameters to those presented in Appendix D and added noise to the signals.

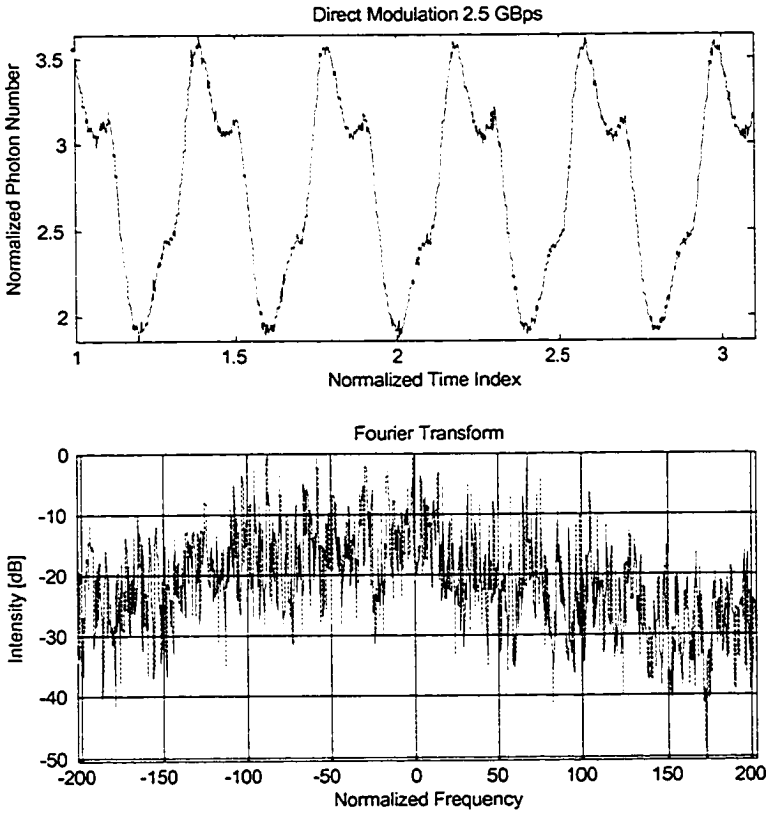

Figure 4.15 Time and power spectral density estimate of direct modulation.

The results of Figure 4.15 are very similar to those presented in [38], where essentially the spectral energy is largely spread out and not concentrated about any particular frequency band which is consistent with the results we achieved in Section 4.3. Also, this figure shows that the binary keying modulation has been severely distorted by the dynamics of the uncontrolled amplitude phase relaxation oscillation coupling penalties associated with direct modulation.

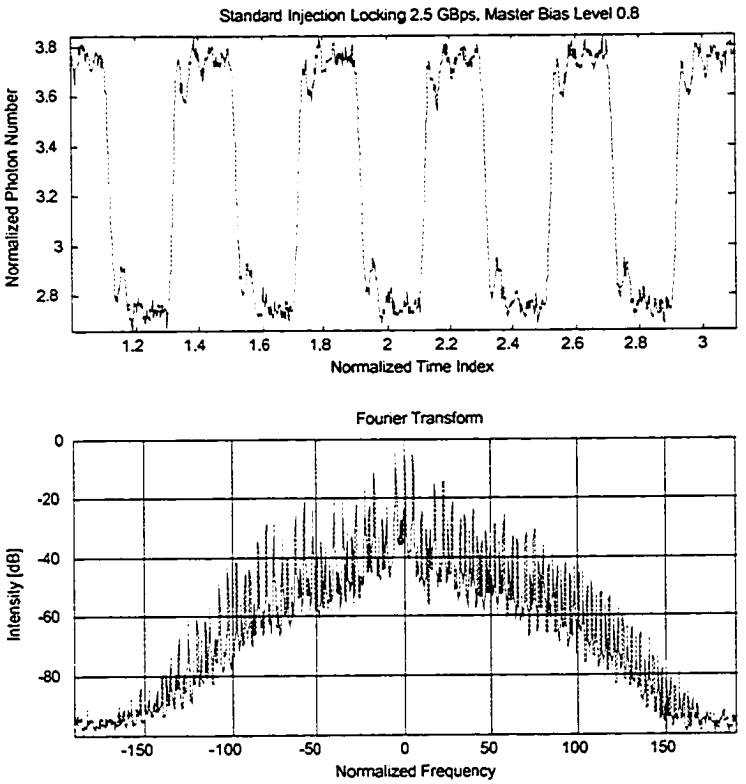

Figure 4.16 Time and power spectral density estimate of standard injection locking.

Figure 4.16 shows modulation sidebands and carrier spikes as expected with good standard injection locking. However, there is a large noise content on the signal that we do not associate with the additive noise we introduced. Insufficient re-sampling and relaxation oscillation effects are possibly responsible for the lack of detail we achieved in this calculation. The result however is consistent, albeit noisily, with the theory of standard injection locking power spectra. As such it shows a better confinement of spectral energy and a spectral structure that begins to mimic one of binary amplitude keying.

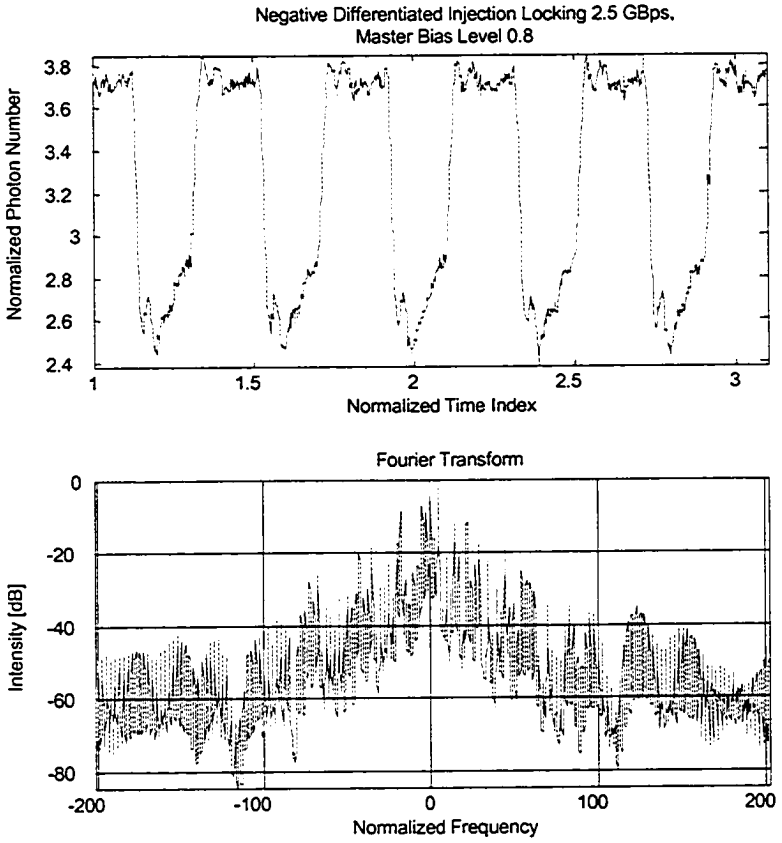

Figure 4.17 Time and power spectral density estimate of negative differentiated injection locking.

In Figure 4.17, we present the power spectrum for negative differentiated optical injection locking. We observe a better modulation sideband energy distinction than with standard injection locking and superior spectral confinement in general for this particular optimization. It is clearly representative of binary modulation and is consistent with the result we achieved in Section 4.3 indicating that the adiabatic and transient effects of frequency chirp have been greatly mitigated.

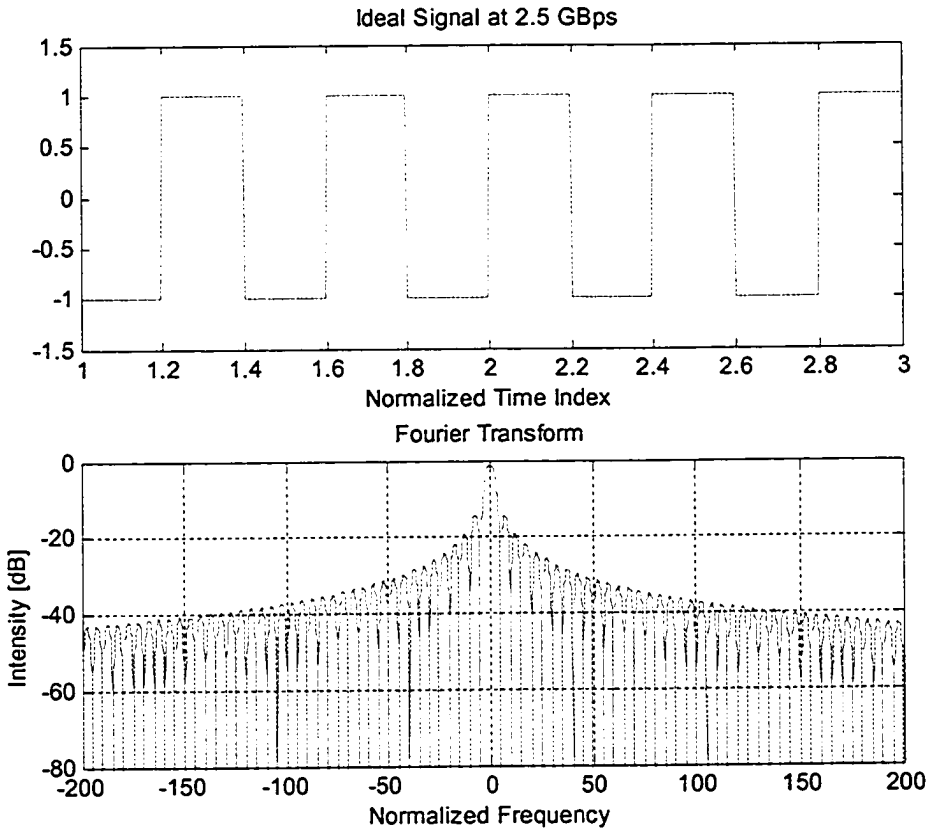

Figure 4.18 Time and power spectral density of ideal signal.

Figure 4.18 depicts the idealized signal and power spectral density representation of the studied signal included to serve as a reference for weighing the modulation mechanisms against each other.

These figures clearly show that, under the common simulation biasing condition of Appendix D, negative differentiated injection locking can improve the spectral performance beyond standard injection locking and direct modulation.

Figures 4.19 and 4.20 show similar results using the VPI simulation package in terms of the spectral confinement efficiency of optical injection locking over direct modulation. Thus we conclude that the results are an acceptably accurate representation of performance.

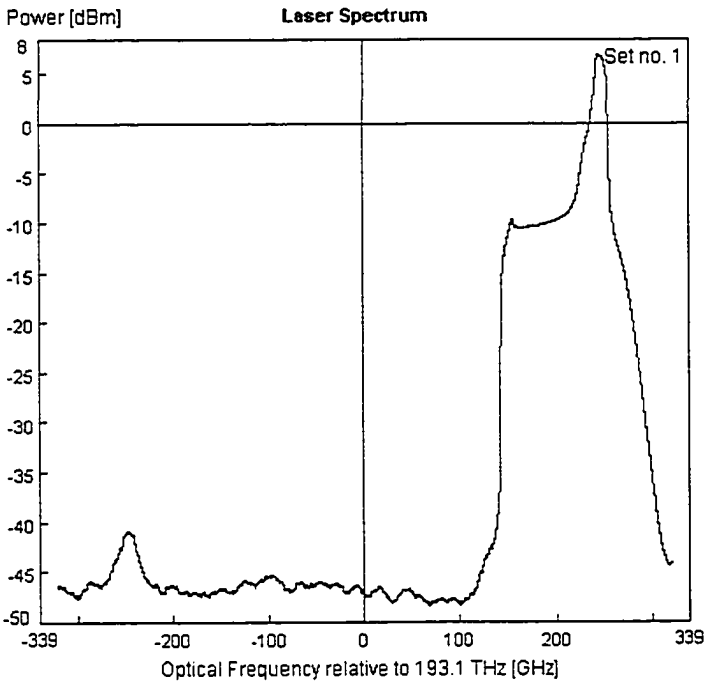

Figure 4.19 Optical spectrum of direct modulation.

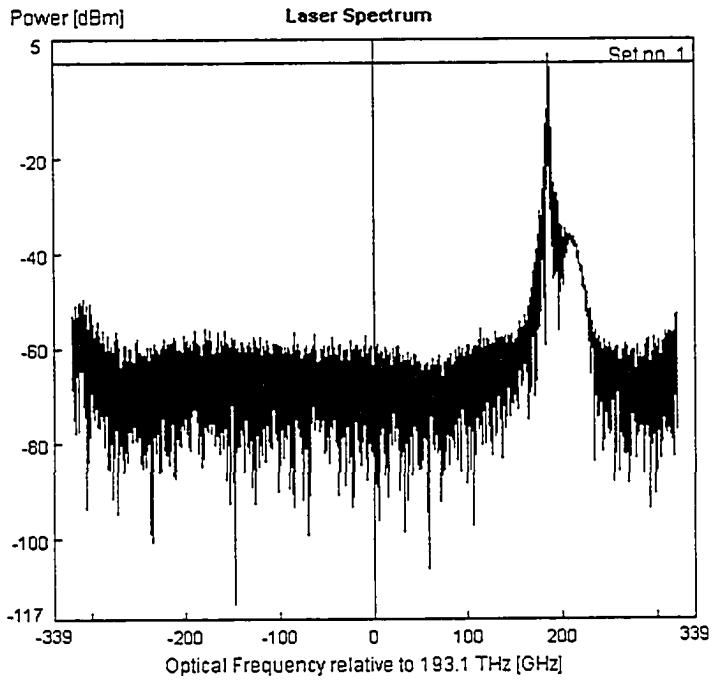

Figure 4.20 Optical spectrum of standard injection locking.

4.6 MODULATION RESPONSE

The modulation response depicts the gain response of a device under modulation relative to its unmodulated output gain. Essentially, it establishes the speed at which a device may be driven with a normalized power output ratio attributed to its modulation speed. One common feature of interest is that generally, the peak gain in the modulation response occurs at the relaxation oscillation frequency of the device [21].

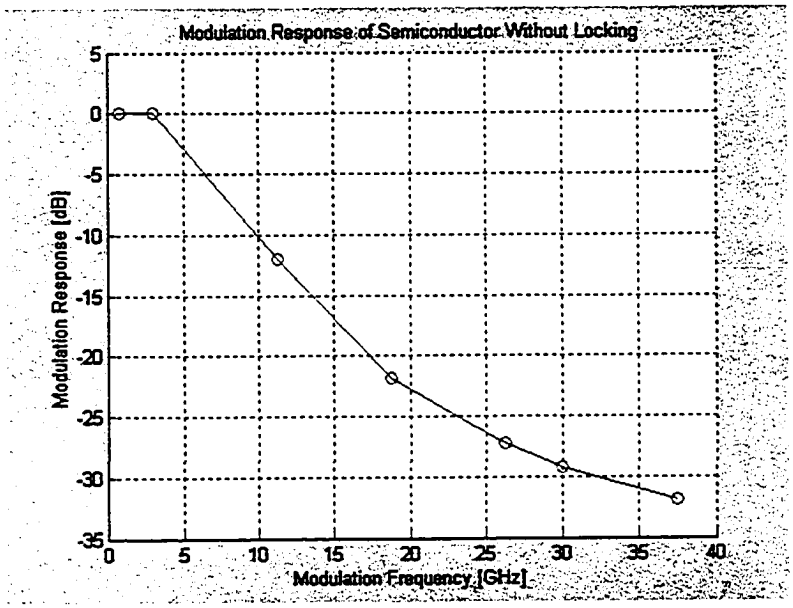

Figure 4.21 Modulation response of direct modulation.

In the above Figure 4.21, we observe that the modulation response of direct modulation using common parameters presented in Appendix D and a gain peak estimate somewhere below 3 GHz due to the limited number of pertinent computed samples available.

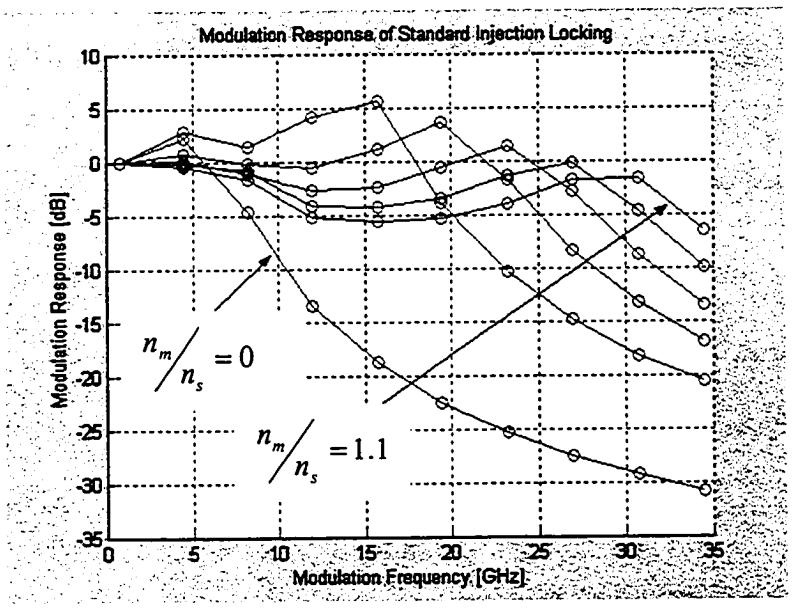

Figure 4.22 Modulation response of standard injection locking over a range of normalized electrical injection ratios from 0 to 1.1.

From Figure 4.22, we note that the gain peak is proportional to the normalized electrical injection ratio of the lasing fields with an apparent maximum gain peak frequency of 31 GHz at a normalized electrical injection ratio of 1.1. This significant enhancement in modulation rate is due to the presence of a coherent field pre-established in the slave laser within the locking range deeply curtailing the cavity photon density build up time through the spontaneous emission mechanism inherent to direct modulation.

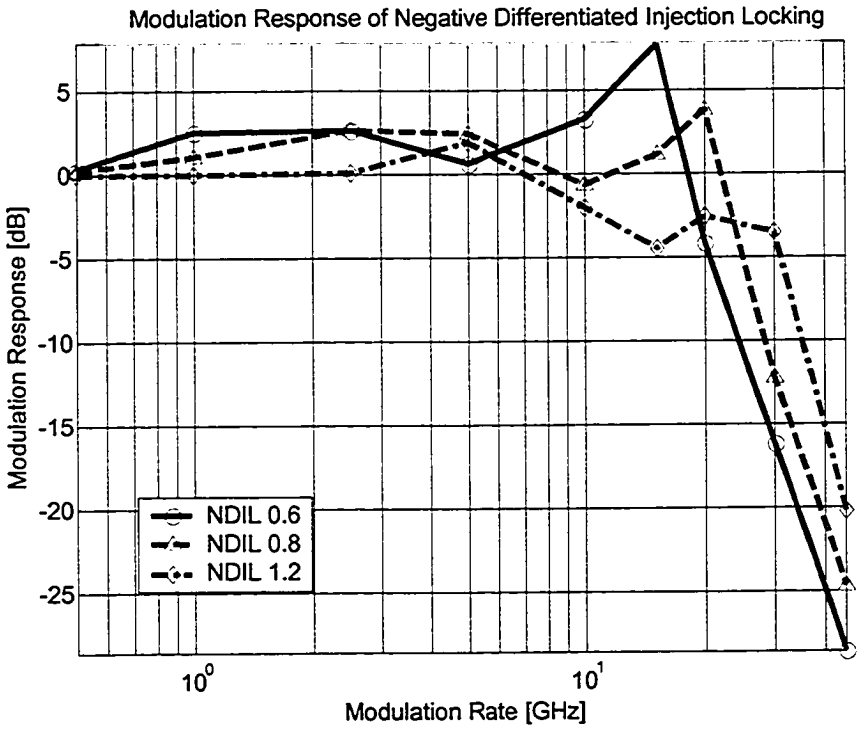

Figure 4.23 Modulation response of negative differentiated injection locking (NDIL).

Finally, in Figure 4.23, we show the modulation response of negative differentiated injection locking, we observe that under common biasing condition to those employed for the analysis of direct and standard injection locking modulations and constrained by Q factor optimized statistics, that we do not discern a significant difference in the gain peaks from the case presented in Figure 4.22 for standard injection locking. The

modulation response mechanism of a coherent lead emission for negative differentiated injection locking at high modulation rates is a near identical mechanism in terms of photon density build up time to that of standard injection locking. However, for an unconstrained optimization of negative differentiated injection locking, Figure 4.24, does show that this form of injection locking can enhance the modulation rate for a normalized electrical injection ratio of 0.6. This result is achieved only at the expense of the Q factor statistic, which is why we shall only consider constrained results in the remainder of our analyses.

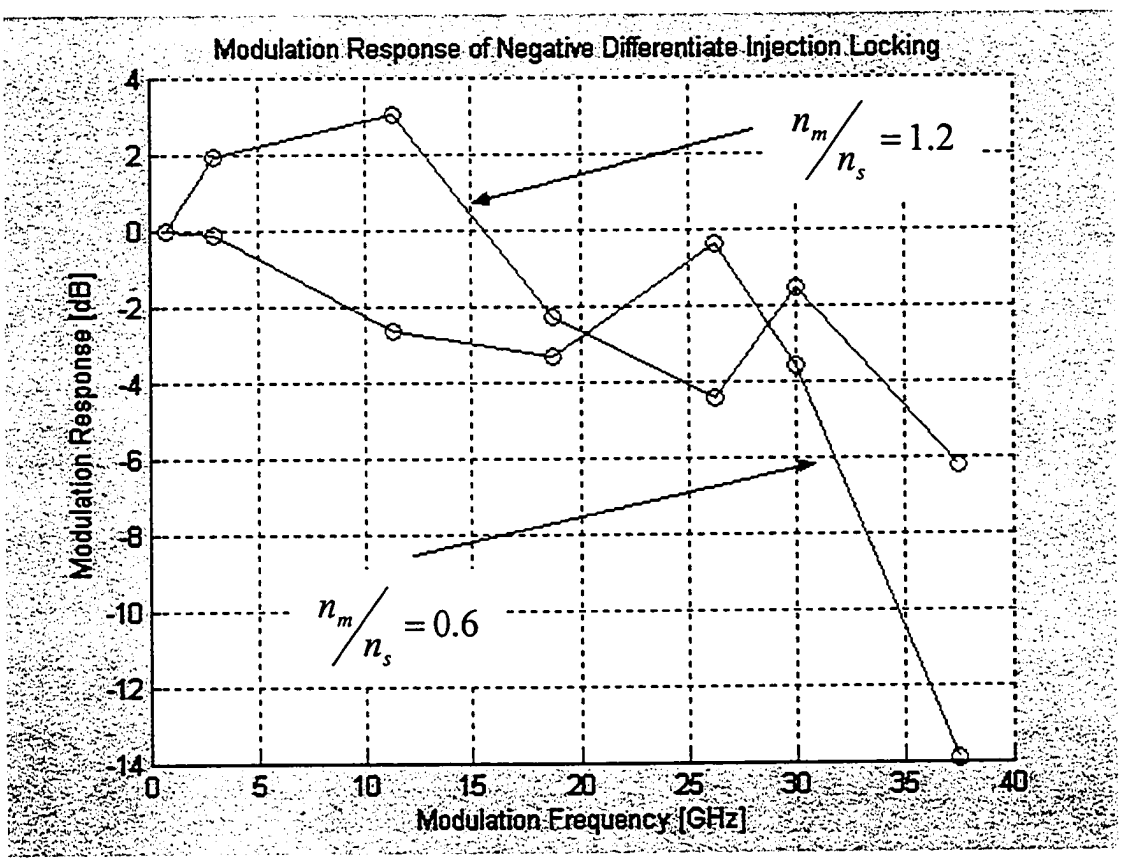

Figure 4.24 Modulation response of unconstrained negative differentiated injection locking over normalized electrical injection ratios of 0.6 and 1.2.

4.7 MASTER LASER OPTICAL FREQUENCY DETUNING

The following diagrams show the unstable and stable operation respectively of standard injection locking with optical frequency detuning of the master laser with respect to the free running slave laser optical frequency as an independent parameter. This was achieved by studying the probability density function of the slave laser output and defining decision threshold levels as indicated in Figure 4.25 b) and Figure 4.26 b) by the figure crossbars. Where significant signal statistics above both the vertical crossbar and outside the horizontal crossbars depict acceptable binary stable performance.

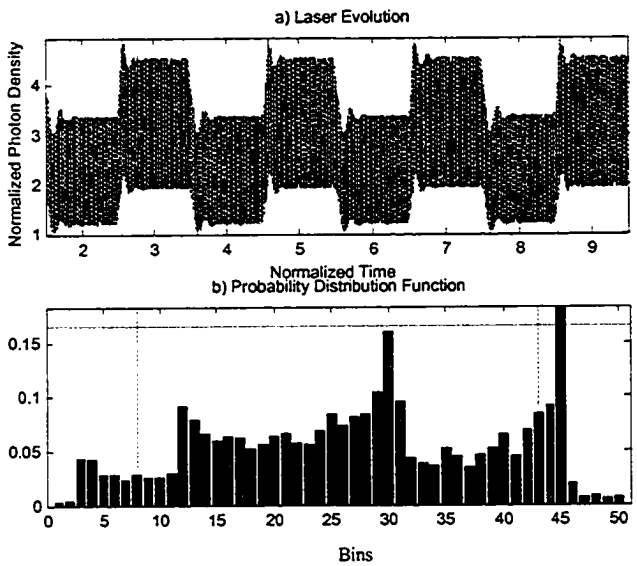

Figure 4.25 a) Slave laser photon density and b) stability plot of a typical unstable 1 Gbps laser under standard injection locking detuned by +50 GHz at a normalize electrical injection level of 0.6.

From the distribution function of Figure 4.25 b), we observe that the signal is dispersed inconsistently with the probability density function of the input raised cosine square wave modulation and fails the criteria for stability depicted by the figure crossbar criteria.

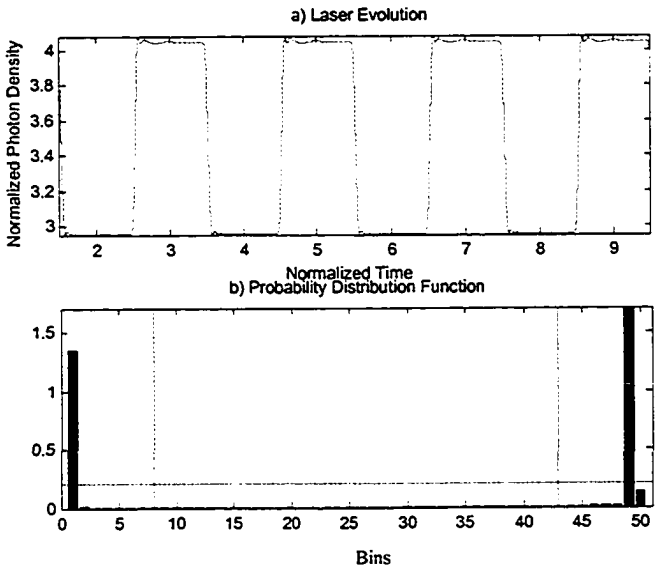

Figure 4.26 a) Slave laser photon density and b) stability plot of a typical stable 1 Gbps laser under standard injection locking detuned by – 25GHz at a normalized electrical injection level of 0.6.

In Figure 4.26 b) contrary to our previous example, we observe that the signal is largely divided between two distinct on-off states consistent with the expected statistics of a square wave modulation and that the stability criteria established by the figure crossbars is met.

Figure 4.27 and Figure 4.28 below, depict an application of the crossbar stability analysis to standard injection locking and negative differentiated injection locking over a 200 GHz range of master laser optical frequency detuning and master laser electrical normalized injection levels ranging from 0.5 to 1.2. In both cases as predicted in Section 3.7.1, these injection locking mechanisms favor negative detuning of the master laser with respect to the frequency of the free running slave laser.

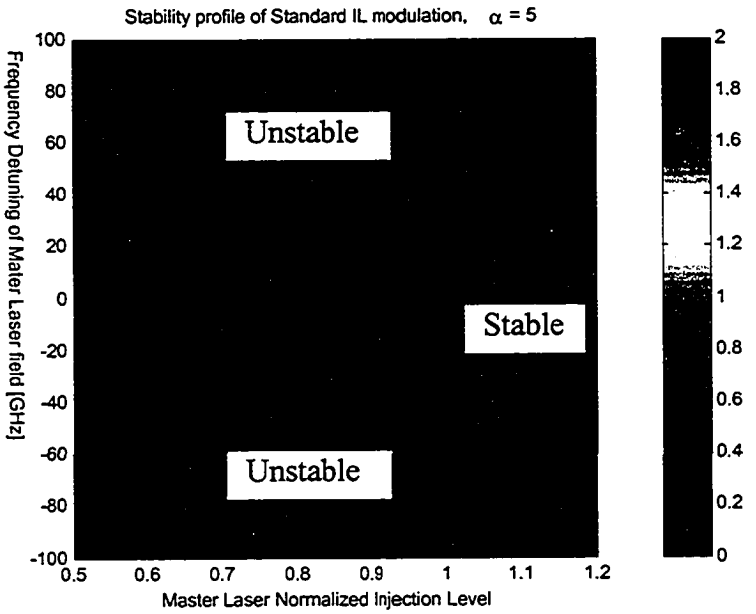

Figure 4.27 Stability response of standard injection locking.

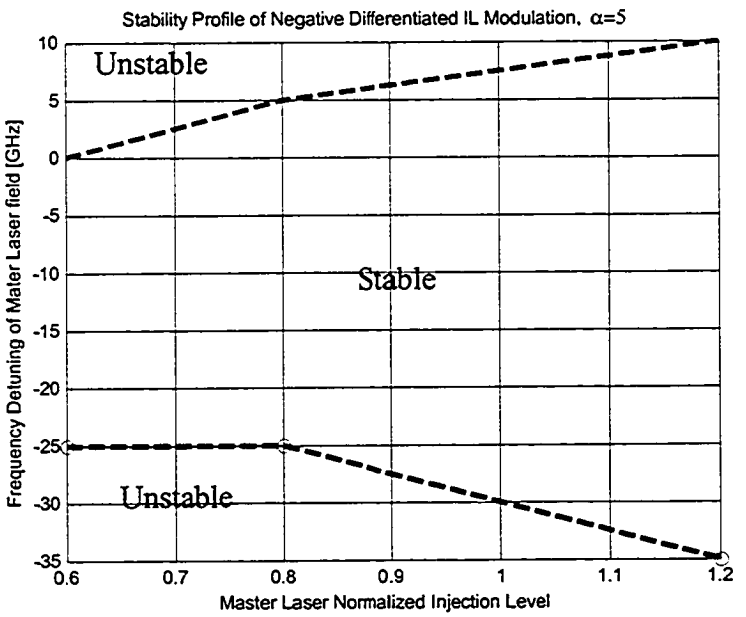

Figure 4.28 Stability response of negative differentiated injection locking.

Figure 4.27 and Figure 4.28, above illustrate the electrical normalized master laser injection level ratios versus master laser optical frequency detuning relative to the free

running slave laser optical frequency under common conditions to those presented in Appendix D with respect to the slave laser stability for standard and negative differentiated injection locking cases. We observed no significant change in stability of either system. However, both systems do follow the expected theoretical shape outlined in Section 3.7.1 favouring negative optical frequency detuning in both instances.

4.8 Optical frequency chirp-power index

Having investigated the Q factor constrained slave laser optical frequency chirp responses for direct, standard and negative differentiated injection locking, it seems logical to index both optical frequency chirp and power as a combined figure of merit. Since output power is related to the spatially uniform photon density according to Green [41], we renormalize chirp and photon density with respect to each other and multiplied them to produce a time resolved optical frequency chirp-power index.

Figure 4.29 depicts the chirp-power index (CPI) for direct, standard injection and negative differentiated injection locking over normalized electrical injection ratios of 0.6, 0.8 and 1.2. In all the studied cases the lowest CPI was achieved by negative differentiated injection locking relating that the chirp-power utilization is most effectively being minimized over modulation rates below 50 Gbps. Standard injection locking similarly showed a lesser improvement in CPI performance over direct modulation for the studied modulation rates.

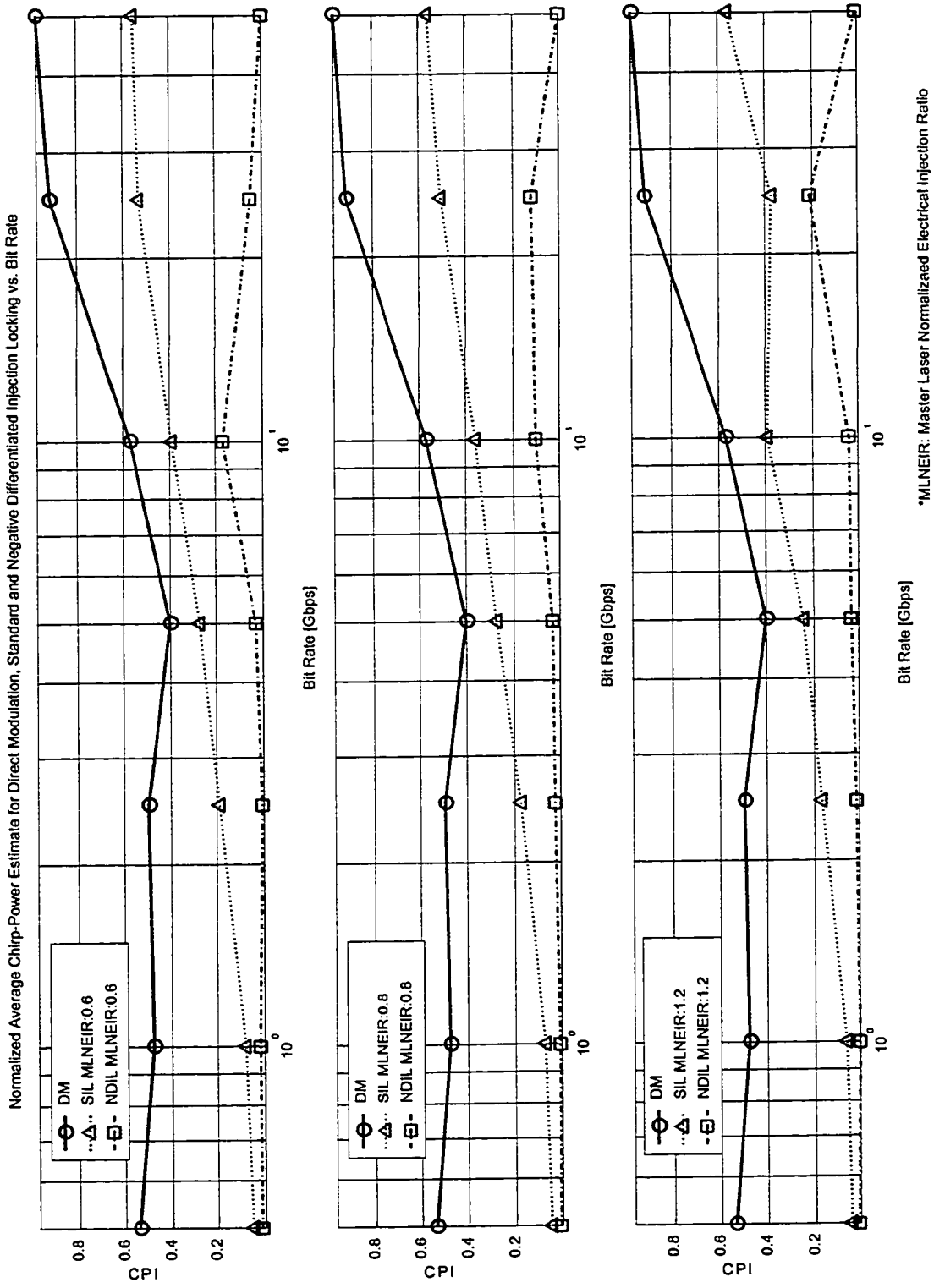

Figure 4.29 Chirp-power index for DM, SIL and NDIL over bit rate and normalized electrical injection ratios of 0.6, 0.8 and 1.2.

4.9 ELECTO-OPTICAL DISTORTION ANALYSIS

In this subsection, we compare the electro-optical distortion of direct modulation, standard and negative differentiated injection locking. Borrowing a technique from synthetic aperture radar theory, we use the cross correlation of the electrical input to optical output of the slave laser to synchronize the signals and then renormalize the signals for distortion comparison.

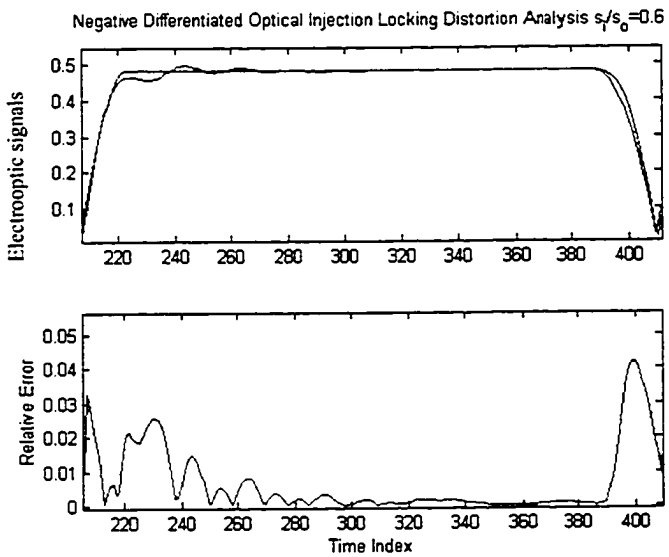

Figure 4.30 Synchronized and normalized electro-optic signals and distortion estimate plot of negative differentiated injection locking at an injection ratio of 0.6.

Figure 4.30 depicts an example of the distortion signal between the slave laser electrical input and its optical output; it is important to stress that distortion analysis does not affect the linearity of the device but does play an important role nonetheless. In characterizing this signal we model the distortion error signal in terms of its mean and standard deviation.

In Figure 4.31, we compare the mean error distortion signal for negative differentiated injection locking, standard injection locking, and direct modulation. Our analysis suggests there are a variety of regimes where each modulation technique is favored. For instance, below 1 Gbps standard injection locking is globally but marginally superior to NDIL and DM in terms of its distortion performance. However above 10 Gbps DM is often superior to either NDIL or SIL which favor slightly SIL independent of injection level. This paints a complex picture that depends on the signal conditioning and purpose. In this case, we again chose parameters that maximized Q factor for NDIL as depicted in Figure 4.13 as an underlying constraint to the analysis.

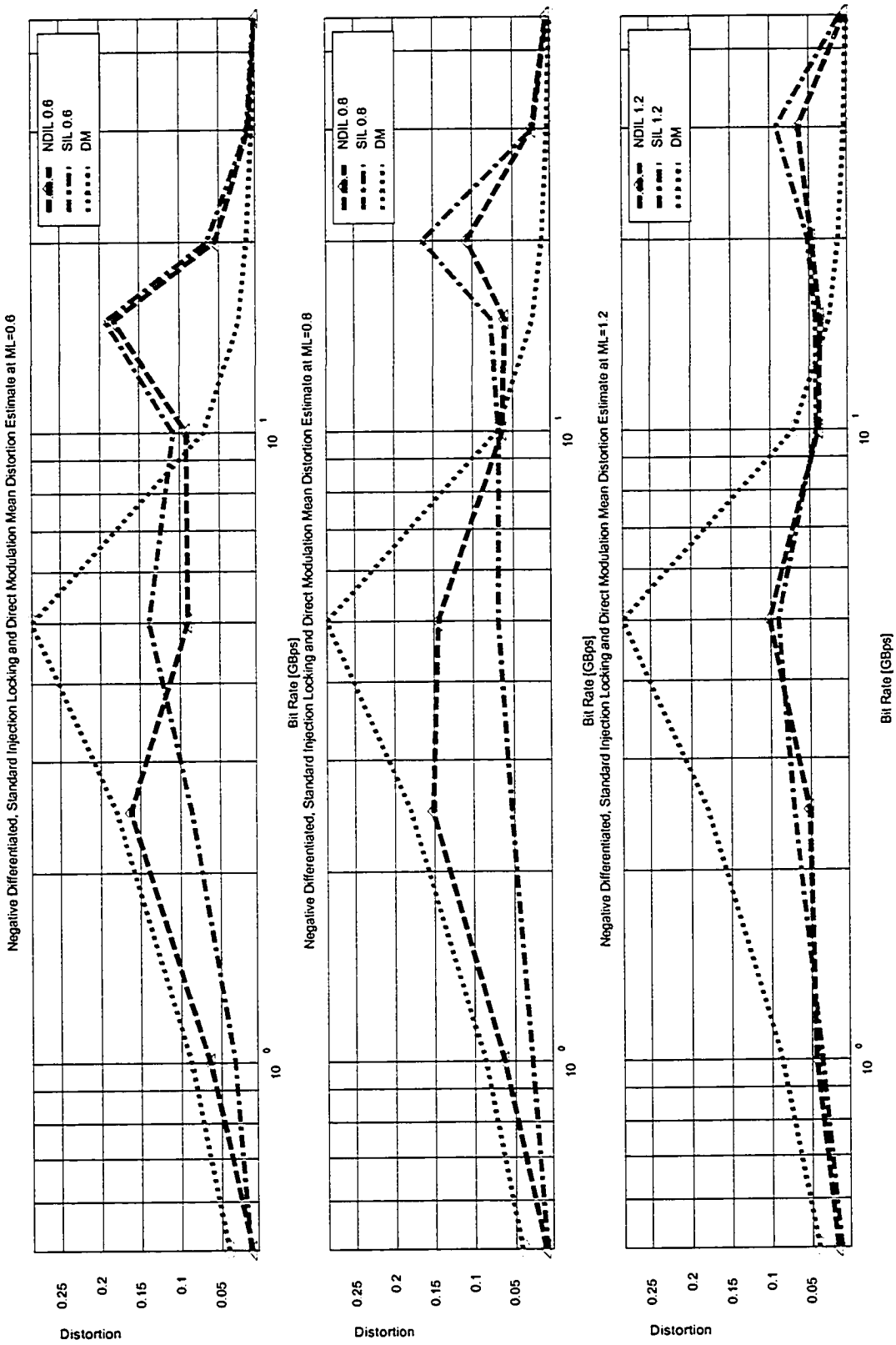

Figure 4.31 Mean distortion error signal for NDIL, SIL and DM over various injection levels.

4.10 NONLINEAR MODULATORS

There are three important technologies that currently attempt to address the shortcomings of direct semiconductor modulation with respect to its typical system penalties of: speed, chirp, and complexity. The first is the Mach-Zehnder modulator, which splits an optical carrier into two paths of different length and relies upon controlled superposition to produce a modulation. Another technique employs an electro absorption modulator that couples a gain cavity with a reverse biased semiconductor producing modulation by varied absorption. Finally, optical injection locking uses direct laser modulation but reduces chirp by reducing spontaneous interaction within the lasing field. These three modulation schemes represent the bulk of current commercial technology for high speed optical modulation. Thus, it is important for us to understand how each addresses the issue of frequency chirp and the technological compromises they engineer to mitigate it.

4.10.1 MACH-ZEHNDER MODULATOR

The Mach-Zehnder modulator consists of an integrated waveguide of an electro-optic material that has an index of refraction that is influenced by an applied voltage over a lithium niobate or gallium arsenide substrate. The device operates by splitting the input light into two branches whose path length must be carefully electrically controlled such that upon recombination, by virtue of the signals optical phase differences, they superimpose constructively or destructively. The advantage of this technology is that, properly configured, there is no spectral broadening due to relaxation oscillations and it has been shown that it is possible to achieve modulation bandwidths well above 50 GHz

[36]. However, the cost and complexity of use are serious disadvantages to this technology. Also, the electro-optic effect in MZ modulators is relatively weak, so they tend to be devices that become walk-off length limited.

The phase relationship for the coupled branches of a MZ modulator are given in Green [42] by,

$$\phi = \frac{2\pi}{\lambda} n(\omega) L ; \tag{4.24}$$

$$n(\omega) = n_0 - \tfrac{1}{2} n_0^3 \cdot \overline{\overline{r}} \cdot \bar{E} , \tag{4.25}$$

where L is the (walk-off) arm length, $\overline{\overline{r}}$ is the linear electro-optic coefficient tensor and $\bar{E}$ is the applied electrical field vector. To obtain a phase shift of π for typical values in GaAs imply a necessary arm walk-off length of about 2 cm and as such implies a minimum transition from minimum to maximum extinction of > 25 ps, which is remarkably fast!

MZ modulators however require specifically adjusted input polarization states, careful attention to thermal compensation, and produce a nonlinear distortion between the electrical and optical modulation. Chirp control with Mach-Zehnder modulators can be achieved by altering the drive conditions on the interferometer arms separately but always at the cost of additional complexity balanced with the walk-off length inherent to the device.

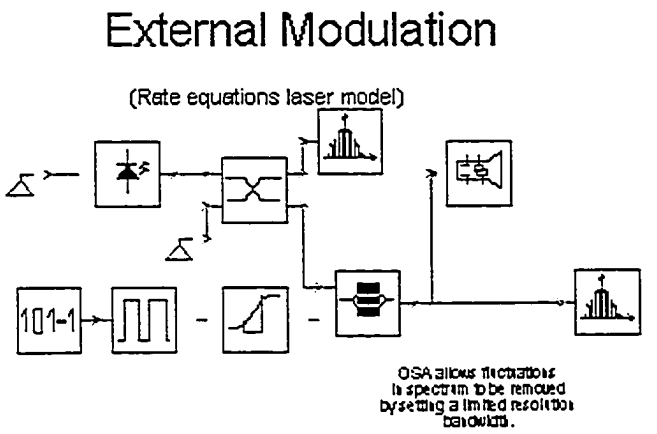

Figure 4.32 Schematic representation of Mach-Zehnder modulator.

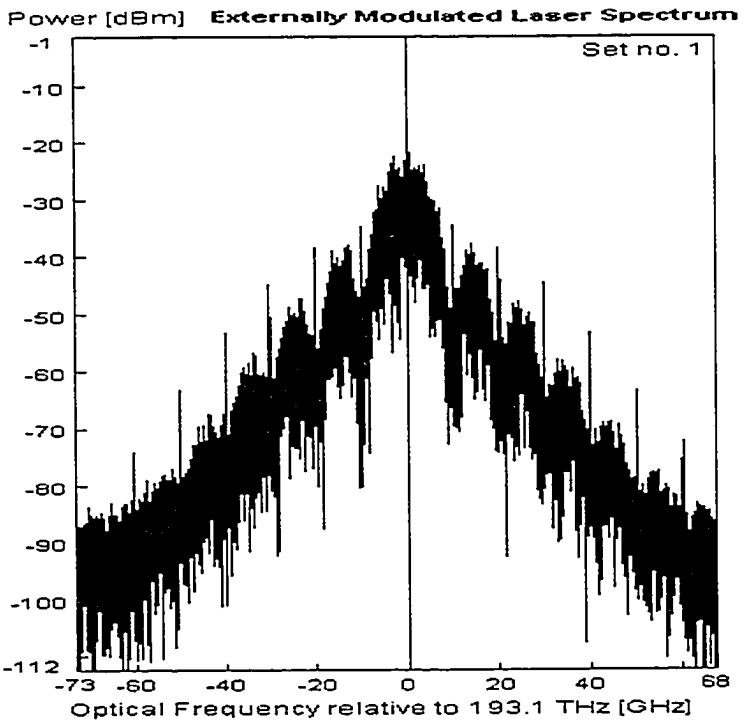

Figure 4.33 Optical spectrum of Mach-Zehnder modulator at 10 Gbps.

Figure 4.33 depicts the optical output spectrum of a typical Mach-Zehnder modulator driven at 10 Gbps. Notice the harmonic spacing is at odd multiples of the bit rate clearly

evident due to the high extinction of this modulation approach. Also with respect to Figure 4.15, Figure 4.16, and Figure 4.17 we note that the binary keying spectrum is clearly defined and modulation spikes are clearly distinguishable. This finding, in terms of time and frequency resolution shows this modulation technology to be superior to our previous simulations of direct modulation, standard injection locking, and negative differentiated injection locking.

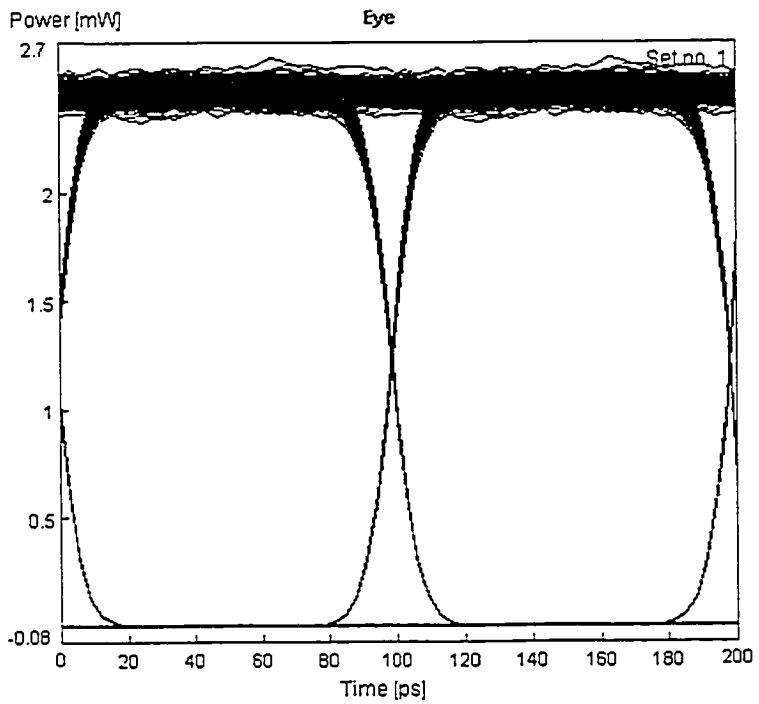

Figure 4.34 Eye diagram of Mach-Zehnder modulator at 10 Gbps.

Figure 4.34 above, is of particular interest because it showcases some of the great strengths and weaknesses of this modulator. The eye diagram in this case is clear and open, relatively jitter free with well defined logic levels. However, the transitions between these levels are nonlinear and follow a trajectory given by [36] as $\cos^2(V)$ where V is the modulating voltage, which limits modulation pulse shaping formats.

Thus Mach-Zehnder modulators exhibit excellent chirp suppression and modulation rate advantages but can also be critiqued in terms of their cost, complexity of control, polarization state controller requirements at the input, nonlinear responsiveness and an insertion loss hit of 1-2 dB.

4.10.2 ELECTRO-ABSORPTION MODULATOR

The electro-absorption modulator uses the effect of adjusting the bandgap of a reverse biased semiconductor to transmit or absorb an injected optical field. The absorption can thus be adjusted to be high loss or transparency depending on the modulating voltage. However, this technique can result in excessive chirp through the same electro-optic refractive index sensitivity to electrical carrier population we discussed throughout this thesis but in the opposite wavelength direction since we are substituting opaqueness for transparency with respect to this modulator. Another consequence is that this effect again degrades the linearity of the electro-optical modulation because absorption is an exponential process according to [36] by,

$$P_{out} = P_{in} e^{\eta V L}, \tag{4.26}$$

where P is power, η is an arbitrary scaling coefficient, V is the modulation voltage and L is the cavity length of the reversed bias semiconductor again referred to as the walk-off length.

The primary advantages of this technology, however, are the ease of producing modulators at low cost for digital links and the fact that these devices can be

monolithically constructed. In [36], it is explained that the device employs an active layer surrounded by a reversed biased blocking layer. These devices offer typically very good modulation responses of about 20 GHz and chirp in the opposite direction of directly modulated lasers (see Figure 4.36). This last point has the advantage of presenting an option where dispersion can be compensated at the source.

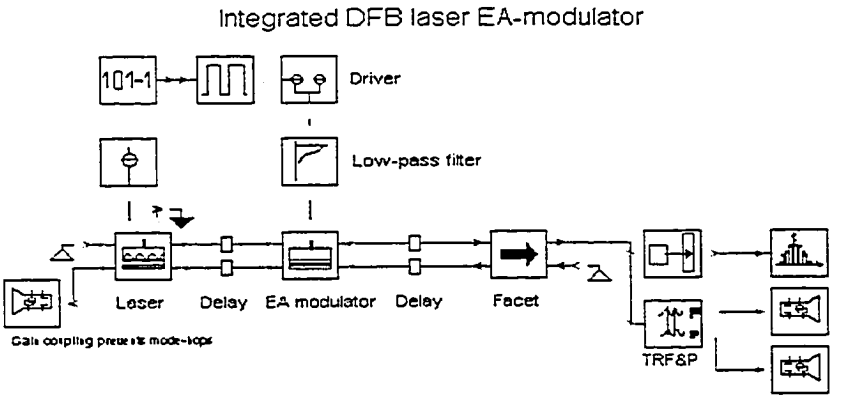

Figure 4.35 Schematic representation of electro-absorption modulator.

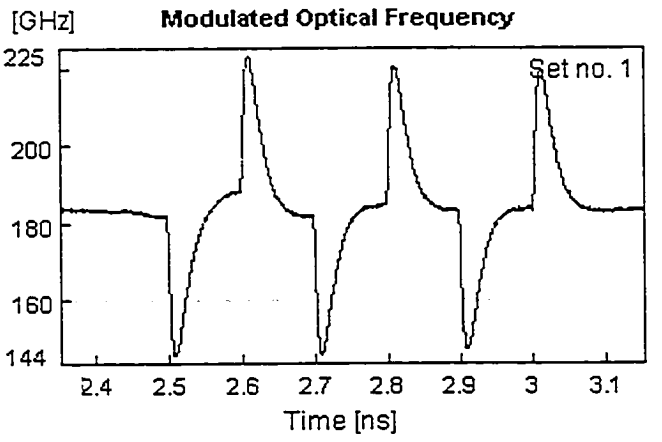

Figure 4.36 Chirp of electro-absorption modulator at 10 Gbps.

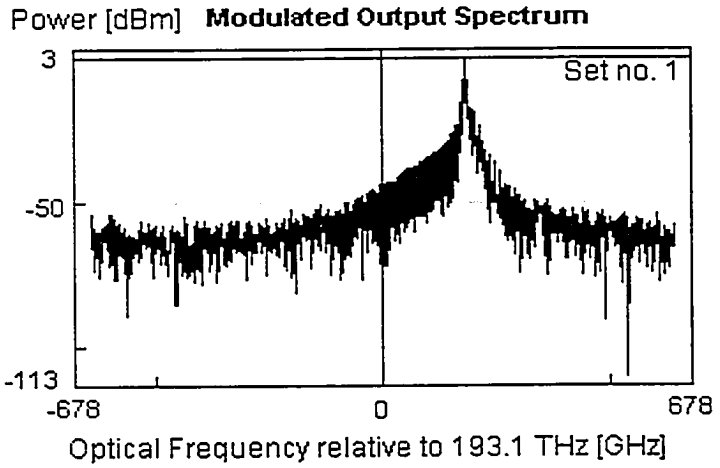

Figure 4.37 Optical spectrum of electro-absorption modulator at 10 Gbps.

Now that we have commented on the advantages of this modulator we shall discuss a few of its disadvantages. This device suffers from a significant insertion loss hit of 6-7 dB. Also, in general, the absorption peak of the reverse bias semiconductor moves in frequency with applied blocking voltage, which results in chirp. This frequency chirp is opposite to fiber dispersion and over long lengths can be used to counter its depressiveness. However, this suggests an increased possibility of cross-talk and poor channel energy utilization. Also, like Mach-Zehnder modulators, these modulators are nonlinear and can only be modulated up to speeds of 40 Gbps presently.

4.11 SUMMARY

In this chapter we presented the results of simulation models for the proposed negative differentiated injection locking, standard injection locking and direct modulation systems, calculating the merit figures of relaxation oscillation duration, frequency chirp, source Q factor statistics, power spectrum of the photon density, chirp-power index, modulation response, effects of master laser frequency detuning and signal distortion estimates. We concluded the chapter with a review of external modulators, contrasting their advantages and disadvantages.

Our simulations of the relaxation oscillation duration analysis showed that the system isn't critically damped at normalized master laser injection levels of 0.6 and 0.8. We observed that negative differentiated injection locking possesses a steeper decay rate and offset than standard injection locking with offset improvements of 0.02 and 0.01 respectively. Our simulations of chirp responses demonstrated that direct modulation exhibited an unconstrained normalized frequency excursion greater than 40. Standard injection locking showed a great improvement in normalized frequency excursion, 10, yet still exhibited a largely unconstrained frequency excursion within this region. Finally, negative differentiated injection locking displayed the smallest normalized frequency excursion, 6, largely constrained within ± 1 indicating adiabatic and transient chirp have been greatly suppressed. The source Q factor statistics revealed that in all cases of the studied normalized electrical injection locking bias ratios and modulation rates that optimized negative differentiated injection locking equalled or outperformed standard injection locking. Of particular interest in these results was the discovery that the

performance of negative differentiated injection locking appears to be bias level and modulation rate dependent. As such at normalized electrical injection ratios of 0.6, 0.8 and 1.2 negative differentiated injection locking outperformed standard injection locking and direct modulation by up to 5 times between the modulation rates of 1 and 20-50 Gbps. The power spectral density analysis of direct modulation, standard injection locking, and negative differentiated injection locking has shown that the spectrum of modulation improves respectively from DM to NDIL. Our investigation of Q factor constrained optical frequency chirp-power index related negative differentiated injection locking over modulation rates from 1 to 50 Gbps with respect to direct and standard injection locking. Looking at their modulation responses however we observed no clear distinction between SIL and NDIL in terms of modulation rate improvement.

Similarly, no clear distinction could be made between SIL and NDIL in terms of the stability responses over various master laser optical frequency detuning. The distortion analysis revealed that within the constraints of Q factor performance, the distortion analysis between DM, SIL and NDL showed no global advantage to any of the studied modulation responses; however, we did find regions where one modulation response could dominate over another over modulation rate and injection ratio.

One dimension where negative differentiated injection locking seems to clearly surpass direct and standard injection locking on a system level analysis is by achieving superior chirp control without changing the electrical bias levels. Thus negative differentiated

injection locking minimizes to a degree the extinction and chirp power penalties beyond the capabilities of either of these two systems.

Finally, we simulated the typical response of the Mach-Zehnder modulator and the electro-absorption modulator. Though we observed superior performance in the MZ modulator in terms of its time-frequency responses, we noted that the complexity, cost and dependence on polarization state control and nonlinear modulation format of this design make it unfavourable for certain applications. Similarly, the nonlinearity, insertion loss penalty and inherent chirp of the electro-absorption modulator also make it unsuitable for certain applications, which may favour direct, standard injection, or negative differentiated injection locking modulations for example, in OCDMA fractal modulation or DWDM metro applications where channel energy utilization, cross talk minimization and control complexity must be balanced.

In this chapter we have investigated a comparison of negative differentiated injection locking with respect to contemporary direct modulation and contemporary external modulation technologies.

5. CONCLUSIONS

5.1 SUMMARY OF THE THESIS

In this thesis, we have presented a new form of optical injection locking which improves slave laser frequency stability by reducing chirp through the relaxation oscillation mechanism. This was accomplished by reducing the relaxation oscillation electro-optical carrier birth-death process caused by instantaneous electrical carrier changes during modulation.

Using the simple harmonic oscillator model, we verified the analysis of [13] and employed the Drude model to relate instantaneous carrier concentration changes through the material dielectric function to a chirp of optical output emission frequency.

Next, we reviewed the rate equation models for direct, standard injection locking, and negative differentiated injection locking. Then we contrasted these simulation models with ones we developed using the Virtual Photonics simulation software.

In addition, we explored the performance of direct modulation, standard optical injection locking, and negative differentiated injection locking by comparing their respective performances to the theory developed in Chapter 3. We contrasted these modulation

schemes with respect to their relaxation oscillation duration, slave laser emission frequency chirp, the source Q factor, slave laser photon power spectral density, chirp-power index, modulation response, master laser optical frequency detuning with respect to slave laser stability, and electro-optical slave laser distortion analysis. Finally, we reviewed two forms of external modulators, the Mach-Zehnder modulator and the electro-absorption modulator and contrasted the general advantages and disadvantages of these with the results achieved by direct modulation devices.

5.2 THESIS CONTRIBUTIONS

Negative differentiated injection locking provides a new means of controlling the relaxation oscillation excursion during direct modulation by opposite optical carrier injection during the instantaneous electrical carrier changes of modulation. We have shown in Chapter 4, that when the relaxation oscillation is not critically damped between the modulation rates of 1 and 20 to 50 Gbps over normalized electrical injection ratios of 0.6, 0.8 and 1.2, negative differentiated optical injection locking greatly improves the source Q factor and chirp-power index estimates over direct modulation and standard injection locking. This results in an improved signal clarity and fidelity. Following from this result, as expected, we observed regions of operation where the spectral profile energy confinement of negative differentiated injection locking was more efficient not only to direct modulation but also to standard injection locking as well.

5.3 SUGGESTIONS FOR FUTURE RESEARCH

There are several ways of achieving high modulation rates while improving the source Q factor in lightwave communication systems. Some external modulators, such as Mach-Zehnder modulators are superior to optical injection modulators with respect to sheer speed and signal clarity but fail to be as proficient in terms of modulation adaptability, operational and design simplicity, linearity or cost. However, our investigation of negative optical injection locking itself is in no way a complete treatment. At the cost of extra complexity, one could investigate the possibility of multiple negative optical injection locking as experimented with using standard injection locking in [46]. Clearly, there is more than a single electro-optic relaxation oscillation in the active layer of a semiconductor laser and multiple negative differentiated optical injection maybe one means of addressing them. Also, investigating the properties of linewidth enhancement factor mismatching between the master and slave lasers could possibly expand the potential of negative optical injection locking by improving the opto-electrical relaxation counter coupling.

It is also important to address the fundamental limitations and constraints of negative differentiated optical injection locking. First and foremost come the effects of temperature expansion and distortion. Though it is easy to compensate for slow effects by retuning the delay between the master and slave laser field evolutions, calculating this relationship and correcting for it over standard commercial or industrial operating ranges presents a clear opportunity for future research. Also, an investigation of the Q factor performance of negative differentiated injection locking simultaneously over bit rate,

injection ratio, and master laser detuning is also worthy of further research. This would allow a more complete picture of overall performance relative to the dynamics of standard injection locking for instance.

Another aspect of this technology that we have not addressed in this thesis is taking into account indirect bandgap phonon heating effects on the locking mechanism as well as isolator feedback contributions. We have learnt that it is possible to have a laser diode and isolator on the same chip. Another possibility for future research would be to investigate the possibility of angled input injection locking and possibly reducing the need for isolators by angling slave laser feedback away from the master laser and adjusting the mode field optical input into the slave laser.

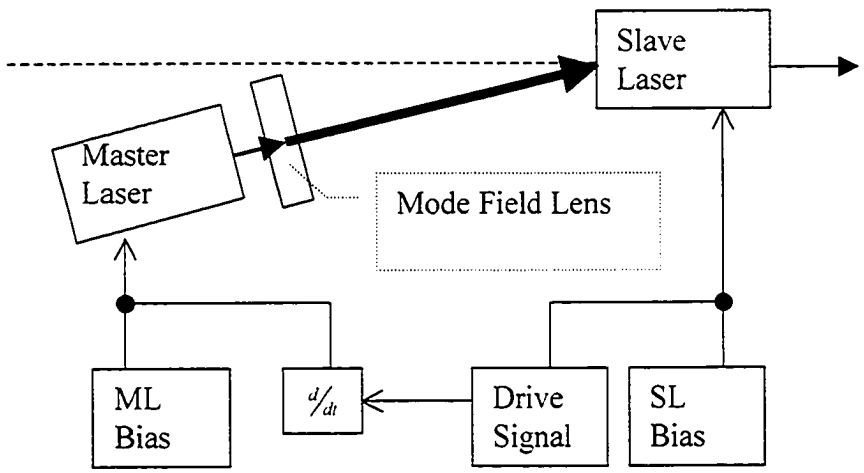

Figure 5.1 Future research isolator free negative differentiated injection locking modulator.

Finally, it may be of significant research interest to pursue an investigation on the effects of positive differentiated injection locking on an electro-absorption modulator.

APPENDIX A - WAVE PROPAGATION AND DISPERSION

The wave propagation constant [31], is described by,

$$\beta = \frac{2\pi n}{\lambda}, \tag{A.1}$$

where β is the wave propagation constant, n is an integer and λ is a wavelength. We can compute the dispersion effects of the wave propagation constant by expanding a Taylor series about a central frequency

$$\beta(\omega) \approx \beta_0(\omega_0) + \beta_1(\omega_0)(\omega - \omega_0) + \frac{1}{2}\beta_2(w_0)(\omega - \omega_0)^2 + \frac{1}{6}\beta_3(w_0)(\omega - \omega_0)^3 + \cdots \tag{A.2}$$

Defining,

$$\beta_m(\omega_0) = \left(\frac{\partial^m \beta}{\partial \omega^m}\right)_{\omega=\omega_o}. \tag{A.3}$$

The first term represents a phase shift and, decomposed into perpendicular components, gives rise to the product

$$pol(z) = \left|\beta_{0x}(\omega_0) - \beta_{0y}(\omega_0)\right| \cdot z, \tag{A.4}$$

where z is the time difference between the x and y components and which describes the polarization evolution of the optical wave. The group delay of the optical wave is given by

$$GD = \beta_1(\omega_0) \cdot z. \tag{A.5}$$

Thus we can calculate the group velocities as

$$V_g(\omega_0) = \frac{1}{\beta_1(\omega_0)}. \tag{A.6}$$

By combining (A.4), (A.5) and (A.6), we can now express the arrival time difference for the orthogonal polarization states we defined earlier. We define the differential group delay or polarization mode dispersion as

$$\Delta\tau_{pol} = z\left|\beta_{1x}(\omega_0) - \beta_{1y}(\omega_0)\right|. \tag{A.7}$$

We observe from (A.2) that the factor β_2 indicates that signal components of different frequencies propagate at different speeds. This spectral velocity dependence results in temporal spreading called chromatic dispersion or group velocity dispersion. This dispersion is quantified as

$$D(\omega_0) = -\frac{2\pi c}{\lambda^2}\beta_2(\omega_0). \tag{A.8}$$

The variation in dispersion with wavelength is characterized by β_3 and defined as the dispersion slope

$$\beta_3(\omega_0) = \frac{\partial\beta_2(\omega_0)}{\partial\omega} = -\frac{\lambda^2}{2\pi c}\frac{\partial\beta_2(\omega_0)}{\partial\lambda}. \tag{A.9}$$

APPENDIX B - DENSITY OF STATES

By expanding on the notions we will develop in exploring the density of states we will learn that quantum confinement on the order of the DeBroglie wavelength results in a quantization of permissible energy levels in the active layer material of a double heterojunction structure. This quantization will demonstrate emission linewidth improvement yet remains sensitive to changes in active layer change in refractive index making this technology particularly complementary to both standard injection locking and negative differentiated injection locking.

When the active layer material thickness becomes on the order of the DeBroglie wavelength [35],

$$\lambda = \frac{h}{mv}. \tag{B.1}$$

The quantum size effects can easily be observed over macroscopic scales as explained in Verdeyen [32], where the initial momentum states of carriers where described as a continuous variable and expressed the density of states as a function of energy as follows

$$\rho(E)dE = \frac{\sqrt{E}}{2\pi^2}\sqrt[3]{\frac{2m^*}{\hbar^2}}dE. \tag{B.2}$$

Within DeBroglie wavelength layer thickness materials, the density of states expression must change accordingly to capture the effect of the quantized momenta perpendicular to the layer plane as shown in Figure B.1.

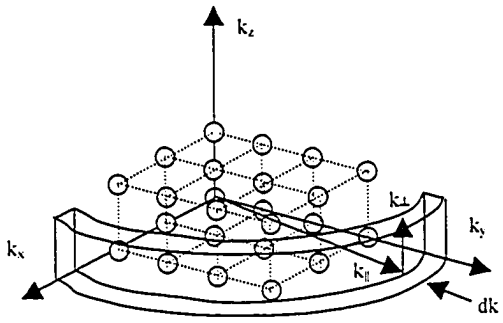

Figure B.1 1D confined quantum state representation.

To count the number of states for this confined configuration as k increases by dk counting only one permitted mode in k_z we may still regard k_x , k_y as continuous variables and re-evaluate the number of allowed states in the interval $k_{\|}$ to $k_{\|} + dk_{\|}$. Thus the number of states between k and $k + dk$ is the quarter-round area multiplied by the number of permitted states in the confined plane multiplied by the two spins of the carrier divided by the volume occupied by one state

$$N_k dk = \left(\frac{2\pi k_{\|} dk_{\|}}{4}\right)\left(\frac{\pi}{L_z}\right)(2)\left(\frac{L_x L_y L_z}{\pi^3}\right), \tag{B.3}$$

now by relating $k_{\|}$ to k

$$k^2 = \left(\frac{\pi}{L_z}\right)^2 + k_{\|}^2, \tag{B.4}$$

and expressing the mode density per unit k with:

$$\frac{N_k dk}{(L_x L_y L_z)} = \rho_k dk = \frac{1}{\pi^2} k dk \left(\frac{\pi}{L_z}\right), \tag{B.5}$$

and again using the energy conversion relationships we obtain

$$E = \frac{(\hbar k)^2}{2m^*} \quad k > \pi / L_z \quad E > E_1 = \frac{[\hbar(\pi / L_z)]^2}{2m^*} \quad q = 1. \tag{B.6}$$

Thus the density of states over the energy interval dE is

$$\rho(E)dE = \frac{1}{2\pi^2}\left(\frac{2m^*}{\hbar^2}\right)\left(\frac{\pi}{L_z}\right)dE \quad E > E_1. \tag{B.7}$$

By choosing L_z we can thus select a base emission frequency. If we permit a second mode in the quantum confinement region, the mathematical development is identical except that it defines another subband that starts at

$$E = E_2 = \frac{\hbar^2(2\pi / L_z)^2}{2m^*}. \tag{B.8}$$

By restricting the number of states in this fashion by mode confinement a greater number of electrons can have the same energy within a band and can be stimulated coherently with much greater efficiency. Also, this confinement can be achieved with a greatly reduced current density allowing such a device to possibly operate at room temperature. However we note the dependence on m^* which depends on the electrical carrier density, which can be related to the index of refraction, and in turn alters the ultimate emission wavelength.

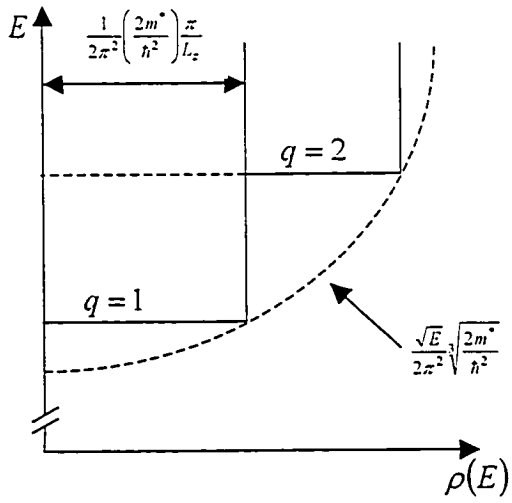

Figure B.2 Density of states under quantum confinement.

APPENDIX C - DESCRIPTION OF SPONTANEOUS EMISSION NOISE

According to the analysis of Schunk [43], spontaneous emission noise is a white noise process with a Gaussian probability distribution. Taking the derivative of the photon number we obtain

$$\frac{dS}{dt} = E_{SL}\frac{dE_{SL}^{*}}{dt} + E_{SL}^{*}\frac{dE_{SL}}{dt} = 2\,\mathrm{Re}\left(E_{SL}^{*}\frac{dE_{SL}}{dt}\right), \tag{C.1}$$

where E_{SL} is the complex slave laser electric field, which can be re-expressed as

$$\frac{dS}{dt} = \left(g(n) - \frac{1}{\tau_{ph}}\right)S + 2k_c\,\mathrm{Re}\left(E_{SL}^{*}E_{ext}\right) + 2\,\mathrm{Re}\left(E_{SL}^{*}E_{N}\right). \tag{C.2}$$

The last term E_N in the previous equation refers to the spontaneous noise. If we express $E_{SL}(t)$ and $E_N(t)$ in the forms

$$\begin{aligned} E_{SL}(t) &= \tilde{E}_{SL}(t)\exp(j\omega_{ML}t) \\ E_N(t) &= E_{sp}(t)\exp(j\omega_{ML}t) \end{aligned}, \tag{C.3}$$

we have then that

$$2\,\mathrm{Re}\left(E_{SL}^{*}E_{N}\right) = 2\,\mathrm{Re}\left(\tilde{E}_{SL}^{*}E_{SP}\right). \tag{C.4}$$

As $E_{SL}, \tilde{E}_{SL}, E_{sp}$ are all correlated, $\left\langle 2\,\mathrm{Re}\left(E_{SL}^{*}E_{N}\right)\right\rangle \neq 0$. If we partition time into sequences of duration $\Delta t = t_{i+1} - t_i$, we can rewrite the spontaneous emission term as

$$\begin{aligned} \tilde{E}_{SL}^{*}E_{sp} &= \tilde{E}_{SL}^{*}(t_i)E_{sp} + \Delta\tilde{E}_{SL}^{*}(t)E_{sp}, \\ \Delta\tilde{E}_{SL}^{*} &= \tilde{E}_{SL}^{*}(t) - \tilde{E}_{SL}^{*}(t_i) \end{aligned} \tag{C.5}$$

where E_{sp} is zero mean and slot independent, so we can approximate the spontaneous emission equation by

$$\tilde{E}_{SL}^{*}E_{sp} \approx \tilde{E}_{SL}^{*}(t_i)E_{sp} + \left\langle \Delta\tilde{E}_{SL}^{*}(t)E_{sp} \right\rangle, \tag{C.6}$$

E_{sp} is expressed by white Gaussian random process, described by

$$E_{sp} = \sqrt{\frac{A}{\Delta t}(x_1 + jx_2)}, \tag{C.7}$$

x_1, x_2 are independent Gaussian random variables with $\langle x_1^2 \rangle = \langle x_2^2 \rangle = 1$ for any timeslot Δt. A has to be chosen such that when E_{ext} is zero it represents a solitary laser. If we consider a solitary laser's photon number rate equation

$$\frac{dS}{dt} = \left(g(n) - \frac{1}{\tau_p} \right) S + R + F_s(t), \tag{C.8}$$

where R, the spontaneous emission rate.

If E_{ext} is zero using (C.2) we have

$$R = 2\,\mathrm{Re}\left\langle \Delta\tilde{E}_{SL}^{*}(t)E_{sp} \right\rangle. \tag{C.9}$$

Also if Δt is sufficiently small

$$\frac{d}{dt}\left(\Delta\tilde{E}_{SL}\right) \approx E_{sp}, \tag{C.10}$$

which yields

$$\begin{aligned} \Delta E_{SL} &= t\sqrt{\frac{A}{\Delta t}(x_1 + jx_2)} \\ \left\langle \Delta \tilde{E}^*_{SL}(t) E_{sp} \right\rangle &= \left\langle \frac{1}{\Delta t}\int_0^{\Delta t} \Delta \tilde{E}^*_{SL} E_{sp}\, dt \right\rangle, \\ &= \left\langle \frac{A}{2}\left(x_1^2 + x_2^2\right) \right\rangle = A \end{aligned} \tag{C.11}$$

and to satisfy (C.9) yields

$$A = \frac{R}{2}, \tag{C.12}$$

where R is the spontaneous emission rate defined by

$$R \equiv \frac{n_{sp}}{\tau_p}. \tag{C.13}$$

With Langevin noise force $F_s(t)$ described by the autocorrelation function

$$\left\langle F_s(t) F_s(t') \right\rangle = 2R\langle S \rangle \delta(t - t'). \tag{C.14}$$

Pulling these equations together we get

$$\tilde{E}^*_{SL} E_{sp} = \tilde{E}^*_{SL}(t_i)\sqrt{\frac{R}{2\Delta t}}(x_1 + jx_2) + \frac{R}{2}. \tag{C.15}$$

Describing the phasor of $\tilde{E}_{SL}$ yields

$$\tilde{E}_{SL}(t) = \sqrt{S(t)}\, e^{j\phi_0(t)}. \tag{C.16}$$

And using this relationship yields

$$\begin{aligned} \tilde{E}_{SL}^{*} E_{SP} &= \sqrt{\frac{S(t_i)}{2\Delta t}}\left(x_e + j x_\phi\right) + \frac{R}{2} \\ x_e &= x_1 \cos\left(\phi_0(t_i)\right) + x_2 \sin\left(\phi_0(t_i)\right), \\ x_\phi &= -x_1 \sin\left(\phi_0(t_i)\right) + x_2 \cos\left(\phi_0(t_i)\right) \end{aligned} \tag{C.17}$$

x_e, x_ϕ are still Gaussian random variables with $\left\langle x_e^2 \right\rangle = \left\langle x_\phi^2 \right\rangle = 1$.

APPENDIX D - SIMULATION PARAMETERS AND MATLAB ENGINE

D.1 MATLAB SEMICONDUCTOR MODULATION CONFIGURATION

```
alpha,5,                          % alpha of semiconductor laser
m_scale,0*-0.15*0.02*[1 -1],      % master laser drive scaling
m_bias,2.2,                       % master laser bias level multiplier
m_delay,0,                        % delay between modulation fields
s_scale,0.5*[1 1],                % slave laser drive scaling
s_bias,2.2,                       % slave laser bias level multiplier
bit_rate,1,                       % bit rate multiplier
beta,0.1,                         % rise/fall time factor (raised cosine shaped)
skip,1.5,                         % reject turn on time
m_rates,[1 2 5 10],               % modulation rate factors or detune if opt 4
i_levels,[0.6 0.8 1.2],           % injection level factors
opt,5,                            % 0:manual DM/SIL 1: BER 2: Distortion
                                  % 3: M Resp 4: detune 5: Relax_osc
mod_id,july 25 ber sil,           % ID label
%estimate_file,c3p0.mat,          % estimation file ie: c3p0.mat
tlimit,[1000 1e-6],               % optimization max cycles and tolerances
end
```

D.2 MATLAB DM,SIL AND NDIL SIMULATION ENGINE

```
function dy = sre21(t,y,varargin)

te=1e-9; % electron lifetime
tp=2e-12; % photon lifetime
T2=7e-12; % cavity round trip time
B=0.001; % fraction of spontaneous emission coupled to the lasing mode
En=0.01; % normalized gain compression factor
nth=1.9; % normalized carrier density at transparency
yamma=500; % ratio between photon and electron lifetimes
% input bias condition from user interface
for n= 1:length(varargin)
   if ischar(varargin{n})
      switch lower(varargin{n})
      case 'm_bias'
         biasm=varargin{n+1};
```

```
      case 'm_delta_scale'
         deltascalem=varargin{n+1};
      case 'beta'
         rcbeta=varargin{n+1};
      case 'bit_rate'
         bitrate=varargin{n+1};
      case 'm_delta_delay'
         deltadelay=varargin{n+1};
      case 's_delta_scale'
         deltascales=varargin{n+1};
      case 's_bias'
         biass=varargin{n+1};
      case 'f_detune'
         dv=varargin{n+1};
      case 'alpha'
         alpha=varargin{n+1};
      case 'bitpatern'
         bitpat=varargin{n+1};
      case 'sustain'
         sustain=varargin{n+1};
         rcbeta2=sustain(1);
         rcbeta3=sustain(2);
      otherwise
         disp(strcat('unrecognized argument',varargin{n}))
      end
   end
end
if bitrate==0
   deltascales=[0 0];
   deltascalem=[0 0];
   bitrate=5;
end
%Roll off and bitrate correction factors
if rcbeta==0
   rcbeta=rcbeta+eps;
end
T= 2/bitrate;
%Pulse shaping of input bit pattern into normal and differentiated output streams
s1=0;
s2=0;
m1=0;
m2=0;

a1=(1-rcbeta)*T/4;
a2=(1+rcbeta)*T/4;
a12=(1-rcbeta2)*T/4;
```

```
a22=(1+rcbeta2)*T/4;
a13=(1-rcbeta3)*T/4;
a23=(1+rcbeta3)*T/4;


t1=(T)*(t/T-floor(t/T));
t2=(T)*(((t-T/2)/T)-floor((t-T/2)/T));
t3=(T)*(((t-deltadelay)/T)-floor((t-deltadelay)/T));
t4=(T)*(((t-T/2-deltadelay)/T)-floor((t-T/2-deltadelay)/T));


b1=2*pi/(T*rcbeta)*(t1-a1)+pi;
b2=2*pi/(T*rcbeta)*(t1-a1-T/2);
b3=2*pi/(T*rcbeta)*(t2-a1)+pi;
b4=2*pi/(T*rcbeta)*(t2-a1-T/2);


c1=2*pi/(T*rcbeta2)*(t3-a12)+pi+deltadelay;
c2=2*pi/(T*rcbeta2)*(t3-a12-T/2)+deltadelay;
c3=2*pi/(T*rcbeta2)*(t4-a12)+pi+deltadelay;
c4=2*pi/(T*rcbeta2)*(t4-a12-T/2)+deltadelay;

c12=2*pi/(T*rcbeta3)*(t3-a13)+pi+deltadelay;
c22=2*pi/(T*rcbeta3)*(t3-a13-T/2)+deltadelay;
c32=2*pi/(T*rcbeta3)*(t4-a13)+pi+deltadelay;
c42=2*pi/(T*rcbeta3)*(t4-a13-T/2)+deltadelay;


flag=0;
if (t1 >= a1) & (t1 <= a2)
   s1=bitpat(2*ceil(t*bitrate/2+eps)-1)*deltascales(1)*0.5*(1+cos(b1));
elseif (t1 > a2) & (t1 <= a1+T/2)
   s1=bitpat(2*ceil(t*bitrate/2+eps)-1)*deltascales(1);
elseif (t1 > a1+T/2) & (t1 <= a2+T/2)
   s1=bitpat(2*ceil(t*bitrate/2+eps)-1)*deltascales(1)*0.5*(1+cos(b2));
end

if (t3 >= a12) & (t3 <= a22)& t>T/2+abs(deltadelay)
   flag=1;
   m1=bitpat(2*ceil((t-deltadelay)*bitrate/2+eps)-1)*deltascalem(1)*-
0.5*2*pi/(T*rcbeta2)*sin(c1);
elseif (t3 > a22) & (t3 <= a12+T/2)& t>T/2
   m1=0;
elseif (t3 > a12+T/2) & (t3 <= a22+T/2)& t>T/2+abs(deltadelay)
   m1=bitpat(2*ceil((t-deltadelay)*bitrate/2+eps)-1)*deltascalem(2)*-
0.5*2*pi/(T*rcbeta2)*sin(c2);
```

```
end

if (t3 >= a13) & (t3 <= a23) & t>T/2+abs(deltadelay) & bitpat(2*ceil((t-
deltadelay)*bitrate/2+eps-0.5))==0
   m1=bitpat(2*ceil((t-deltadelay)*bitrate/2+eps)-1)*deltascalem(1)*-
0.5*2*pi/(T*rcbeta3)*sin(c12);
   flag=1;
end


if (t2 >= a1) & (t2 <= a2) & t>T/2
   s2=bitpat(2*ceil(t*bitrate/2+eps-0.5))*deltascales(2)*0.5*(1+cos(b3));
elseif (t2 > a2) & (t2 <= a1+T/2) & t>T/2
   s2=bitpat(2*ceil(t*bitrate/2+eps-0.5))*deltascales(2);
elseif (t2 > a1+T/2) & (t2 <= a2+T/2) & t>T/2
   s2=bitpat(2*ceil(t*bitrate/2+eps-0.5))*deltascales(2)*0.5*(1+cos(b4));
end

if (t4 >= a12) & (t4 <= a22) & t>T/2+abs(deltadelay)
   if flag==1 & abs(m1)>0
      m2=bitpat(2*ceil((t-deltadelay)*bitrate/2+eps-0.5))*deltascalem(1)*-
0.5*2*pi/(T*rcbeta2)*sin(c3);
   else
      m2=bitpat(2*ceil((t-deltadelay)*bitrate/2+eps-0.5))*deltascalem(2)*-
0.5*2*pi/(T*rcbeta2)*sin(c3);
   end
elseif (t4 > a22) & (t4 <= a12+T/2) & t>T/2
   m2=0;
elseif (t4 > a12+T/2) & (t4 <= a22+T/2) & t>T/2+abs(deltadelay)
   if flag==1 & abs(m1) >0
      m2=bitpat(2*ceil((t-deltadelay)*bitrate/2+eps-0.5))*deltascalem(1)*-
0.5*2*pi/(T*rcbeta2)*sin(c4);
   else
      m2=bitpat(2*ceil((t-deltadelay)*bitrate/2+eps-0.5))*deltascalem(2)*-
0.5*2*pi/(T*rcbeta2)*sin(c4);
   end
end

if (t4 >= a13) & (t4 <= a23) & t>T/2+abs(deltadelay) & bitpat(2*ceil((t-
deltadelay)*bitrate/2+eps)-1)==0
   m2=bitpat(2*ceil((t-deltadelay)*bitrate/2+eps-0.5))*deltascalem(1)*-
0.5*2*pi/(T*rcbeta3)*sin(c32);
end

ss=s1+s2+biass;
mm=m1+m2+biasm;
```

```
if y(1)<=0
   y(1)=eps;
end
if y(4)<=0
   y(4)=eps;
end
r2d2=y(1)/y(4);
if y(4)== eps & y(1) ==eps
   r2d2 = 0;
end
% Rate equation for master and slave laser diodes
np=mm-gc(y(2),y(1),nth,En)*y(1)-y(2);
sp=yamma*(nth*gc(y(2),y(1),nth,En)*y(1)-y(1)+nth*B*y(2));
dy =real([
  yamma*(nth*gc(y(2),y(1),nth,En)*y(1)-y(1)+nth*B*y(2))
  mm-gc(y(2),y(1),nth,En)*y(1)-y(2)
  y(7)
  yamma*(nth*gc(y(5),y(4),nth,En)*y(4)-y(4)+...
     nth*B*y(5)+2*tp/T2*(r2d2)^.5*y(4)*cos(y(6)))
  ss-gc(y(5),y(4),nth,En)*y(4)-y(5)
  y(7)+yamma*(-alpha/2*(nth*gc(y(5),y(4),nth,En)-1)...
     -tp/T2*(r2d2)^.5*sin(y(6)))
  -alpha*yamma/2*(nth*(np*(1-En*y(1))-En*sp*(y(2)-1/nth+1)))
  s1+s2
  m1+m2
]);
% Gain function with gain compression factor based on photon density
function g=gc(a1,a2,nth,En);
g=(a1+1/nth-1)*(1-En*a2);
```

REFERENCES

1. Kroemer H., "A Proposed Class of Hetero-junction Injection Lasers," Proc. IEEE, Vol. 51, No.12, Dec. 1963, pp. 1782-1783.
2. Dingle R., Weigmann W., and Henry C.H., "Quantum States of Confined Carriers in Very Thin AlxGa1-xAs-GaAs-AlxGa1-xAs Heterostructures," Phys. Rev. Lett., Vol. 33, No. 14, Sept. 1974, pp. 827-830.
3. Verdeyen J., Laser Electronics, Prentice Hall, New Jersey, 1995, pp. 464-466.
4. Verdeyen J., Laser Electronics, Prentice Hall, New Jersey, 1995, pp. 467-470.
5. Cassey H.C. and Panish M. B., "Composition dependence of the $Al_xGa_{1-x}As$ direct and indirect energy gaps," J. Appl. Phys., 1969, Vol. 40,p. 4910.
6. Cassey H.C., Sell D., and Panish M., "Refractive index of $Al_xGa_{1-x}As$ between 1.2eV and 1.8eV," Appl. Phys. Lett., 1974, Vol. 24, pp. 63-65.
7. Verdeyen J., Laser Electronics, Prentice Hall, New Jersey, 1995, p. 442-444.
8. Keiser G., Optical Fiber Communications, McGraw-Hill, Toronto, 2000, pp. 180-181.
9. Keiser G., Optical Fiber Communications, McGraw-Hill, Toronto, 2000, p. 347.
10. Verdeyen J., Laser Electronics, Prentice Hall, New Jersey, 1995, pp. 151-154.
11. Morikuni J. and Kang S., Computer-Aided Design of Optoelectronic Integrated Circuits and Systems, Prentice Hall Inc., New Jersey, 1997, pp. 50-61.

12. Petitbon I., Gallion P., Debarge G., and Chabran C., 'Locking Bandwidth and Relaxation Oscillations of an Injection-Locked Semiconductor Laser', IEEE Journal of Quantum Electronics, 1998, vol 24, pp. 148-153.

13. Yu P., Cardona M., 'Fundamentals of Semiconductors', New York, 1999, pp. 282-305.

14. Henry C.H., Logan R.A., and Bertness K.A., 'Spectral dependence of the change in refractive index due to carrier injection in GaAs lasers', J. Appl. Phys, July 1981, vol 52., pp. 4453-4461.

15. Hass M., Lattice reflections, in Optical Properties of III-V Compounds, Semiconductors and Semimetals, Vol. 3, Academic Press, New York, 1967, pp. 3-16.

16. Henry C., Theory of the Phase Noise and Power Spectrum of a Single Mode Injection Laser, IEEE Journal of Quantum Electronics, September 1983, Vol. QE-19, NO. 9, pp.259-265.

17. Freed C., Bielinski J., and Lo W., "Fundamental linewidth in solitary ultranarrow output $PbS_{(1-x)}Se_{(x)}$ diode lasers," Appl. Phys. Lett., 1983.

18. Daino B., Spano P., Tamburrini M., and Piazzolla S., "Phase noise and spectral line shape in semiconductor lasers," IEEE J. Quantum Electronics, Mar. 1983, Vol. QE-19, pp. 266-270.

19. Henry C., "Theory of the linewidth of semiconductor lasers," IEEE J. Quantum Electronics, 1982, Vol. QE-18, pp. 259-264.

20. Morikuni J., Kang S., Computer-Aided Design of Optoelectronic Integrated Circuits and Systems, Prentice Hall Inc., New Jersey, 1997, p. 311.

21. Derickson D., 'Fiber Optic Test and Measurement', Prentice Hall, New Jersey, 1998, pp. 257-258.

22. Agrawal G. and Dutta N., Long-Wavelength Semiconductor Lasers, Van Nostrand Reinhold, New York, 1986.

23. Kikuchi K. and Okoshi T., "Estimation of linewidth enhancement factor of AlGaAs lasers by correlation measurements between FM and AM noises", IEEE Journal of Quantum Electronics, 1985, Vol. QE-21, no. 6, pp. 669-673.

24. Keiser G., Optical Fiber Communications, McGraw-Hill, Toronto, 2000, pp. 347-350.

25. Morikuni J., Kang S., Computer-Aided Design of Optoelectronic Integrated Circuits and Systems, Prentice Hall Inc., New Jersey, 1997, pp. 294-316.

26. Agrawal G.P. and Dutta N.K., Long-Wavelength Semiconductor Lasers, Van Nostrand Reinhold, New York, 1986.

27. Ikegami T. and Suematsu Y., "Large-signal characteristics of directly modulated semiconductor injection lasers", Electronics and Communications in Japan, 1970, Vol. 53-B, no. 9, pp. 69-75.

28. Linke R., "Modulation Induced Transient Chirping in Single Frequency Lasers", Journal of Quantum Electronics, 1985, Vol. QE-21, No. 6, pp. 593-597.

29. Keiser G., Optical Fiber Communications, McGraw-Hill, Toronto, 2000, pp. 282-297.

30. Verdeyen J., Laser Electronics, Prentice Hall, New Jersey, 1995, pp. 531-533.

31. Keiser G., Optical Fiber Communications, McGraw-Hill, Toronto, 2000, pp. 582-583.

32. Verdeyen J., Laser Electronics, Prentice Hall, New Jersey, 1995, pp. 517-531.

33. Verdeyen J., Laser Electronics, Prentice Hall, New Jersey, 1995, pp. 444-449.

34. Verdeyen J., Laser Electronics, Prentice Hall, New Jersey, 1995, pp. 476-482.

35. Verdeyen J., Laser Electronics, Prentice Hall, New Jersey, 1995, pp. 470-476.

36. Spirit D.M. and Mahony O., 'High Capacity Optical Transmission Explained', Wiley, Toronto, 1995, pp. 35-37.

37. Agrawal G., 'Power Spectrum of Directly Modulated Single-Mode Semiconductor Lasers: Chirp-Induced Fine Structure', IEEE Journal of Quantum Electronics, 1985, Vol. QE-21, pp. 680-687.

38. Mohrdiek S., Burkhard H. and Walter H., 'Chirp Reduction of Directly Modulated Semiconductor Lasers at 10Gb/s by Strong CW Light Injection', Journal of Lightwave Technology, 1994, Vol. 12, pp. 418-423.

39. Foschini G., Jopson R.M., Nelson L., and Kogelnik H., 'The Statistics of PMD-Induced Chromatic Fiber Dispersion', Journal of Lightwave Technology, 1999, Vol. 17, pp. 1560-1565.

40. Green P., Fiber Optic Networks, Prentice Hall, New Jersey, 1993, pp. 417-456.

41. Green P., Fiber Optic Networks, Prentice Hall, New Jersey, 1993, pp. 198-199.

42. Green P., Fiber Optic Networks, Prentice Hall, New Jersey, 1993, pp. 254-258.

43. Schunk N. and Petermann K., Noise Analysis of Injection-Locked Semiconductor Injection Lasers, IEEE Journal of Quantum Electronics, 1986, Vol. QE-22, pp. 642-650.

44. Serway R., Physics for Scientiscts and Engineers, Saunders College Publishing, Toronto, 1990, p. 663.

45. Papoulis A., Probability, Random Variables, And Stochastic Processes, McGraw-Hill, Inc., Toronto, 1991, pp. 649-650.

46. Teshima M., Frequency Stabilization of Tunable DBR Laser Using Multiwavelength Light Injection Locking Technique, Journal of Lightwave Technology, 1996, Vol. 14, pp. 2749-2755.

47. Ikegami T. and Suematsu Y., Resonance-Like Characteristics of the Direct Modulation of a Junction Laser, Proc. IEEE, 1967, Vol. 55, p.122.

48. R. Adler, A study of locking phenomena in oscillators, Proc. IRE, 1946, Vol. 34, pp. 351-357.

Bibliography

1. Ibsen M., Eggleton B., Sceats M. and Ouellette F., 'Broadly tunable DBR fibre laser using sampled fiber Bragg grating', Electron. Lett., 1995, Vol. 31, pp. 37-39.
2. Loh W., Zhou F., and Pan J., 'Sampled Fiber Grating Based-Dispersion Slope Compensator', IEEE Photonics Technical Letters, 1999,Vol. 11, pp. 1280-1282.
3. Grunnet J., Johnson A., Maniloff E., Mossberg T., Munroe M. and Sweetser, 'Demonstration of All-Fiber Sparse Lightwave CDMA Based on Temporal Phase Encoding', IEEE Photonics Technical Letters, 1999,Vol. 11, pp. 1283-1285.
4. Lee S., Khosravani, Peng J., Grubky V., Starodubov D., Willner A.E., Feinberg J., 'Adjustable Compensation of Polarization Mode Dispersion Using a High-Birefringence Nonlinearly Chriped Fiber Bragg Grating', IEEE Photonics Technical Letters, 1999, Vol. 11, pp. 1283-1285.
5. Koch T., Alferness R., 'Dispersion Compensation by Active Predistorted Signal Synthesis', Journal of Lightwave Technology, 1985, Vol. 3, pp. 800-805.
6. Chen X., Fan C., Luo Y., Xie S., Hu S., 'Novel Flat Multichannel Filter Based on Strongly Chirped Sampled Fiber Bragg Grating', IEEE Photonics Technology Letters, 2000, Vol. 12, pp. 1501-1503.
7. Chen X., Luo Y., Fan C., Wu T., Xie S., 'Analytical Expression of Sampled Bragg Gratings with Chirp in the Sampling Period and Its Application in Dispersion Management Design in a WDM System', IEEE Photonics Technology Letters, 2000, Vol. 12, pp. 1013-1015.

8. Griffel G., 'Synthesis of Optical Filters Using Ring Resonator Arrays', IEEE Photonics Technology Letters, 2000, Vol. 12, pp. 810-812.
9. Komukai T., Inui T., Nakazawa M., 'Group Delay Ripple Reduction and Reflectivity Increase in a Chirped Fiber Bragg Grating by Multiple-Overwriting of a Phase Mask with an Electron-Beam, IEEE Photonics Technology Letters, 2000, Vol. 12, pp. 816-818.
10. Eldada L., Amin J., Sharps R., 'Dispersive Properties of Planar Polymer Bragg Gratings', IEEE Photonics Technology Letters, 2000, Vol. 12, pp. 819-821.
11. Wedding B., 'New Method For Optical Transmission Beyond Dispersion Limit', Electronics Letters, 1992, Vol. 28, pp. 1298-1300.
12. Tatham M.C., Sherlock G. and Westbrook L.D., 'Compensation fiber chromatic dispersion by optical phase conjugation in a semiconductor laser amplifier', Electronics Letters, 1993, Vol. 29, pp. 1851-1852.
13. Izadpanah H, Goldstein E., Lin C., 'Broadband Multiwavelength Simultaneous Dispersion Compensation near 1550nm Through singlemode Fibers Optimised For 1310nm', Electronics Letters, 1993, Vol. 29, pp. 364-365.
14. Takesue H., Yamamoto F., Sugie T., 'Novel Node Configuration for DWDM Photonic Access Ring Using CMLS', IEEE Photonics Technology Letters, 2000, Vol. 12, pp. 1698-1700.
15. Xie Y.,Lee S. Pan Z., Cai J.-X, Willner A.E., Grubsky V., Starodubov D.S., Salik E. and Feinberg J., 'Tunable Compensation of the Dispersion Slope Mismatch in Dispersion-Managed Systems Using a Sampled Nonlinearly Chirped FBG', IEEE Photonics Technology Letters, 2000, Vol. 12, pp. 1417-1419.

16. Belloti G., Bigo S., Cortès P., Gauchard S. and Larochelle S., '10 x 10 Gb/s Cross-Phase Modulation Suppressor for Multispan Transmissions Using WDM Narrow-Band Fiber Bragg Gratings', IEEE Photonics Technology Letters, 2000, Vol. 12, pp. 1403-1405.

17. Guan B., Tam H., Tao X. and Dong X., 'Highly Stable Fiber Bragg Gratings Written in Hydrogen-Loaded Fiber', IEEE Photonics Technology Letters, 2000, Vol. 12, pp. 1349-1351.

18. Boivin L., Taccheo S., Doerr C.R., Stulz L.W., Monnard R., Lin W., Fang W.C., 'A Supercontinuum Source Based on an Electroabsorption-Modulated Laser for Long Distance DWDM Transmission', IEEE Photonics Technology Letters, 2000,Vol. 12, pp. 1695-1697.

19. Chin M.K., Youtsey C., Zhao W., Pierson T., Ren Z., Wu S.L., Wang Y.G. and Ho S.T., 'GaAs Microcavity Channel-Dropping Filter Based on a Race-Track Resonator', IEEE Photonics Letters, 1999, Vol. 11, pp. 1620-1622.

20. Madsen C.K., Lenz G., Bruce A.J., Cappuzzo M.A., Gomez L.T. and Scotti R.E., 'Integrated All-Pass Filters for Tunable Dispersion and Dispersion Slope Compensation', IEEE Photonics Letters, 1999, Vol. 11, pp. 1623-1625.

21. Neophytou A.I., White I. H., Quinian S.M. and Garrett B., 'All Optical Switching Of Integrated Hybrid Distributed Feedback Bistable Laser', Electronics Letters, 1992, Vol. 28, pp. 1300-1301.

22. Little B.E., Chu S.T., Haus H.A., Foresi J., Laine J.-P., 'Microring Resonator Channel Dropping Filters', Journal of Lightwave Technology, 1997,Vol. 15, pp. 998-1005.

23. Chen L., Cooper J.F. and Smith P., 'Transmission Filters With Multiple Flattened Passbands Based on Chirped Moiré Gratings', IEEE Photonics Technology Letters, 1998, Vol. 10, pp. 1283-1285.

24. Chen L.R, Loka H.S., Cooper D.J.F., Smith P.W.E., Tam R. and Gu X., 'Fabrication of Transmission filters with single or multiple flattened passbands based on chirped Moiré gratings', Electronics Letters, 1999, Vol. 35, pp. 584-585.

25. Hübner J., Zauner D. and Kristensen M., 'Strong Sampled Bragg Gratings for WDM Applications', IEEE Photonics Letters, 1998, Vol. 10, pp. 552-554.

26. Park K., Young T., Kim M., Lee K. and Won Y., 'All-Fiber Drop-Pass with Fiber Bragg Gratings', IEEE Photonics Letters, 1998, Vol. 10, pp. 555-557.

27. Kwong W.C. and Yang G.-C., 'Allocation of unequal-spaced channels in WDM lightwave systems', Electronics Letters, 1995, Vol. 31, pp. 898-899.

28. Ouellette F., Krug P.A., Stephens T., Dhosi G. and Eggleton B., 'Broadband and WDM dispersion compensation using chirped sampled fiber Bragg gratings', Electronics Letters, 1995, Vol. 31, pp. 899-901.

29. Rizvi N.H., Gower M.C., Goodall F.C., Arthur G. and Herman P., 'Excimer laser writing of submicrometre period fiber Bragg gratings using phase-shifting mask projection', Electronics Letters, 1995, Vol. 31, pp. 901-902.

30. Avrutsky I., Fay M., Xu J.M., 'Multiwavelength Diffraction and Apodization Using Binary Superimposed Gratings', IEEE Photonics Letters, 1998, Vol. 10, pp. 839-841.

31. Ibsen M., Burkin K., Cole J. and Laming R., 'Sinc-Sampled Fiber Bragg Gratings for Identical Multiple Wavelength Operation', IEEE Photonics Letters, 1998, Vol. 10, pp. 842-844.

32. Imai T., Komukai T. and Nakazawa M., 'Dispersion Tuning of a Linearly Chirped Fiber Bragg Grating Without a Center Wavelength Shift by Applying a Strain Gradient', IEEE Photonics Letters, 1998, Vol. 10, pp. 845-847.

33. Saito T., Henmi N., Fujita S., Yamaguchi M. and Shikada M., 'Prechirp Technique for Dispersion Compensation for a High-Speed Long-Span Transmission', IEEE Photonics Technology Letters, Vol. 3, pp. 74-76.

34. Cheng Y. H., 'Optimal Design for Direct-Detection System with Optical Amplifiers and Dispersion Compensators', Journal of Lightwave Technology, Vol. 11, pp. 1495-1499.

35. Deparis O., Kiyan R., Salik E., Starodubov D., Feinberg J., Pottiez O., Mégret P. and Blondel M., 'Round Trip Time and Dispersion Optimization in a Dual-Wavelength Actively Mode-Locked Er-Doped Fiber Lase Including Nonchirped Fiber Bragg Gratings', IEEE Photonics Technology Letters, 1999, Vol. 11, pp. 1238-1240.

36. Chew Y.H., Tjhung T., Thiang and Mendis F., 'An Optical Filter of Adjustable Finesse Using and Amplified Fiber Ring Resonator', Journal of Lightwave Technology, 1997, Vol. 15, pp. 364-370.

37. Fonjallaz P., Limberger H. and Salathé R., 'Bragg Gratings with Efficient and Wavelength-Selective Fiber Out-Coupling', Journal of Lightwave Technology, 1997, Vol. 15, pp. 371-376.

38. Willner A.E., Feng K.-M, Cai J., Lee S., Peng J. and Sun H., 'Tunable Compensation of Channel Degrading Effects Using Nonlinearly Chirped Passive Fiber Bragg Gratings', IEEE Journal of Selected Topics in Quantum Electronics, 1999, Vol. 5, pp. 1298-1311.

39. Jinguji K. and Oguma M., 'Optical Half-Band Filters', Journal of Lightwave Technology, 2000, Vol. 18, pp. 252-259.

40. Ebberg A., Auracher F. and Borchert, '10 Gbit/s transmission using directly modulated uncooled MQW ridge waveguide DFB lasers in TO package', Electronics Letters, 2000, Vol. 36, pp. 1476-1477.

41. Dantec R., Benyattou T., Guillot G., Spisser C., Seassal C., Leclercq J.L., Viktorovitch P., Rondi D., and Blondeau R.,'Tunnable Microcavity Based on InP-Air Bragg Mirrors', IEEE Journal of Selected Topics in Quantum Electronics, 1999, Vol. 5, pp. 111-114.

42. Fehse R., Sweeney S.J., Adams A.R., O'Reilly E.P., Egorov A.Y., Riechert H., and Illek S., 'Insights into carrier recombination processes in 1.3μm GaInAs-based semiconductor laser attained using high pressure', Electronics Letters, 2001, Vol. 37, pp. 92-93.

43. Gaff K.W., Ladouceur F., and Love J.D., 'Two-wavelength planar add/drop WDM filter employing a three-mode coupling Bragg grating', Electronics Letters, 2000, Vol. 36, pp. 1142-1144.

44. Daza M., Liu H.F., Tsuchiya M., Ogawa Y., and Kamiya T., 'All-Optical WDM-to-TDM Conversion with Total Capacity of 33 Gb/s for WDM Network Links',

IEEE Journal of Selected Topics in Quantum Electronics, 1997, Vol. 3, pp. 1287-1294.

45. Takada K., Abe M., Hida Y., Shibata T., Ishii M., Himeno A., and Okamoto K., 'Fabrication of 2GHz-spaced 16-channel arrayed-waveguide grating demultiplexer for optical frequency monitoring applications', Electronics Letters, 2000, Vol. 36, pp. 1643-1644.
46. Lam C.F., Geuer M.D., and Frigo N.J., 'Performance of pin and APD receivers in high speed WDM data transmission systems employing spectrally sliced spontaneous emission sources', Electronics Letters, 2000, Vol. 36, pp. 1572-1574.
47. Lee Jaedeuk, Song H., Paek U., and Seo Y., 'Design and fabrication of dispersion-managed fibers by periodic etching during the MCVD process', Electronics Letters, 2001, Vol. 37, pp.11-12.
48. Diminstein O., Gorbatov N., and Tur M., 'Dispersion-based differential wavelength measurements for Bragg grating sensors', Electronics Letters, 2001, Vol. 37, pp. 12-14.
49. Tanaka K., Morita I., Edagawa N., and Suzuki M., 'Impact of nonlinear crosstalk in 0.8nm-spaced 40Gbit/s DWDM systems', Electronics Letters, 2000, Vol. 36, pp. 1217-1218.
50. Shimizu N., Murata K., Hirano A., Miyamoto Y., Kitabayashi H., Umeda Y., Akeyoshi T., Furuta T., and Wantanabe N., '40Gbit/s monolithic digital OEIC composed of unitravelling-carrier photodiode and InP HEMTs', Electronics Letters, 2000, Vol. 36, pp. 1220-1221.

51. Timofeev F.N., Bayvel P., Mikhailov V., Lavrova O.A., Wyatt R., Kashyap R., Robertson M., Midwinter J.E., '2.5Gbit/s directly-modulated fiber grating laser for WDM networks', Electronics Letters, 1997, Vol. 33, pp. 1406-1407.

52. Lender A., 'Correlative Digital Communication Techniques', IEEE Transactions on Communications Technology, 1964, Vol. COM-12, pp. 128-135.

53. Yonenaga K., and Kuwano S., 'Dispersion-Tolerant Optical Transmission System Using Duobinary Transmitter and Binary Receiver', Journal of Lightwave Technology, 1997, Vol. 15, pp. 1530-1537.

54. Gu X., and Blank L.C., '10Gbit/s unrepeatered three-level optical transmission over 100 km of standard fiber', Electronics Letters, 1993, Vol. 29, pp. 2209-2210.

55. Price A.J., Mercier N. Le, 'Reduced bandwith optical digital intensity modulation with improved chromatic dispersion tolerance', Electronics Letters, 1995, Vol. 31, pp. 58-59.

56. May G., Solheim A., and Conradi J., 'Extended 10 Gb/s Fiber Transmission Distance at 1538 nm Using a Duobinary Receiver', IEEE Photonics Technology Letters, 1994, Vol. 6, pp. 648-650.

57. Yonenaga K., Hirano A., Yoneyama M., Miyamoto Y., Hagimoto K., and Noguchi K., 'Expansion of tolerable dispersion range in a 40 Gbit/s optical transmission system using and optical duobinary signal', Electronics Letters, 1998, Vol. 34, pp. 385-386.